



HAL
open science

Contribution of interictal and ictal epileptic sources to scalp EEG

Georgia Ramantani

► **To cite this version:**

Georgia Ramantani. Contribution of interictal and ictal epileptic sources to scalp EEG. Signal and Image processing. Université de Lorraine, 2018. English. NNT : 2018LORR0034 . tel-01792027

HAL Id: tel-01792027

<https://theses.hal.science/tel-01792027>

Submitted on 15 May 2018

HAL is a multi-disciplinary open access archive for the deposit and dissemination of scientific research documents, whether they are published or not. The documents may come from teaching and research institutions in France or abroad, or from public or private research centers.

L'archive ouverte pluridisciplinaire **HAL**, est destinée au dépôt et à la diffusion de documents scientifiques de niveau recherche, publiés ou non, émanant des établissements d'enseignement et de recherche français ou étrangers, des laboratoires publics ou privés.



AVERTISSEMENT

Ce document est le fruit d'un long travail approuvé par le jury de soutenance et mis à disposition de l'ensemble de la communauté universitaire élargie.

Il est soumis à la propriété intellectuelle de l'auteur. Ceci implique une obligation de citation et de référencement lors de l'utilisation de ce document.

D'autre part, toute contrefaçon, plagiat, reproduction illicite encourt une poursuite pénale.

Contact : ddoc-theses-contact@univ-lorraine.fr

LIENS

Code de la Propriété Intellectuelle. articles L 122. 4

Code de la Propriété Intellectuelle. articles L 335.2- L 335.10

http://www.cfcopies.com/V2/leg/leg_droi.php

<http://www.culture.gouv.fr/culture/infos-pratiques/droits/protection.htm>



Ecole Doctorale BioSE (Biologie-Santé-Environnement)

THÈSE

Présentée et soutenue publiquement pour l'obtention du titre de
DOCTEUR DE L'UNIVERSITE DE LORRAINE

Mention: « Sciences de la Vie et de la Santé »

par

Georgia Ramantani

**Contribution des sources épileptiques
inter-critiques et critiques à l'EEG de scalp**

Le 29 mars 2018 à Nancy

Membres du jury

Rapporteurs Mr Philippe Derambure Professeur, Université de Lille, France
Mr Serge Vulliemoz Professeur assistant, Université de Genève, Suisse

Examineurs

Mr Louis Maillard Professeur, Université de Lorraine, France,
Directeur de Thèse
Mr Laurent Koessler CNRS – Université de Lorraine, France,
Co-Directeur de Thèse
Mme Martine Gavaret Professeur, Université Paris 5 René
Descartes, Paris, France
Mme Valérie Louis-Dorr Professeur, Université de Lorraine, France

THANKS AND ACKNOWLEDGEMENTS

My thanks to Pr. Martine Gavaret, Pr. Philippe Derambure, Pr. Serge Vulliémoz, and Pr. Valérie Louis-Dorr who have done me the honor of agreeing to take part in my thesis committee, and for taking the time to judge this work.

A special thanks is necessary to Pr. Louis Maillard and Dr. Laurent Koessler for their unwavering support and assistance and their insightful suggestions and stimulating discussions.

Thanks are also necessary to my collaborators in the Epilepsy Centre Freiburg, Germany, Dr. Matthias Dümpelmann, Dr. Delphine Cosandier, and Armin Brandt, for their valuable contribution to the published works.

RÉSUMÉ LONG

CONTRIBUTION DES SOURCES ÉPILEPTIQUES INTER-CRITIQUES ET CRITIQUES À L'EEG DE SCALP

INTRODUCTION

Depuis l'existence des enregistrements électroencéphalographiques (EEG) invasifs avec des électrodes intracrâniennes positionnées dans un contexte clinique, il est admis qu'un nombre considérable de décharges épileptiques intercritiques ou critiques ne sont pas visibles en électroencéphalographie (EEG) de scalp lors des interprétations visuelles de routine. Ce problème méthodologique est majeur dans la prise en charge des épilepsies car l'EEG de scalp est la technique la plus utilisée dans le diagnostic initial, dans la classification, dans la définition des zones cérébrales à explorer avec l'EEG intracrânien voire même dans l'exérèse chirurgicale d'emblée de la zone épileptogène. Dans le contexte de la chirurgie des épilepsies, les enregistrements EEG invasifs représentent la méthode de référence pour définir la localisation et l'étendue de la zone épileptogène. Ces enregistrements invasifs présentent cependant des limites. L'électrocorticographie (ECoG), avec des multi-capteurs placés à la surface du cortex, offre une excellente surface d'exploration des sources cérébrales superficielles mais présente un biais d'échantillonnage spatial pour les sources profondes, comme par exemple celles situées dans le fond des sillons. La stéréoelectroencéphalographie (SEEG), avec des capteurs multi-contacts implantés en profondeur dans le cortex, offre une excellente profondeur d'exploration et permet notamment l'investigation des sources profondes mais présente un biais d'échantillonnage spatial en raison du faible nombre d'électrodes implantées et la couverture irrégulière des sources cérébrales latérales notamment celles situées sur la convexité. L'investigation des corrélations entre les sources épileptiques et les signaux EEG enregistrés de façon non-invasive sur le scalp est donc devenue particulièrement importante et nécessaire dans le champ de la chirurgie des épilepsies avec notamment l'avènement récent des méthodes de localisation de sources basées sur l'EEG de scalp. Le

développement des enregistrements EEG simultanés multi-échelles avec des capteurs de scalp, subduraux et/ou de profondeur, réalisés dans un contexte clinique, offre une opportunité unique d'investiguer et de résoudre la problématique de ces corrélations mal connues et non quantifiées à ce jour. De même, les développements technologiques et méthodologiques de ces dernières années, notamment ceux réalisés dans le domaine de l'imagerie de sources électriques (ISE) non invasive, offrent des perspectives très intéressantes dans l'investigation de cette question d'interrelation entre les sources cérébrales et les signaux EEG de surface. Ces développements rapides dans le domaine des neurosciences computationnels nécessitent néanmoins de résoudre des problématiques complexes en terme de modélisation et de résolution de problème inverse. Dans la littérature, des études ont montré que l'investigation des sources profondes (comme c'est le cas dans les épilepsies temporo-mésiales) mais aussi des sources néocorticales au niveau du lobe temporal et des autres lobes (comme c'est particulièrement fréquent dans les épilepsies de l'enfant ou de l'adolescent en association avec une dysplasie corticale focale) s'avère également importante à étudier.

Cette thèse vise à étudier la contribution des sources épileptiques à l'EEG de surface en utilisant une approche par enregistrement EEG simultané multi-échelle et par imagerie de sources électriques non-invasives. Ce travail s'est réparti de la façon suivante : 1) clarifier l'origine corticale exacte des activités épileptiques intercritiques corticales enregistrées en EEG de scalp, 2) identifier les caractéristiques qui déterminent la visibilité des sources cérébrales en EEG de surface et 3) mettre en évidence les zones cérébrales qui ne sont pas visibles, et donc échappent, à l'EEG de surface. Dans ce but, une revue détaillée de la littérature à la fois médicale et neuroscientifique a été réalisée. Ensuite les études expérimentales ont été menées pour 1) étudier la contribution des sources temporales internes (profondes) à l'EEG de surface en utilisant la SEEG comme méthode de référence, 2) étudier l'apport de l'ISE dans les épilepsies frontales et mettre en rapport les signaux enregistrés en ECoG avec ceux enregistrés simultanément en EEG de surface et 3) étudier

la contribution des sources internes, basales et latérales du lobe frontal en ECoG et en EEG de surface. Enfin, une analyse a été effectuée pour étudier la pertinence des résultats obtenus et définir les perspectives de cette thèse.

CONTRIBUTION DES SOURCES TEMPORO-MÉSIALES A L'EEG DE SURFACE

Dans cette étude, 1) j'ai étudié la contribution des sources épileptiques localisées purement dans le lobe temporal interne à l'EEG de surface puis 2) j'ai comparé les différentes projections électriques (cartographies de scalp) des sources cérébrales temporales mésiales, mésio-latérales et latérales sur le scalp. Pour cela, j'ai utilisé une approche basée sur des enregistrements simultanés EEG-SEEG chez des patients présentant une épilepsie temporale pharmaco-résistante. Cette approche s'avère particulièrement innovante et pertinente pour plusieurs raisons. En effet, par comparaison avec les précédentes études qui utilisaient uniquement des électrodes subdurales ou du foramen ovale, j'ai pu investiguer simultanément de nombreuses régions cérébrales notamment profondes et superficielles mais aussi celles situées dans les fonds de sillons. De plus, la SEEG grâce à ces capteurs multi-contacts, permet de localiser très précisément les sources cérébrales via la présence d'inversion de phase sur les signaux enregistrés. Enfin, la SEEG grâce à son excellente résolution temporelle permet l'identification précise de l'activation temporelle des sources et donc un séquençage précis qui est nécessaire à la caractérisation des sources en EEG de surface. Cette étude a été la première dans la littérature à étudier la contribution des sources temporales en EEG de surface via l'identification de différents réseaux de sources du lobe temporal (mésiaux, mésiaux plus néocorticaux et néocorticaux). D'un point de vue méthodologie, un pipeline automatique, utilisant à la fois une expertise humaine et statistique, a été développé. Des décharges épileptiques intercritiques, utilisées comme biomarqueurs, ont été moyennés puis classés sur la base de la SEEG selon les différents réseaux énoncés ci-dessus. Ce pipeline a été développé de façon à être utilisable pour l'investigation de tous les signaux EEG multi-échelles. Le résultat majeur de cette étude concerne la mise en évidence de la contribution en EEG de surface des sources temporales

mésiales. Cette contribution, même si elle n'est pas visible spontanément à l'EEG de surface sans moyennage, existe de façon statistiquement significative. Il s'agit de la première étude à montrer que les sources temporales mésiales, contribuent à l'EEG de surface malgré leur géométrie enroulée (champ électrique « fermé »), leur profondeur (plusieurs centimètres du scalp) et l'activation électrique permanente des sources temporales latérales (activité de fond). Bien que cette contribution soit faible (en moyenne 7 μ V), elle est extractible du bruit de fond EEG. Cette découverte permet de résoudre une question très ancienne qui est posée depuis le début des enregistrements EEG et SEEG. Elle permet de démontrer que, malgré l'enroulement anatomique des structures temporales internes et la position diamétralement opposée du subiculum et du gyrus parahippocampique, les sources temporales internes peuvent être détectées en EEG de surface. En outre, cela démontre aussi que la conduction volumique s'applique quel que soit le type de sources cérébrales même si elles sont distantes de la surface.

Concernant la projection des différents réseaux de sources temporales sur l'EEG de surface, nous avons démontré que les sources temporales mésiales ont une projection différente des autres réseaux (mésiaux plus latéraux et latéraux). En effet les sources mésiales plus latérales et les sources latérales présentent un pôle électrique négatif au niveau des électrodes de scalp temporales ipsi-latérales et un pôle électrique positif au niveau des électrodes du vertex (région fronto-centro-pariétale) alors que les sources mésiales pures ne présentent qu'un seul pôle négatif au niveau des électrodes temporales basales ipsi-latérales. Cette observation démontre l'importance de couvrir l'ensemble du scalp avec les électrodes EEG et de considérer l'intégralité des champs électriques sur le scalp et non dans une région donnée, notamment quand il s'agit de localiser la source d'une activité EEG de scalp visible.

L'identification de nouveaux biomarqueurs en EEG de surface, issus de sources temporales mésiales, représente une nouvelle voie de recherche très intéressante pour permettre, à terme, d'éviter les enregistrements EEG invasifs dans le cadre des épilepsies pharmaco-

résistantes et spécialement chez les patients souffrant d'épilepsie du lobe temporal (étiologie la plus fréquente). Ce travail a fait l'objet d'un article original.

Koessler L, Cecchin T, Colnat-Coulbois S, Vignal JP, Jonas J, Vespignani H, **Ramantani G**, **Maillard LG**. Catching the invisible: mesial temporal source contribution to simultaneous EEG and SEEG recordings. *Brain Topogr.* 2015 Jan;28(1):5-20.

IMAGERIE DE SOURCES ELECTRIQUES DES SOURCES CEREBRALES FRONTALES ET DE LEURS CORRELATS SUBDURAUX.

L'ISE, issue des signaux EEG, représente de nos jours une méthode reconnue dans le domaine de l'épilepsie permettant une représentation dans un volume cérébral en 3D des sources épileptiques. Cependant, malgré les progrès récents et des résultats prometteurs, l'ISE n'a pas encore réussi à remplacer les enregistrements EEG invasifs qui ont une résolution supérieure notamment dans les régions explorées. L'extension de l'ISE en utilisant des signaux ECoG pourrait pallier cette problématique. Dans cette étude, j'ai analysé des signaux EEG-ECoG simultanés issus de patients épileptiques pharmaco-résistants du lobe frontal et intégrés dans un bilan pré-chirurgical. Nous avons réalisé des études d'ISE, à partir de signaux ECoG avec la présence de pointes épileptiques intercritiques, pour comparer 1) les localisations de sources obtenues avec les localisations anatomiques issues des interprétations électrocliniques conventionnelles de la zone épileptogène et irritative et 2) les résultats post-chirurgicaux dans les cas où les localisations de sources étaient incluses dans la zone de résection chirurgicale avec les résultats où les localisations de sources étaient uniquement partielles ou non incluses dans la zone de résection chirurgicale. J'ai utilisé les algorithmes MUSIC et sLORETA, deux méthodes complémentaires et connues pour donner des localisations de sources valides que ce soit à partir de signaux ECoG simulés ou réels. Cette approche d'ISE en ECoG, c'est-à-dire l'utilisation d'une échelle EEG différente du scalp, est nouvelle par comparaison aux nombreuses études réalisées dans la littérature. Il s'agit ici de la première étude qui valide l'utilisation d'une telle méthode, qui démontre une grande précision et surtout qui montre

l'utilité clinique de cette nouvelle approche méthodologique qui était jusqu'alors utilisée sur des cas uniques ou sur des signaux simulés. L'avantage majeur de l'ISE couplée à l'ECoG repose sur la résolution du biais d'échantillonnage spatial de l'ECoG utilisée seule. D'autre part, cela permet de donner une dimension supplémentaire, en profondeur, aux résultats d'ECoG classiques. Les épilepsies du lobe frontal représentent le second type le plus fréquent parmi les épilepsies pharmaco-résistantes et dont le taux de patients libres de crises après la chirurgie est le plus bas. Les avancées obtenues par cette étude d'ISE issue de signaux ECoG devraient permettre d'améliorer le taux de réussite chirurgicale de ce type d'épilepsie difficile à traiter. L'ISE en ECoG a donné dans cette étude des résultats anatomiquement concordants par comparaison avec les analyses conventionnelles faites à partir de signaux seuls mais a surtout permis d'obtenir de meilleures localisations pour les sources profondes. Cette observation suggère que l'utilisation de méthodes de résolution de problèmes inverses basés sur l'ECoG devrait combler les lacunes liées à l'utilisation de capteurs subduraux en cas de sources profondes. Toutefois, bien que les résultats d'imagerie de sources soient concordants d'un point de vue anatomique notamment dans les cas de sources mésiales et orbito-frontales, nous avons mis en évidence que seules les sources bien échantillonnées spatialement par les capteurs subduraux sont localisables. Cette limitation est cependant contrebalancée par le fait que la couverture spatiale des régions cérébrales d'intérêt est toujours soigneusement définie à partir des résultats électro-cliniques pré-chirurgicaux et des données de neuro-imagerie. L'utilisation de l'algorithme sLORETA sur les signaux ECoG a montré des résultats très diffus tandis que MUSIC a donné des localisations de sources plus limitées spatialement. Ceci est inhérent aussi aux contraintes fixées par ces algorithmes, à savoir l'utilisation d'une décomposition en valeur propre par MUSIC et l'utilisation de sources distribuées à la fois spatialement mais aussi temporellement (étude du décours temporel) pour sLORETA. La maîtrise de ces outils méthodologiques est donc cruciale pour l'interprétation correcte des résultats obtenus et dans la suppression de sources incongrues ou fantômes. Les localisations de sources doivent être appréhendées et interprétées comme une

approximation de l'étendue réelle des sources cérébrales et donc ne doivent pas être comparées au volume de résection chirurgicale (souvent plus vaste). D'autre part, la comparaison des localisations de sources peut aussi s'avérer complexe lorsque deux méthodes différentes de résolution de problème inverse (notamment familles d'algorithmes différentes : L1-norm, L2-norm, dipole fit, ...) ont été utilisées. Ceci a été démontré dans une étude récente de simulation avec l'utilisation de modèles biophysiques réalistes et de méthodes de localisation de sources distribuées. Les résultats ont montré une surestimation de l'étendue des sources cérébrales reconstruites. Par conséquent, le choix de l'algorithme de résolution de problème inverse est une donnée essentielle à prendre en compte lors d'investigations futures.

Dans notre étude, la présence de localisation de sources dans la zone de résection était très fortement corrélée avec le résultat excellent de la chirurgie (patients libres de crises) du lobe frontal. Ceci démontre l'utilité clinique de l'ISE-ECOG dans la définition des limites anatomiques de l'exérèse chirurgicale. La valeur ajoutée de cette nouvelle méthode devra être validée de façon prospective, en incluant d'autres types de sources cérébrales dans le lobe frontal (position et extension). Si l'on considère que la délimitation de la zone épileptogène ne doit pas seulement être issue de l'utilisation des pointes épileptiques comme marqueurs de la zone épileptogène, l'étape suivante sera d'appliquer cette méthode sur les décharges critiques et de réaliser une comparaison prospective avec les méthodes conventionnelles utilisées actuellement. Ce travail a fait l'objet d'un article original.

Ramantani G, Cosandier-Rimélé D, Schulze-Bonhage A, **Maillard L**, Zentner J, Dümpelmann M. Source reconstruction based on subdural EEG recordings adds to the presurgical evaluation in refractory frontal lobe epilepsy. Clin Neurophysiol. 2013 Mar;124(3):481-91.

ETUDE DES CORRELATS ELECTROPHYSIOLOGIQUES EEG-ECOG DANS LES EPILEPSIES FRONTALES

Toutes les études qui utilisent des données simultanées EEG-ECoG, récentes ou anciennes, se sont intéressées au lobe temporal. Pourtant, les sources cérébrales extra-temporales ont une prévalence identique aux sources cérébrales temporales dans la chirurgie des épilepsies en pédiatrie. Par conséquent, elles représentent un challenge important pour la compréhension des corrélations électro-cliniques et des résultats post-chirurgicaux obtenus. En particulier, les études réalisées dans les épilepsies du lobe frontal ont montré que 12 à 37% des patients ne présentaient pas de pointes épileptiques en EEG de scalp. Les facteurs qui contribuent aux difficultés d'interprétation des pointes EEG et de leurs corrélats en profondeur reposent sur l'inaccessibilité d'une large partie du lobe frontal aux électrodes de surface, l'importance des connexions cortico-corticales rapides intra-lobaires et inter-lobaires, et la présence de co-activation de sources bilatérales. L'observation en EEG de scalp de pointes épileptiques intercritiques focales a surtout été faite avec des sources cérébrales dorso-latérales frontales, tandis que les sources mésiales et orbito-frontales sont généralement associées à des pointes bi-frontales ou unilatérales et controlatérales à la source à l'EEG de surface. Ces disparités engendrent très souvent l'utilisation d'enregistrements EEG invasifs pour la délimitation de la zone épileptogène.

Dans cette étude, nous avons étudié la détectabilité des sources cérébrales du lobe frontal telles que définies par des enregistrements ECoG. Nous avons étudié l'influence de la localisation, de l'extension et de l'amplitude des sources sur la présence des pointes intercritiques à EEG enregistrées simultanément sur le scalp. Nous avons utilisé la même cohorte de patients que pour l'étude précédente et nous avons utilisé les mêmes sources cérébrales car très bien caractérisées et localisées par l'ISE-ECoG et les résultats post-chirurgicaux. Cette étude est innovante pour plusieurs raisons : 1) il s'agit de la première étude utilisant des signaux simultanés EEG-ECoG pour étudier les sources frontales et leurs corrélats électriques sur le scalp ; 2) il s'agit de la première utilisation concomitante de l'analyse visuelle et de l'ISE issue de l'ECoG pour améliorer la définition spatiale des sources et pour ajouter une dimension supplémentaire (3D) aux sources corticales.

Plusieurs résultats de cette étude sont importants et nouveaux. Notre étude a démontré l'invisibilité des pointes épileptiques en EEG de surface pour la majorité des sources épileptiques intercritiques frontales: seulement 14% des sources sont visibles spontanément sur l'EEG de scalp. Ce résultat est crucial pour l'évaluation pré-chirurgicale. De plus, notre étude a démontré l'absence de visibilité en EEG de scalp de la majorité des sources situées dans la partie basale et mésiale du lobe frontal, ce qui corrobore des études plus anciennes qui n'utilisaient pas de signaux EEG simultanés multi-échelles. Enfin, nos résultats montrent l'influence très grande de l'activité de fond EEG dans la visibilité ou non des décharges épileptiques en EEG de scalp. L'élimination de cette activité de fond (par moyennage) permet de détecter clairement les sources mésiales et basales mais aussi les sources dorso-latérales qui n'étaient pas visibles par analyse visuelle de routine. Ceci explique le taux très faible de pointes épileptiques visibles en EEG de scalp dans les épilepsies frontales. Ce résultat suggère que le manque de visibilité des sources frontales en EEG de scalp était lié surtout à l'activité électrique des sources cérébrales physiologiques sus-jacentes. Notre étude est la première à avoir quantifié ce paramètre in-vivo et dans le contexte des épilepsies du lobe frontal. Les pointes dont l'origine anatomique est située sur la convexité latérale sont souvent invisibles tandis que les sources situées dans le gyrus frontal mésial, ou dans le fond des sillons dorso-latéraux, ou dans le cortex fronto-orbitaire sont détectables après moyennage des signaux EEG de scalp, remettant en cause le postulat théorique largement répandu que ces régions ne sont pas détectables en EEG de scalp. Enfin, il s'agit de la première étude à avoir étudié l'influence de l'extension et de l'amplitude des sources sur la visibilité des signaux en EEG de scalp. La médiane de l'extension spatiale de sources à activer pour détecter un signal en EEG de scalp est de 6 cm². Ce résultat est comparable avec les études réalisées in-vitro en l'absence d'activité de fond ou encore avec les études réalisées en simulation. Ce résultat est par contre en dessous des 10 à 20 cm² qui ont été proposés dernièrement dans une étude réalisée in-vivo et in-vitro dans le lobe temporal. Cet écart est peut être dû à la différence de sources étudiées (frontales versus temporales). Cependant, cet écart peut aussi souligner la

différence entre les sources qui sont visibles lors des interprétations de routine clinique et les sources petites ou profondes qui sont détectables seulement après un moyennage qui atténue le bruit de fond physiologique. Si l'on considère la grande différence de couverture spatiale (profondeur et extension corticale) entre les explorations avec les capteurs ECoG et les capteurs SEEG, nous souhaitons étendre cette étude en utilisant cette fois-ci des signaux EEG-SEEG avec ces mêmes sources frontales. Nous utiliserons pour quantifier les relations le même pipeline que celui utilisé pour l'étude sur les sources du lobe temporal (voir plus haut). Ce travail a été valorisé par l'article original suivant.

Ramantani G, Dümpelmann M, **Koessler L**, Brandt A, Cosandier-Rimélé D, Zentner J, Schulze-Bonhage A, **Maillard LG**. Simultaneous subdural and scalp EEG correlates of frontal lobe epileptic sources. *Epilepsia*. 2014 Feb;55(2):278-88.

CONCLUSION

Cette thèse avait pour but d'étudier les corrélats électriques en EEG de scalp de sources cérébrales investiguées selon différentes méthodes invasives. Ces études ont été réalisées grâce à des enregistrements EEG simultanés multi-échelles et dans un contexte de bilans pré-chirurgicaux d'épilepsie pharmaco-résistante. Pour mener à bien ces études, j'ai développé des méthodes innovantes d'analyse notamment dérivées de l'imagerie de sources électriques. Les données EEG multi-échelles ont facilité l'analyse des corrélats électriques étant donné la synchronie des signaux enregistrés et l'échantillonnage spatial des sources depuis la profondeur jusqu'à la surface. Les méthodes d'imagerie de sources électriques permettent d'améliorer encore l'analyse de ces signaux. Les sources cérébrales profondes, comme celles situées dans la partie mésiale lobe temporal ou dans la partie fronto-basale du lobe frontale, ne sont pas visibles spontanément en EEG de scalp mais sont détectables. Les pointes épileptiques visibles sur l'EEG de scalp sont issues généralement d'activation de sources très étendues spatialement et dont le rapport signal sur bruit est généralement très grand. La résolution spatiale de l'EEG de scalp pose des limites intrinsèques pour la détection et la localisation des sources. Ces études menées lors

de la thèse démontrent l'importance majeure de continuer à développer des outils d'analyse des signaux EEG de scalp pour obtenir de nouveaux outils diagnostiques qui permettent de surmonter le biais d'échantillonnage spatial des explorations EEG invasives et pourront, peut-être à terme, éviter l'utilisation des méthodes EEG invasives.

Mots clés: électroencéphalographie, pointes épileptiques, imagerie de sources électriques, enregistrements EEG invasifs, épilepsie pharmaco-résistante, chirurgie des épilepsies

ABSTRACT

CONTRIBUTION OF INTERICTAL AND ICTAL EPILEPTIC SOURCES TO SCALP EEG

Ever since the implementation of invasive EEG recordings in the clinical setting, it has been perceived that a considerable proportion of epileptic discharges present at a cortical level are missed by routine scalp EEG. Several *in vitro*, *in vivo*, and simulation studies have been performed in the past decades aiming to clarify the interrelations of cortical sources with their scalp and invasive EEG correlates. The amplitude ratio of cortical potentials to their scalp EEG correlates, the extent of the cortical area involved in the discharge, as well as the localization of the cortical source and its geometry, have been each independently linked to the recording of the cortical discharge with scalp electrodes. The need to elucidate these interrelations has been particularly imperative in the field of epilepsy surgery with its rapidly growing EEG-based localization technologies. Simultaneous multiscale EEG recordings with scalp, subdural and depth electrodes, applied in presurgical epilepsy workup, offer an excellent opportunity to shed some light on this fundamental issue. Whereas past studies have considered predominantly neocortical sources in the context of temporal lobe epilepsy, the present work also addresses deep sources, as in mesial temporal epilepsy, and extratemporal sources. We could show that multiscale EEG recordings and source localization tools considerably facilitate the analysis of interrelations between cortical sources and their scalp EEG correlates. Deep sources, such as those in mesial temporal or fronto-basal regions, are not visible, but they are detectable in scalp EEG. Scalp EEG spikes correlate with extensive activation of the cortical convexity and high spike-to-background amplitude ratios. The decoding of the interrelations between invasive and scalp EEG can facilitate the validation of diagnostic tools such as ESL, MEG, and fMRI. These novel computational tools may serve as surrogates for the shortcomings of current EEG recording methodology and promote further development in modern electrophysiology.

Keywords: interictal spikes, source localization, intracranial recordings, refractory epilepsy, epilepsy surgery, electroencephalography

ABBREVIATIONS

CT: computer tomography

ECoG: electrocorticography

EEG: electroencephalography

ESL: electrical source localization

fMRI: functional magnetic resonance imaging

MEG: magnetoencephalography

SEEG: stereoelectroencephalography

TABLE OF CONTENTS

Thanks and Acknowledgements	2
Résumé long	3
Abstract	14
Abbreviations	15
CHAPTER 1: INTRODUCTION	17
1. <i>General Introduction</i>	17
2. <i>Cortical sources and their EEG correlates</i>	19
A. Medical context	19
B. Scientific context	20
3. Need for simultaneous intracranial and scalp EEG recordings	26
4. Findings from past studies of simultaneous invasive and scalp EEG	27
CHAPTER 2: EXPERIMENTAL	30
2.1 <i>The Contribution of Mesial Temporal Sources to EEG and SEEG</i>	31
A. Introduction	31
B. Catching the Invisible: Mesial Temporal Source Contribution to Simultaneous EEG and SEEG Recordings	33
C. Discussion & Perspectives	34
2.2 <i>Source localization in the study of frontal lobe sources and their subdural correlates</i>	36
A. Introduction	36
B. Source reconstruction based on subdural EEG recordings adds to the presurgical evaluation in refractory frontal lobe epilepsy	38
C. Discussion & Perspectives	39
2.3 <i>Simultaneous subdural and scalp EEG correlates of frontal lobe epileptic sources</i>	41
A. Introduction	41
B. Simultaneous subdural and scalp EEG correlates of frontal lobe epileptic sources	43
C. Discussion & Perspectives	44
CHAPTER 3: DISCUSSION	46
<i>Perspectives</i>	48
<i>Conclusion</i>	50
BIBLIOGRAPHY	51
APPENDIX	56
ABSTRACT/RESUME	57

CHAPTER 1: INTRODUCTION

1. GENERAL INTRODUCTION

Ever since the implementation of invasive EEG recordings with chronically implanted electrodes in the clinical setting, it has been observed that a considerable proportion of interictal and ictal epileptic discharges present at a cortical level are missed by routine scalp EEG^{1,2}. This observation thus gave rise to the following critical questions regarding the contribution of epileptic sources to the signals recorded on the scalp level:

- a. What is the exact cortical origin of a rhythm recorded by scalp EEG?
- b. Which features determine the visibility of cortical sources in scalp EEG?
- c. Are there cortical regions that fail to contribute to scalp EEG signals?

This issue is of cardinal importance in epilepsy management, with scalp EEG constituting a major localizing tool³ from the primary diagnosis and epilepsy classification to the planning of an intracranial investigation or of a resection in the case of a refractory course. Several *in vitro*, *in vivo*, and simulation studies have been conducted to clarify the interrelations of scalp and intracranial EEG findings^{1,4-9}. The need to elucidate these interrelations has been particularly imperative in the field of epilepsy surgery with its rapidly growing EEG-based localization technologies. The development of electrical source localization (ESL), magnetoencephalography (MEG), and functional magnetic resonance imaging (fMRI)¹⁰⁻¹⁶, all deriving from interictal EEG spikes, has rendered the correlation of cortical to scalp epileptic discharges even more crucial. Simultaneous multiscale EEG recordings with scalp, subdural and depth electrodes, applied in the presurgical evaluation of patients with refractory focal epilepsy, offer an excellent opportunity to shed some light on this fundamental issue. Technological advances of the last decades, as implemented in the fast-growing field of ESL, have the potential to resolve these complex interrelations. Past studies have considered predominantly neocortical sources in the context of temporal lobe epilepsy, but

deep sources, as in mesial temporal epilepsy, as well as extratemporal sources, also warrant further investigation.

This thesis aimed to evaluate the contribution to answering questions a-c provided by this simultaneous multiscale EEG recording approach, extended by the application of source localization methodologies. This aim is achieved by:

1. A detailed review of the relevant primary literature in both a medical and scientific context.

2. Experimental work addressing:

a. The Contribution of Mesial Temporal Sources to EEG and SEEG: Koessler et al. (2015) Catching the invisible: mesial temporal source contribution to simultaneous EEG and SEEG recordings. Published: *Brain Topogr*,28:5-20.

b. Source localization in the study of frontal lobe sources and their subdural correlates: Ramantani et al. (2013) Source reconstruction based on subdural EEG recordings adds to the presurgical evaluation in refractory frontal lobe epilepsy. Published: *Clin Neurophysiol*, 124:481-91.

c. The contribution of mesial, basal and dorsolateral frontal lobe sources to EEG and iEEG: Ramantani et al. (2014) Simultaneous subdural and scalp EEG correlates of frontal lobe epileptic sources. Published: *Epilepsia*,55:278-88.

3. Discussion of the significance of this experimental work, and perspectives deriving from it.

2. CORTICAL SOURCES AND THEIR EEG CORRELATES

A. MEDICAL CONTEXT

Ever since the first recordings in humans, performed by Hans Berger in 1924¹⁷, scalp EEG has been a key instrument in epilepsy workup, guiding primary diagnosis, epilepsy classification, and treatment. However, the first intracranial EEG recordings, performed by Reginald Bickford in epilepsy patients in 1948², revealed a striking discrepancy between seemingly negative scalp EEGs and an abundance of epileptic discharges in invasive EEGs (Figure 1).

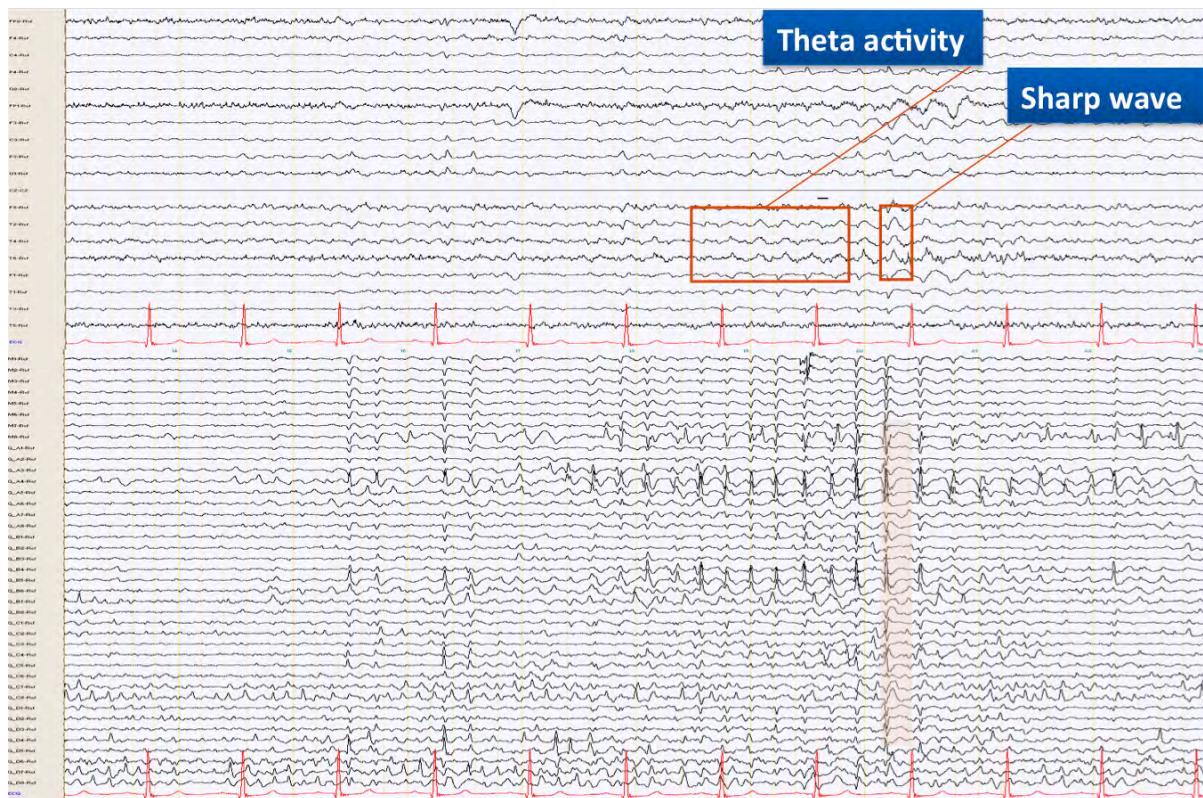


Figure 1: Simultaneous scalp (upper rows) and subdural (lower rows) EEG traces, recorded during the invasive exploration of a patient with refractory focal frontal lobe epilepsy. Note the discrepancy between the abundant spikes over numerous subdural EEG contacts, often corresponding to theta activity and rarely to sharp waves in scalp EEG.

The correlation of cortical sources with their corresponding scalp EEG discharges is particularly crucial for epilepsy surgery that has since been established as a safe and effective treatment option for pharmacoresistant patients^{18–22}. In this context, scalp EEG is a

primary localizing tool that determines invasive electrode placement or even surgical resection, whereas invasive EEG constitutes the gold standard for defining the localization and extent of the epileptogenic zone²³. The current methodology of invasive explorations in epilepsy patients has, however, inherent limitations, thus rendering multimodal comparisons particularly challenging²⁴. Subdural recordings offer extensive cortical coverage but are prone to sampling limitations for deep sources, such as those in the depth of a sulcus^{13,14,25}. Depth electrode recordings provide information for selected deep structures^{11,25,26} but are plagued from sampling limitations due to incomplete and irregular cortical coverage on the brain convexity.

Rapid developments in computational studies, including simulation as well as source localization methods, address the urgent need to compensate for the shortcomings of both subdural and depth recordings and, most of all, to clarify their correlation with scalp EEG recordings^{8,14,26,27}. On the other hand, several novel technologies have been established in the last decade that derive from interictal EEG spikes, such as ESL, magnetoencephalography (MEG), and functional magnetic resonance imaging (fMRI)¹⁰⁻¹⁶. This development renders the correlation of cortical to scalp epileptic discharges even more crucial.

B. SCIENTIFIC CONTEXT

i. Electrogenesis

The field potential of a population of neurons equals the sum of the field potentials of the individual neurons (Figure 2). To understand EEG phenomena, the activity of populations of neurons must always be considered. EEG phenomena can be measured only at a considerable distance from the source if the responsible neurons are regularly arranged and activated in a more or less synchronous way. A typical regular arrangement is a palisade, in which the neurons are distributed with the main axes of the dendritic trees parallel to each other and perpendicular to the cortical surface. When the neurons in such a population (e.g., the pyramidal neurons of cortical layers III and V) are more or less simultaneously activated

by way of synapses lying at the proximal dendrites, extracellular currents will flow. Their longitudinal components (i.e., parallel to the main axes of the neurons) will add, whereas their transverse components will tend to cancel out. The result is a laminar current along the main axes of the neurons²⁸.

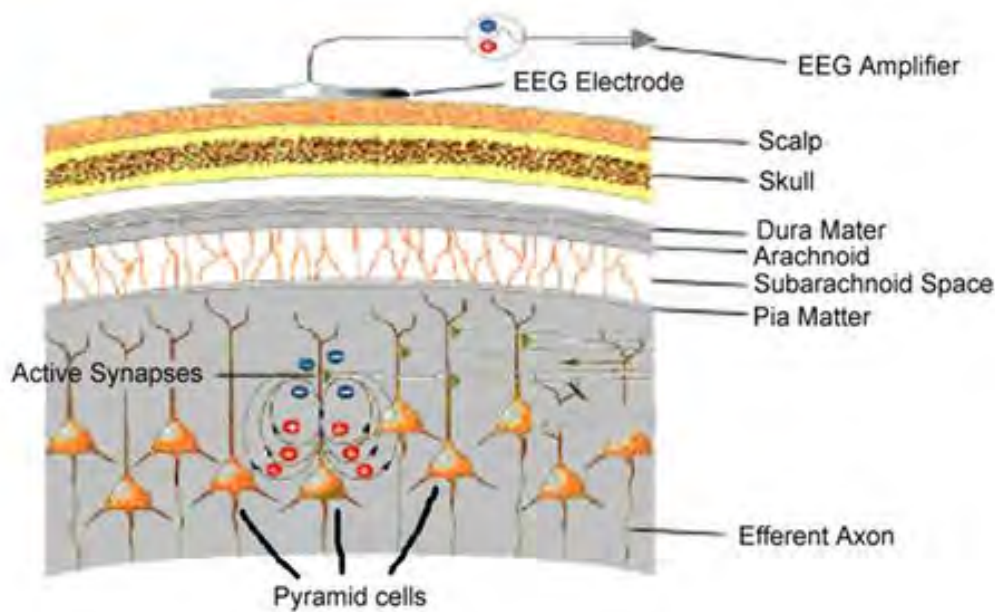


Figure 2: Schematic illustration of EEG generation in the pyramidal neurons of the brain.

Most epileptiform transients are initially negative when recorded from electrodes on or above the cortical surface. Electrodes on the opposite side of the generating cortical layer, whether in the underlying white matter or even on the scalp at the other side of the head, record a positive potential. Accordingly, spike and seizure voltage fields typically have dipolar configurations, i.e., two maxima, one negative and one positive, both readily recordable, unless the orientation of the cortical source is such that one of the maxima is located at the base of the skull, a region beyond the reach of scalp electrodes. At a macroscopic level, it may, therefore, be stated that the potential field generated by a synchronously activated palisade of neurons behaves like that of a dipole layer²⁸.

ii. Biophysical model of propagation

It has been assumed that the brain could be considered an infinite homogeneous medium, but in reality, this is not the case. The field potentials are influenced not only by the geometry of the neuronal populations and the electrical properties of individual neurons but also by the existence of regions with different conductivities in the head, i.e., by the presence of inhomogeneities. For an interpretation of field potentials measured at the scalp, it is therefore important to take into consideration the layers lying around the brain: the cerebrospinal fluid (CSF), the skull, and the scalp. These layers account, at least in part, for the attenuation of EEG signals measured at the scalp as compared to those recorded at the underlying cortical surface^{28,29}.

In addition, it is known that the conductivity of the various tissues is not homogeneous. The conductivity of the skull varies with its thickness and bone structure. Studies by Law et al.³⁰ supported that there is an inverse relation between skull resistivity and thickness. Cuffin³¹ and Eshel et al.³² investigated the effects of varying the conductivity of the skull; the former determined the impact of local variations in skull and scalp thickness on the EEG while the latter showed a correlation between interhemispheric asymmetry in skull thickness and the amplitude of the scalp EEG. The comprehensive studies of Haueisen³³ on the influence of various combinations of conductivities on the EEG showed that the scalp EEG is most influenced by the conductivities of the skull and the scalp. It should be noted that the conductivity of the tissues of the head can also present anisotropy. Indeed, it is known that in brain tissue, the conductivity measured in a direction parallel to a fiber tract can be ten times larger than in the perpendicular direction, whereas the anisotropy of the skull causes the smearing-out of the distribution of the EEG over the scalp.

In addition, it is relevant to emphasize that the skull does not have a homogeneous surface, due to both the existence of regions with different thickness and the occipital and the eye socket openings. The presence of holes in the skull, for example, due to surgical interventions, also influences the distribution of the EEG over the scalp (Figure 3).

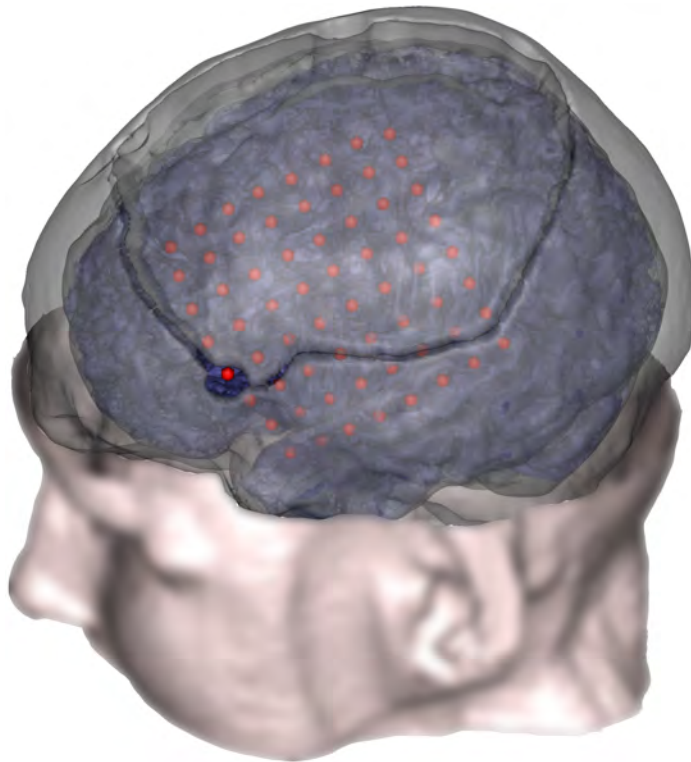


Figure 3: Depiction of the multiple layers of scalp and skull in a realistic head model deriving from the MRI data of a patient undergoing presurgical evaluation for refractory epilepsy. The grid array electrodes are illustrated with red dots. Note the burr hole through the skull, performed for subdural electrode implantation.

iii. Factors influencing the scalp visibility of a cortical source

The scalp voltage field of an epileptiform discharge depends on both the physical and functional properties of its cerebral source. Physical factors include the location, the extent of activation, and the orientation of the cortical generator. Functional factors include the discharge amplitude, frequency, and synchrony⁵.

It should be noted that the location of a cortical generator determines the distribution of its voltage field only in relation to source area and orientation. If the amount of synchronously activated cortex is not large enough, no discernible field will be recorded at the scalp after attenuation by the skull and scalp, in spite of the large amplitude of the cortical epileptiform discharge. This is a common observation in invasive EEG recordings with intracranial electrodes for the presurgical evaluation of refractory focal epilepsy patients: abundant focal spikes are recorded from multiple subdural and intracerebral electrodes, whereas only a few

spikes are detected at the scalp level. This phenomenon is often due to the limited generator extent. The dependence of scalp potential amplitude on the extent of the generator is most easily appreciated in the seminal paper by Gloor³⁴.

Source orientation is an equally crucial feature determining the visibility of cortical generators in scalp EEG recordings. Electrodes placed directly above a given cortical generator only record the maximum voltage if the net orientation of the active cortical area is parallel to the skull, thus producing a radial field orthogonal to the active cortical area. The field maximum is further displaced as the orientation of a source becomes more tangential. The extreme case is an entirely tangential source, such as one on the bank of a sulcus or major lobar fissure: an electrode directly above this tangential source is on the zero isopotential line and records no voltage. The positive and negative maxima are on either side and have a more extensive separation with increasing source depth. In the case of widespread sources, voltage fields from opposing sulcal walls may cancel, leaving the fields from gyral crowns to predominate. This observation underlines the critical role of source orientation in determining scalp field configuration. The overall contour of lobar surfaces influences voltage topography, rather than individual gyri and sulci, given the typically large source area of scalp-recordable spikes⁵.

The distance between the source and the sensor is another crucial factor in the visibility of cortical source activation in scalp EEG recordings. Superficial sources produce smaller fields with higher voltages and steeper gradients, whereas deeper sources produce larger fields of lesser amplitude and shallower gradients. The temporal evolution of the voltage field indicates propagation and its direction. Voltage fields that show only a change in field magnitude but not in basic shape or location are generated by discrete sources with little or no propagation. Spike voltage fields that change in shape or demonstrate movement of maxima during the course of a spike indicate altered source geometry, most commonly a reflection of propagation⁵.

In 1999, Merlet et al.³⁵ analyzed simultaneous scalp EEG and stereoelectroencephalography (SEEG) recordings and compared dipole localizations with the distribution of SEEG potentials concurrent with scalp EEG discharges. The cortical discharges that corresponded to scalp EEG spikes were never focal but involved 8-21 SEEG contacts for temporal and 15-10 SEEG contacts for extratemporal sources. Interestingly, no scalp EEG spikes were observed that corresponded exclusively to focal activity limited to mesial temporal structures. The authors concluded that the involvement of lateral temporal neocortex, additional to the mesial temporal structures, is required for the generation of scalp-visible EEG spikes. They further suggested that modeling a scalp-visible EEG spike by a single source located in the medial aspect of the temporal lobe might be unreliable.

iv. Findings from in vitro studies

Of all studies attempting to determine the extent of cortical activation required to produce epileptic discharges recordable in scalp EEG, that of Cooper et al.⁴ has gained the most widespread acceptance, proposing a minimum of 6 cm² of synchronized cortical activity. This estimation, however, is based on a head-phantom using in-vitro measurements of a piece of fresh cadaver skull, a pulse generator connected to saline-soaked cotton balls placed on the inside of the skull, an artificial dura made of polyethylene, and EEG electrodes recording from the exterior of the skull. The 6 cm² estimate of the required extent of cortical sources derived from the area of multiple pinholes punched into the polyethylene sheet when EEG signals were first recorded from the electrodes on the outside of the skull. Additionally, measurements estimating the source area were made in the absence of EEG background activity, thus rendering any conclusions uncertain³⁶.

v. Findings from computational studies

The relationship between the EEG signals and the spatiotemporal configuration of the underlying cortical sources was more recently addressed in the study of Cosandier-Rimélé et al., using a realistic model of the simultaneous scalp and intracerebral EEG generation⁸ (Figure 4).

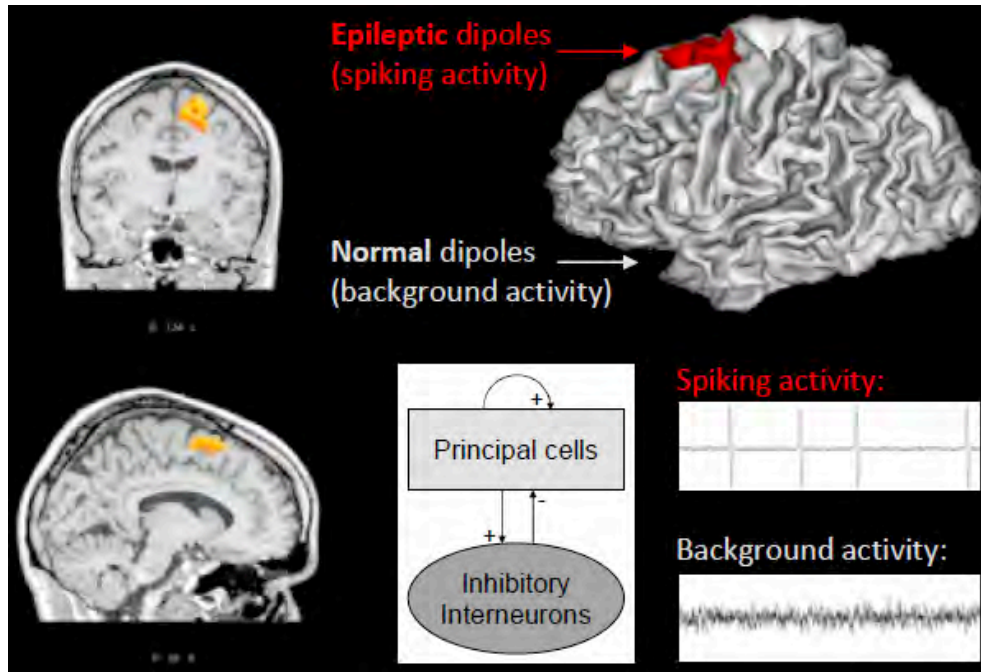


Figure 4: The computational model of EEG^{8,27,37} combines a neurophysiologically relevant description of the EEG sources (3D geometry and activity of cortical populations of neurons) with a biophysically pertinent description of the transmission of cortical activity to recording electrodes.

The proposed model includes both an anatomically realistic description of the spatial features of the sources, as a convoluted dipole layer, and a physiologically relevant description of their temporal activities, as coupled neuronal populations. The authors confirmed that the cortical area involved in scalp EEG spikes is rather extensive since a spike-to-background amplitude ratio of > 2.8 corresponded to a cortical source of 24 cm^2 for the intracerebral EEG and 30 cm^2 for the scalp EEG. Furthermore, it was shown that the location of the cortical generator relative to the recording electrodes strongly influences EEG signal properties, thus underlining the importance of source geometry in this context.

3. NEED FOR SIMULTANEOUS INTRACRANIAL AND SCALP EEG RECORDINGS

Simultaneous recordings from intracranial and scalp electrodes allow assessing the relationships among source properties, such as location, extent, and amplitude, and the resultant scalp voltage field in candidates for epilepsy surgery. Additional to the denser sampling of cortical generators provided by subdural recordings compared to a 10-20 scalp

EEG coverage, intracranial EEG shows little field spread, whereas scalp EEG visibility depends on widespread synchronized activity^{7,14}. Overall, multiscale EEG studies provide a unique opportunity to investigate the interrelations between cortical generators and their scalp correlates.

However, the spatial sampling with intracranial electrodes is nearly always far from optimal, due to the small number of measurement sites, given that brain regions are only explored when they are presumed to participate in the epileptogenic zone or to carry eloquent functions, overlapping with the planned resection area. Further limitations are evident in the use of subdural electrodes for determining the extent of a given underlying source since the sulcal area is not taken into account, with sulcal voltage fields tending to suffer voltage cancellation.

4. FINDINGS FROM PAST STUDIES OF SIMULTANEOUS INVASIVE AND SCALP EEG

Further to simulation studies, several in vivo studies have been conducted to clarify the relationship between the epileptic discharges recorded at the cortical level and their scalp correlates, especially regarding the amplitude of the original discharge and the extent of the cortical activation.

Penfield and Jasper, deriving from intraoperative electrocorticography (ECoG) recordings, were the first to propose that a critical minimum amplitude of cortical activity is necessary for epileptic discharges to be recorded by scalp EEG³⁸. They suggested a ratio of 10 to 1 between the amplitudes of cortical and scalp discharges, below which cortical discharges would likely be missed on the scalp, whereas the amplitude of the scalp potentials would increase with the amplitude of the original cortical discharge. This ratio, however, was obtained indirectly by comparing the average amplitude of the routine EEG before surgery with the amplitude of the subsequent intraoperative ECoG and was challenged by others that reported considerably lower ratios.

Simultaneous chronic scalp and invasive EEG recordings provided a more suitable setting to determine the correlations of the scalp to cortical potentials in the following years. The first combined scalp, subdural and depth recordings for clinical purposes were performed in temporal lobe epilepsy patients by Abraham and Ajmone-Marsan in 1957¹, verifying that the amplitude of cortical spikes determines their recording by scalp EEG electrodes, at least to a certain extent. The authors proposed that the extent of the activated cortical area, but not the morphology or the duration of the resulting cortical discharge, determines the presence and amplitude of its scalp EEG correlate.

Two further studies in animals^{39,40} verified the role of the scalp as a spatial averager of electrical activity, exclusively transmitting components common to and synchronous over extensive cortical areas.

In a seminal study, Tao et al⁷ analyzed the simultaneous scalp and subdural grid recordings of temporal lobe epilepsy patients, aiming to determine the extent of cortical sources that produce scalp EEG spikes. Cortical discharges with and without scalp EEG correlates were visually identified, and the extent of cortical activation was estimated from the number of electrode contacts demonstrating concurrent depolarization. The authors concluded that cortical sources of scalp EEG spikes commonly involved a synchronous activation of at least 10 cm² of gyral cortex, whereas much larger cortical source areas of 20-30 cm² corresponded to prominent scalp EEG spikes, and cortical source areas of <6 cm² never resulted in scalp EEG spikes.

The same methodology was applied two years later to ictal discharges in temporal lobe epilepsy patients, aiming to delineate the cortical substrates necessary for generating scalp EEG patterns^{41,42}. In this study, less than half of subdural EEG ictal discharges presented a scalp EEG correlate, with a mean latency of 0.4 seconds for seizures of neocortical origin and 7 seconds for seizures of mesial-temporal origin. Ictal onset was apparently missed in scalp EEG for mesial temporal cortical sources, whereas the delayed ictal pattern occurring

in scalp EEG with a latency of up to 16 seconds mirrored propagation and served rather to lateralize than to localize the cortical seizure onset. The authors concluded that sufficient extent of cortical activation of $>10 \text{ cm}^2$ as well as synchrony, gradually achieved in the course of propagation, were required for scalp-recordable EEG patterns, in line with their findings for interictal discharges.

CHAPTER 2: EXPERIMENTAL

In this chapter, experimental work will be discussed in depth and related to the issues outlined in the introduction.

2.1 THE CONTRIBUTION OF MESIAL TEMPORAL SOURCES TO EEG AND SEEG

A. INTRODUCTION

In this study, we aimed to investigate 1) the contribution in scalp EEG of epileptic sources confined to mesial temporal structures, and (2) the distinction of their scalp EEG correlates from those of mesial plus neocortical and neocortical networks. For this purpose, we analyzed simultaneous scalp and intracerebral EEG recordings with depth electrodes (SEEG: stereo-electroencephalography) in temporal lobe epilepsy patients undergoing presurgical evaluation.

As depicted in figure 5, this approach is both novel and relevant in several ways. First of all, as opposed to previous studies conducted solely with foramen ovale or subdural electrodes^{7,41-43}, we took advantage of SEEG performed with depth electrodes to simultaneously record all structures from the lateral to the medial aspect of the temporal lobe, including infolded sulcal cortex, with an excellent spatial resolution⁴⁴. A further benefit of this approach is that SEEG constitutes the only available methodology permitting to record electrophysiological activity directly within cortical sources, as reflected by a phase reversal between contiguous contacts. Finally, SEEG facilitates the distinction of the different sources constituting a given network, as indicated in the common observation of slightly delayed multiple phase reversals between co-occurring intracerebral spikes. SEEG thus allows identifying the leader source that generates the earliest and highest amplitude intracerebral spike within a given network.

This is the first simultaneous SEEG and scalp EEG study addressing the issue of mesial temporal lobe source contribution to scalp EEG signals that derives from a precise characterization of the underlying mesial, mesial plus neocortical and purely neocortical networks. This approach serves to disentangle the activity generated by solely mesial sources from the activity generated by neocortical sources using electrodes placed within the mesial temporal lobe.

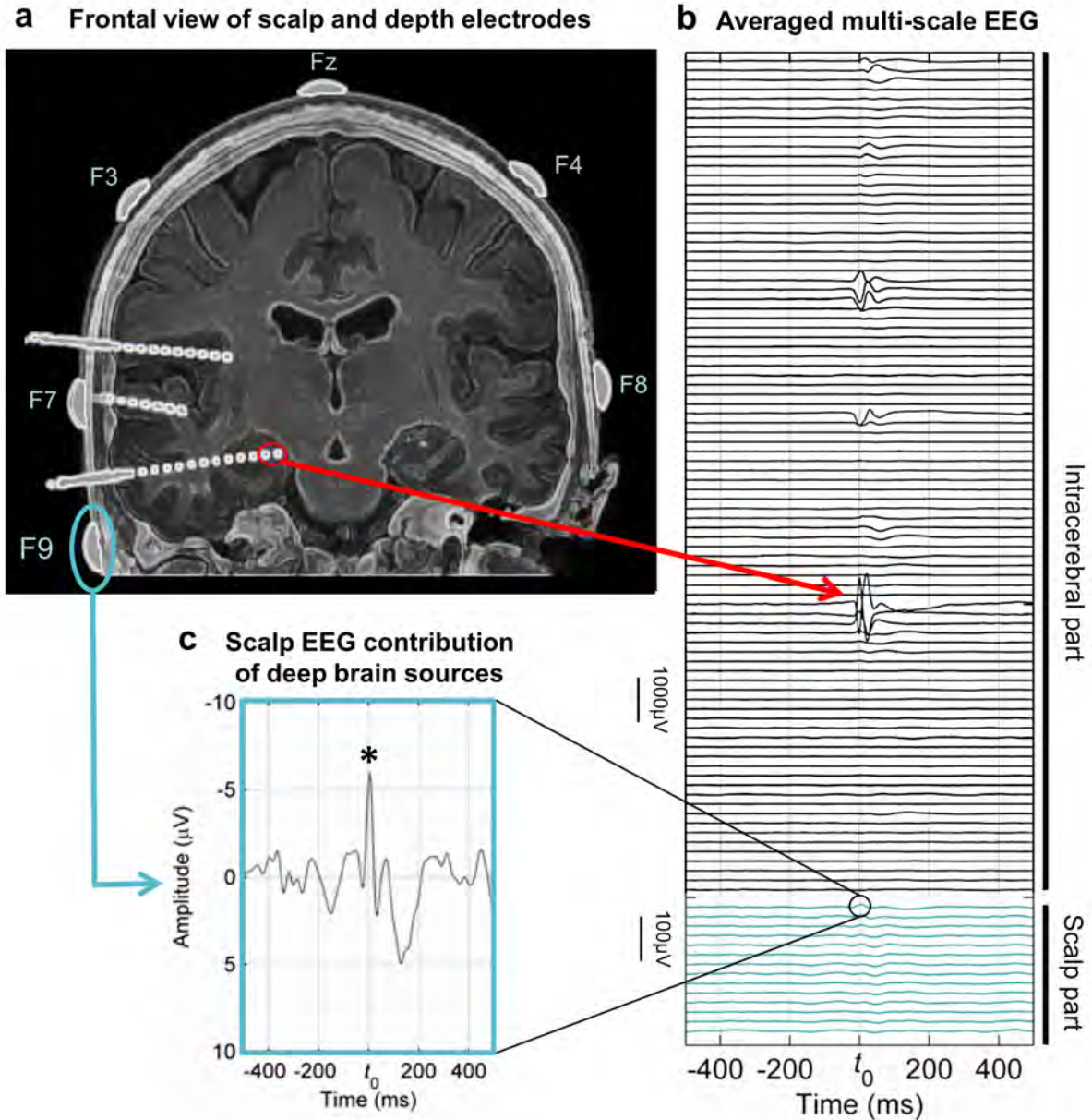


Figure 5: Contribution of multiscale EEG recordings to the detection of deep (medial) epileptic sources in an illustrative case of temporal lobe epilepsy²⁶ **(a)** Schematic illustration of a coronar MRI-CT co-registration with the six scalp (names in blue) and three intracerebral electrodes (trajectories in white) used for multiscale EEG recordings. Intracerebral electrodes presented 5 to 15 platinum multi-contacts. Scalp electrodes consisted of sterile silver-silver chloride disks. Intracerebral contacts circled in red were situated in the medial part of the temporal lobe and indicated the position of the epileptic source. **(b)** Averaged multiscale EEG signals derived from 368 epileptic events, confined to the medial part of the temporal lobe, automatically detected and marked (t_0). The maximum mean amplitude was $-826 \mu\text{V}$ and the signal to noise ratio 20.4 dB . **(c)** Magnification of the scalp signal in the averaged multiscale EEG recording. The medial epileptic source contribution to the scalp part of the multiscale EEG was recorded with maximum amplitude in the F9 scalp electrode. The star indicates that the corresponding averaged multiscale EEG signal recorded from the F9 scalp electrode at t_0 was statistically significant ($\alpha = 0.05$).

B. CATCHING THE INVISIBLE: MESIAL TEMPORAL SOURCE CONTRIBUTION TO SIMULTANEOUS EEG AND SEEG RECORDINGS

Catching the Invisible: Mesial Temporal Source Contribution to Simultaneous EEG and SEEG Recordings

Laurent Koessler · Thierry Cecchin · Sophie Colnat-Coulbois · Jean-Pierre Vignal · Jacques Jonas · Hervé Vespignani · Georgia Ramantani · Louis Georges Maillard

Received: 14 May 2014 / Accepted: 8 November 2014
© Springer Science+Business Media New York 2014

Abstract Mesial temporal sources are presumed to escape detection in scalp electroencephalographic recordings. This is attributed to the deep localization and infolded geometry of mesial temporal structures that leads to a cancellation of electrical potentials, and to the blurring effect of the superimposed neocortical background activity. In this study, we analyzed simultaneous scalp and intracerebral electroencephalographic recordings to delineate the contribution of mesial temporal sources to scalp electroencephalogram. Interictal intracerebral spike networks were classified in three distinct categories: solely mesial, mesial as well as neocortical, and solely neocortical. The highest and earliest intracerebral spikes generated

by the leader source of each network were marked and the corresponding simultaneous intracerebral and scalp electroencephalograms were averaged and then characterized both in terms of amplitude and spatial distribution. In seven drug-resistant epileptic patients, 21 interictal intracerebral networks were identified: nine mesial, five mesial plus neocortical and seven neocortical. Averaged scalp spikes arising respectively from mesial, mesial plus neocortical and neocortical networks had a 7.1 ($n = 1,949$), 36.1 ($n = 628$) and 10 ($n = 1,471$) μV average amplitude. Their scalp electroencephalogram electrical field presented a negativity in the ipsilateral anterior and basal temporal electrodes in all networks and a significant positivity in the fronto-centro-parietal electrodes solely in the mesial plus neocortical and neocortical networks. Topographic consistency test proved the consistency of these different scalp electroencephalogram maps and hierarchical clustering clearly differentiated them. In our study, we have thus shown for the first time that mesial temporal sources (1) cannot be spontaneously visible (mean signal-to-noise ratio -2.1 dB) on the scalp at the single trial level and (2) contribute to scalp electroencephalogram despite their curved geometry and deep localization.

Electronic supplementary material The online version of this article (doi:10.1007/s10548-014-0417-z) contains supplementary material, which is available to authorized users.

L. Koessler (✉) · T. Cecchin · J.-P. Vignal · J. Jonas · H. Vespignani · G. Ramantani · L. G. Maillard
UMR 7039, CRAN, CNRS - Université de Lorraine, 2 Avenue de la forêt de Haye, 54516 Vandoeuvre-Lès-Nancy, France
e-mail: laurent.koessler@univ-lorraine.fr

L. Koessler · T. Cecchin · J.-P. Vignal · J. Jonas · H. Vespignani · G. Ramantani · L. G. Maillard
UMR 7039, CRAN, CNRS, Vandoeuvre-Lès-Nancy, France

L. Koessler · J.-P. Vignal · J. Jonas · H. Vespignani · L. G. Maillard
Service de Neurologie, Centre Hospitalier Universitaire de Nancy, 54000 Nancy, France

S. Colnat-Coulbois
Service de Neurochirurgie, Centre Hospitalier Universitaire de Nancy, Nancy 54000, France

G. Ramantani
Epilepsy Center, University Hospital Freiburg, 79106 Freiburg, Germany

Keywords Simultaneous EEG–SEEG recordings · Deep brain sources · Source localization · Mesial temporal lobe epilepsy · Hippocampus · Volume conduction

Abbreviations

IIS	Interictal intracerebral spikes
ISS	Interictal scalp spikes
M	Mesial epileptic network
NC	Neocortical epileptic network
M + NC	Mesial and neocortical epileptic network
MTL	Mesial temporal lobe
SEEG	Stereoencephalography

Introduction

The contribution of electrical potentials arising from deep brain sources in scalp EEG recordings is still under debate. This issue is particularly crucial in temporal lobe epilepsy, due to the involvement of complex mesial and/or neocortical, epileptogenic networks (Maillard et al. 2004; Barba et al. 2007; Bartolomei et al. 2008). Currently, it is widely accepted that localized hippocampal interictal or ictal discharges do not correspond to concomitant visible correlates in scalp EEG (International League against Epilepsy commission's report of the electroclinical features of mesial temporal lobe (MTL) epilepsy; Wieser 2004). Thus, evidence of MTL involvement in refractory partial epilepsy is commonly indirect, deriving from seizure semiology and hippocampal sclerosis in structural- and/or hypometabolism in functional imaging (Gil-Nagel and Risinger 1997; Williamson et al. 1998; Chassoux et al. 2004). The indication for MTL resection is set when the sum of criteria is fulfilled. Otherwise, direct evidence of MTL involvement in the epileptogenic network derives solely from intracerebral recordings with depth electrodes. The identification of scalp EEG biomarkers of MTL involvement is therefore crucial for the delineation and differentiation of mesial from neocortical sources, since this may constitute a potential surrogate for invasive recordings (Harroud et al. 2012).

This issue has been previously addressed by comparative studies of simultaneous intracranial and scalp EEG recordings that facilitate the study of cortical potential contribution to scalp EEG recordings. These studies derive from invasive investigations performed mainly with foramen ovale or subdural electrodes (Baumgartner et al. 1995; Alarcon et al. 1994, 1997; Lantz et al. 1996; Merlet et al. 1998; Nayak et al. 2004; Yamazaki et al. 2012; Wennberg and Cheyne 2014) and seldom with depth electrodes (Abraham and Ajmone-Marsan 1958; Lieb et al. 1976; Alarcon et al. 1994). These studies, deriving from the routine visual analysis of concomitant scalp EEG, have supported that interictal (Alarcon et al. 1994; Merlet et al. 1998) or ictal discharges (Lieb et al. 1976) confined to MTL structures escape detection in scalp EEG recordings. This was primarily attributed to physical reasons, including (1) the specific geometric and anatomic configuration of MTL structures (Sedat and Duvernoy 1990) that produce a presumably closed electrical field (Jayakar et al. 1991; Ebersole 2000), (2) the distance between MTL structures and scalp electrodes (Lopes Da Silva and Van Rotterdam 1993), and (3) the amplitude of background activity originating from basal and lateral neocortical regions that towers over the conducted MTL signals (Mikuni et al. 1997). Further studies, deriving from the analysis of averaged scalp EEG concomitant with intracranial signals, have suggested that

temporal lobe sources are detectable in scalp EEG only if interictal or ictal discharges (1) are not solely confined to MTL structures and (2) simultaneously involve the lateral part of the temporal lobe (Alarcon et al. 1994; Lantz et al. 1996; Merlet and Gotman 1999; Wennberg and Cheyne 2014). However, the major limitation of these observations relying on foramen ovale or subdural electrodes is the inherent difficulty to disentangle the activity generated by solely mesial from the activity generated by neocortical sources with electrodes placed in the vicinity of—as opposed to within the MTL. Thus, there is an urgent need to address the question of purely MTL contribution to scalp EEG potentials deriving from intracerebral hippocampal, subhippocampal and neocortical recordings.

In this study, epileptic sources localized solely in mesial (M), in mesial as well as neocortical (M + NC) and solely in neocortical (NC) temporal regions, as defined by stereoelectroencephalography (SEEG) recordings, were investigated with simultaneous scalp and intracerebral EEG recordings to comparatively assess the contribution of MTL and neocortical sources to scalp EEG signals.

Materials and Methods

Patients

Seven patients (three female) with temporal lobe epilepsy (TLE, three right TLE) and a mean age of 38 years (Table 1) were selected from 40 consecutive patients that underwent simultaneous scalp EEG and SEEG recordings in the context of presurgical investigations for refractory partial epilepsy in 2009–2012 in the University Hospital of Nancy, France. Prior comprehensive evaluation included a detailed medical history, full neurological examination, neuropsychological assessment, high resolution MRI, interictal PET, interictal and ictal (when available) SPECT, and 64-channel long-term scalp video-EEG recordings, as well as electrical source imaging (Maillard et al. 2009; Koessler et al. 2010). We enrolled patients with (1) an epileptogenic zone confined to the temporal lobe and (2) at least one interictal intracerebral spike (IIS) source confined to the MTL, as defined by SEEG recordings. All patients gave their informed consent prior to participation. The study was granted approval by the local ethics committee.

Intracerebral and Scalp EEG Electrodes

SEEG was performed using 0.8 mm-diameter depth electrodes with 8–15 2 mm-long contacts per electrode and a 1.5 mm intercontact distance (DIXI Microtechniques, Besançon, France). For electrode placement, a Leksell G-frame (Elekta, Stockholm, Sweden) was positioned on

Table 1 Main clinical features of all seven patients (P1–P7)

Patients	Gender	Age (years)	Epileptogenic zone defined by SEEG	Laterality	MRI	Interictal EEG	Surface electrodes	Depth electrodes
P1	M	49	Mesial	R	bilateral HS	R temporal slow waves—spikes	8	9 (R) + 3 (L)
P2	F	27	Mesial, pole	R	DNT	R temporal slow waves—no spikes	25	8 (R) + 1 (L)
P3	M	32	Mesial	L	Normal	L ant. temporal spikes	14	2 (R) + 9 (L)
P4	M	51	Mesial	L	L HS	L ant. temporal slow waves—spikes	14	1 (R) + 10 (L)
P5	F	46	Mesial, pole	L	L HS	L ant. temporal spikes	14	1 (R) + 8 (L)
P6	M	29	Mesial, ant. and mid. basal part	L	L ITG atrophy	L mid. temporal slow waves—spikes	13	1 (R) + 8 (L)
P7	F	31	Mesial, pole, insula	R	R HS and pole atrophy	R mid. temporal slow waves—spikes	21	10 (R) + 2 (L)

IIS interictal intracerebral spikes, *M* mesial, *NC* neocortical, *F* female, *M* male, *y* years, *L* left, *R* right, *ant* anterior, *mid* middle, *HS* hippocampal sclerosis, *DNT* dysembryoplastic neuroepithelial tumor, *ITG* inferior temporal gyrus

the patient's head and a stereotactic MRI (3D SPGR T1-weighted sequence with double injection of gadolinium) was performed. The MRI was subsequently imported into a computer-assisted stereotactic module (Leksell Surgiplan®; Elekta, Stockholm, Sweden) and electrode trajectories were delineated according to the presurgical implantation scheme, carefully avoiding vascular structures. The presurgical implantation scheme derived from a standardized approach simultaneously sampling mesial, basal and lateral temporal lobe structures that was individually adapted according to the presumed localization of the epileptogenic and propagation zones (Koessler et al. 2010; Ramantani et al. 2013). A postoperative stereotactic CT was performed and fused with the preoperative MRI to determine the exact position of each intracerebral contact. These positions have been carefully checked by the investigators (SCC, LGM and JPV).

The following structures were sampled in all patients: amygdala; anterior and posterior hippocampus; entorhinal cortex; collateral fissure; parahippocampal gyrus; internal and external temporal pole; superior, middle and inferior temporal gyri; temporo-occipital junction; fusiform gyrus; insula.

In average, 10 ± 2 depth electrodes were placed within the temporal lobe ipsilateral to the presumed epileptogenic zone and 1.5 ± 1 depth electrodes were placed in the contralateral temporal lobe, amounting to an average of 90 intracerebral contacts in total. The scalp EEG was mounted using 16 ± 6 sterile Ag/AgCl electrodes of 10 mm diameter (Table 1). Occasionally one or two scalp electrodes were slightly displaced from the standard positions of the 10–20 system, due to the surgical scars resulting from depth electrode insertion. Scalp electrode positions were calculated by a 3D digitizer system (3 Space Fastrak;

Polhemus, Colchester, VT, USA). Two main scalp regions were sampled: the fronto-centro-parietal region and the lateral and basal temporal regions ipsi- and contralateral to the presumed epileptogenic zone (F9/F10, FT9/FT10, P9/P10, AF7/AF8, T7/T8; Koessler et al. 2009). Further electrodes were occasionally placed (F7/F8, Fp1/Fp2, P7/P8, C5, FC5, CP5, O1/O2, Oz) according to the spatial distribution of interictal spikes in 64-channel EEG recordings and the respective electroclinical hypothesis.

Simultaneous EEG and SEEG Recordings

Simultaneous EEG and SEEG recordings were performed using a 128 channel system (LTM128; Micromed, Beaune, France). The EEG and SEEG acquisition signals were referenced to the Fpz scalp electrode. Signals were sampled at 512 Hz and filtered with an analog 0.15 Hz high-pass filter. Simultaneous EEG and SEEG recordings were performed for 5 days, 20/24 h. 2–3 h of simultaneous scalp EEG and SEEG recordings during calm wakefulness were selected for interictal spike analysis, avoiding ictal events or preictal changes.

Data Collection and Analysis

Data collection and analysis were performed in four consecutive steps: (1) interictal intracerebral spike (IIS) selection and characterization, (2) IIS network classification, (3) averaged interictal scalp spike (ISS) validation and characterization and (4) averaged ISS automatic clustering (Fig. 1).

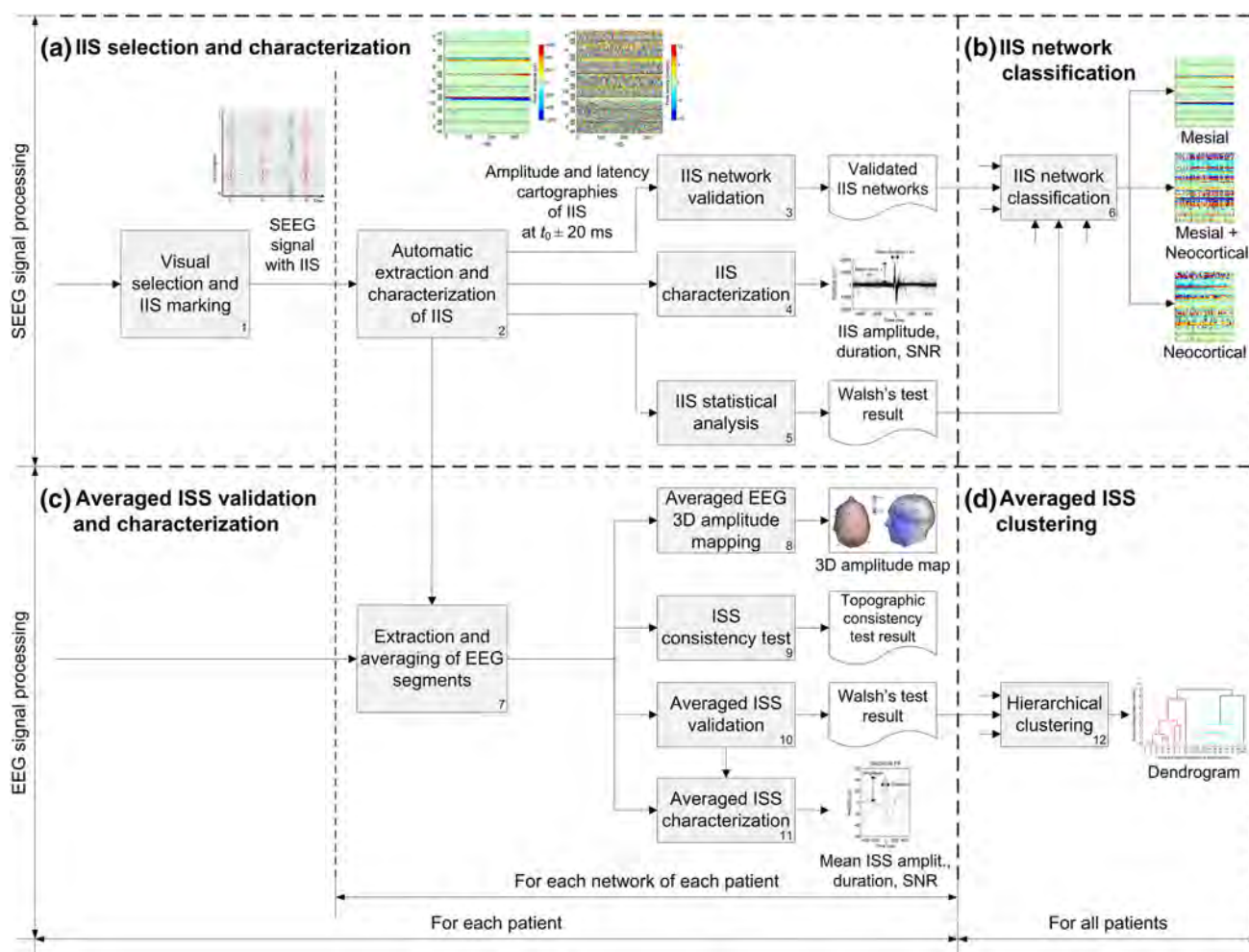


Fig. 1 Overview of data collection and analysis. *IIS* interictal intracerebral spikes, *ISS* interictal scalp spikes, *SNR* signal-to-noise ratio

Interictal Intracerebral Spike (IIS) Selection and Characterization

IIS Visual Selection and Classification

SEEG recordings were visually analyzed by three experienced neurophysiologists (LK, LGM and JPV) using a bipolar montage, that provides the potential difference between two contiguous contacts and discards events generated by far field potentials, thus exclusively depicting events from focal and adjacent sources. The IIS were identified according to the definition of the International Federation of the Society for Electroencephalography and Clinical Neurophysiology (IFSECN) as transient events, clearly distinguishable from the background activity (at least two times higher in amplitude), with a pointed peak at conventional screen display and a duration from 20 to less than 70 ms (Chang et al. 2011a). The main component of these IIS was generally negative and had variable

amplitude. For each patient, IIS networks were defined by the reproducible co-occurrence of IIS in different temporal lobe structures. These IIS networks were classified as: mesial (M) if IIS co-occurred within the MTL comprising the amygdala, hippocampus, entorhinal cortex, parahippocampal gyrus and collateral sulcus; neocortical (NC) if IIS co-occurred within any other temporal neocortical structures lateral to the collateral sulcus (fusiform, inferior, middle, and superior temporal gyri) and mesial plus neocortical (M + NC) if IIS co-occurred within both MTL and neocortical structures. This classification has been previously validated for ictal discharges on both clinical and neurophysiological grounds (Bartolomei et al. 2001; Maillard et al. 2004). Within each of these networks, the earliest IIS with the highest amplitude were manually marked with a trigger (t_0) at the peak of the initial component for subsequent averaging; the corresponding source was considered the leader source of the network.

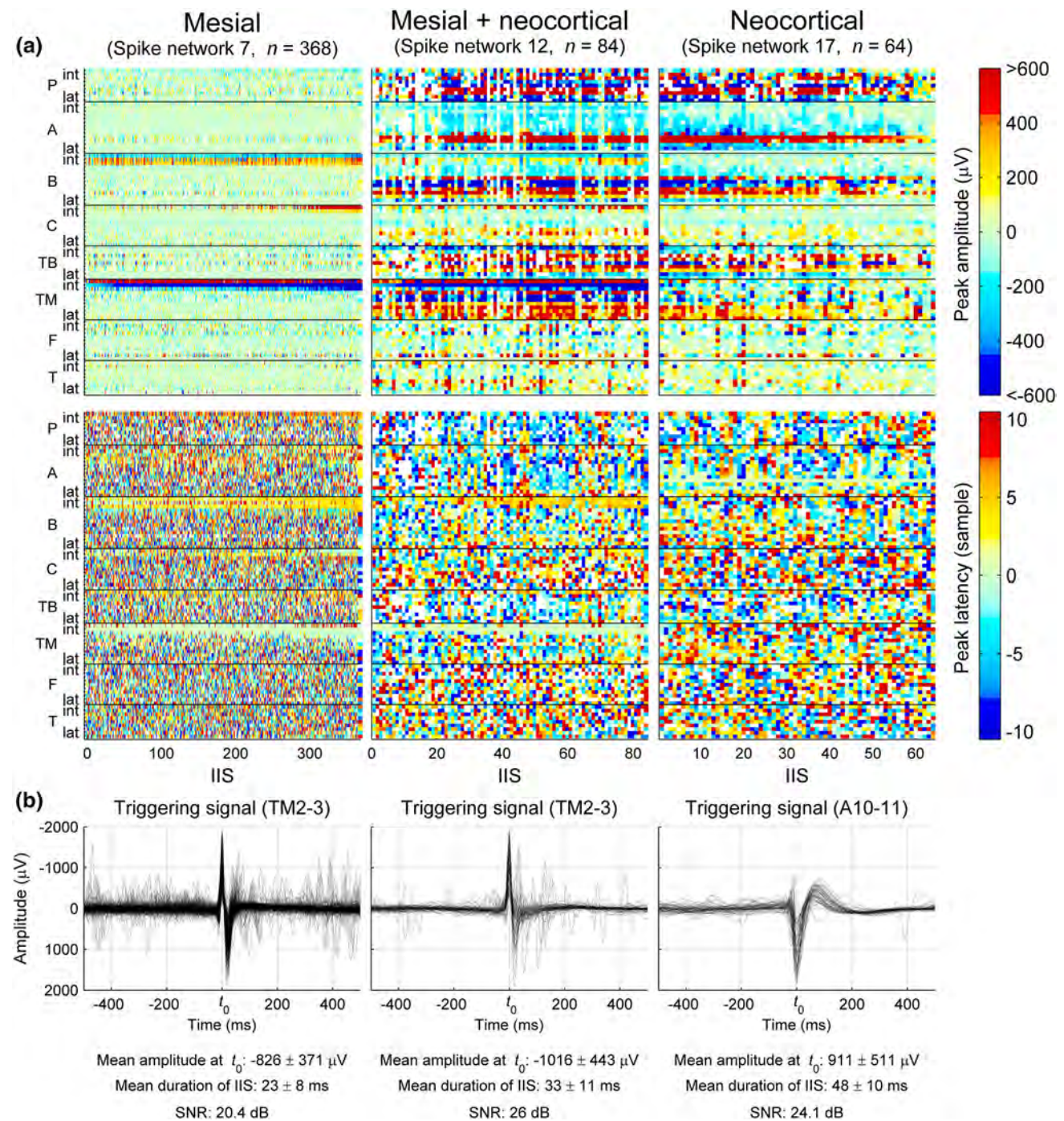


Fig. 2 SEEG characterization for the three distinct IIS networks in patient 5. **a** Spatial and temporal distributions of the three networks depicted by condensed amplitude and latency cartographies around $t_0 \pm 20$ ms. The IIS are sorted by increasing peak amplitude values: e.g. in the M network the highest spike amplitudes were observed in the

IIS Automatic Extraction, Characterization and IIS Network Validation

Condensed cartographies of IIS amplitude and latency (Fig. 2a) were obtained for each network in order to (1)

internal contacts of *TM*, *B* and *C* (located in hippocampus) with a phase reversal in *TM* and *B*. The earliest spikes were observed in the internal contacts of *TM* and followed by spikes in the internal contacts of *B* with a 5 ms delay. **b** Overlay of each segment recorded in the same contact of the highest and earliest peak and their characteristics at t_0

ascertain that the selected IIS was indeed the earliest event with the highest amplitude within the network, and to (2) verify that all individual spikes presented an identical intracerebral distribution and therefore belonged to the same network.

For this purpose, SEEG segments of 1 s centered on t_0 were automatically extracted. For each SEEG segment, local extremes corresponding to IIS were automatically detected within an interval of ± 10 samples (± 19.5 ms) around the trigger instant (t_0). The amplitude and latency of this extreme were automatically calculated. All values of amplitude and latency at t_0 were converted into a corresponding color scale (Fig. 2a). SEEG segments without a peak were coded with white.

IIS Characterization

For each IIS, we computed the amplitude, duration and signal-to-noise ratio (SNR) at t_0 in the triggering channel (Fig. 2b). SEEG signals were filtered with a 1.5 Hz high-pass filter that allowed suppressing slow baseline drifts. Spike duration was generally estimated automatically as the latency between the first detected time-axis crossing before and after t_0 . In case of baseline fluctuation that would lead to an overestimation of spike duration by this approach, we commenced the analysis from the spike peak at t_0 and searched for the extremes around the peak. For SNR computation of the whole set of IIS, we proceeded as follows. Let $x(i, t)$ be the value of the filtered triggering signal of the i th recording ($i = 1, \dots, n$) at time t , we had:

$$x(i, t_0) = s(i) + v(i, t_0)$$

where $s(i)$ represents the peak value of the spike for the i th recording and $v(i, t)$ the “noise”, that is the background activity. We assumed that $s(i)$ and $v(i, t)$ were random variables and that v had a zero mean. We defined the SNR as:

$$\text{SNR(dB)} = 10 \log_{10} \left(\frac{E[s^2]}{\sigma_v^2} \right)$$

Here $E[\cdot]$ denotes the expected value and σ_v^2 the variance of v . To estimate this variance, we first extracted the values corresponding to $[-500, -250] \cup [250, 500]$ ms for each IIS segment; we assumed that these intervals contained only noise and that the spike was contained in the interval $[-250, 250]$ ms. We further concatenated all intervals corresponding to the n IIS in a single vector representing the variance.

IIS Statistical Analysis of M Networks

For M network, in order to check that non-mesial contacts were not activated at time zero during the discharges classified as purely mesial, we performed a *quantitative* validation. Each IIS were compared to background activity, in every intracerebral contact, by a statistical test of outlier rejection under the null hypothesis that the amplitude of the peak did not significantly differ from the amplitude of the

background activity as measured in the intervals $[-500, -250]$ and $[250, 500]$ ms around t_0 . We used the Walsh nonparametric test (Walsh 1959), since preliminary tests indicated that the background activity was not normally distributed. The significance level was set at $\alpha = 0.05$. Then, we computed the percentage of significant response (positivity or negativity) in non-mesial contacts.

IIS Network Classification

Condensed cartographies with similar IIS distribution were concatenated and classified using visual expert and statistical analysis (see “IIS statistical analysis” section) into one of three distinct categories (Fig. 2a): (1) M if IIS were recorded only within mesial temporal structures (i.e. anterior and posterior hippocampus, entorhinal cortex, parahippocampal and collateral fissure); (2) NC if IIS were recorded in structures lateral to the collateral fissure (i.e. basal and lateral part of the temporal lobe); (3) M + NC if IIS were recorded simultaneously or within a maximum latency of 20 ms in both mesial and neocortical temporal structures.

Averaged Interictal Scalp Spike (ISS) Validation and Characterization

Extraction and Averaging of Scalp EEG Segments

Scalp EEG segments were extracted using the same 1 s epoch centered on t_0 as SEEG segments. Segments with scalp EEG amplitude > 150 μV that represented $< 10\%$ of all segments were rejected as artifacts. The remaining segments were band-pass filtered with cut-offs at 1.5 and 30 Hz and averaged using the same t_0 triggers as for simultaneous IIS (Fig. 3).

Visual Analysis of Averaged EEG 3D Amplitude Maps

Realistic head models (boundary element models: BEM) and 3D amplitude cartographies were used to delineate the propagation of cortical sources to the scalp. The head models were obtained from the individual MRI by a semi-automatic segmentation procedure (ASA software, Enschede, The Netherlands). The 3D positions of scalp electrodes in each patient were digitized and subsequently co-registered with the 3D head reconstruction using fiducial landmarks (nasion, left and right tragus). 3D amplitude maps served to represent the amplitude distribution of the averaged EEG segments at t_0 (Fig. 4b; supplementary figures). The amplitude values between electrodes were interpolated by 3D spline functions. In order to compare the scalp projections of all IIS networks, regardless of their lateralization, all corresponding averaged ISS were

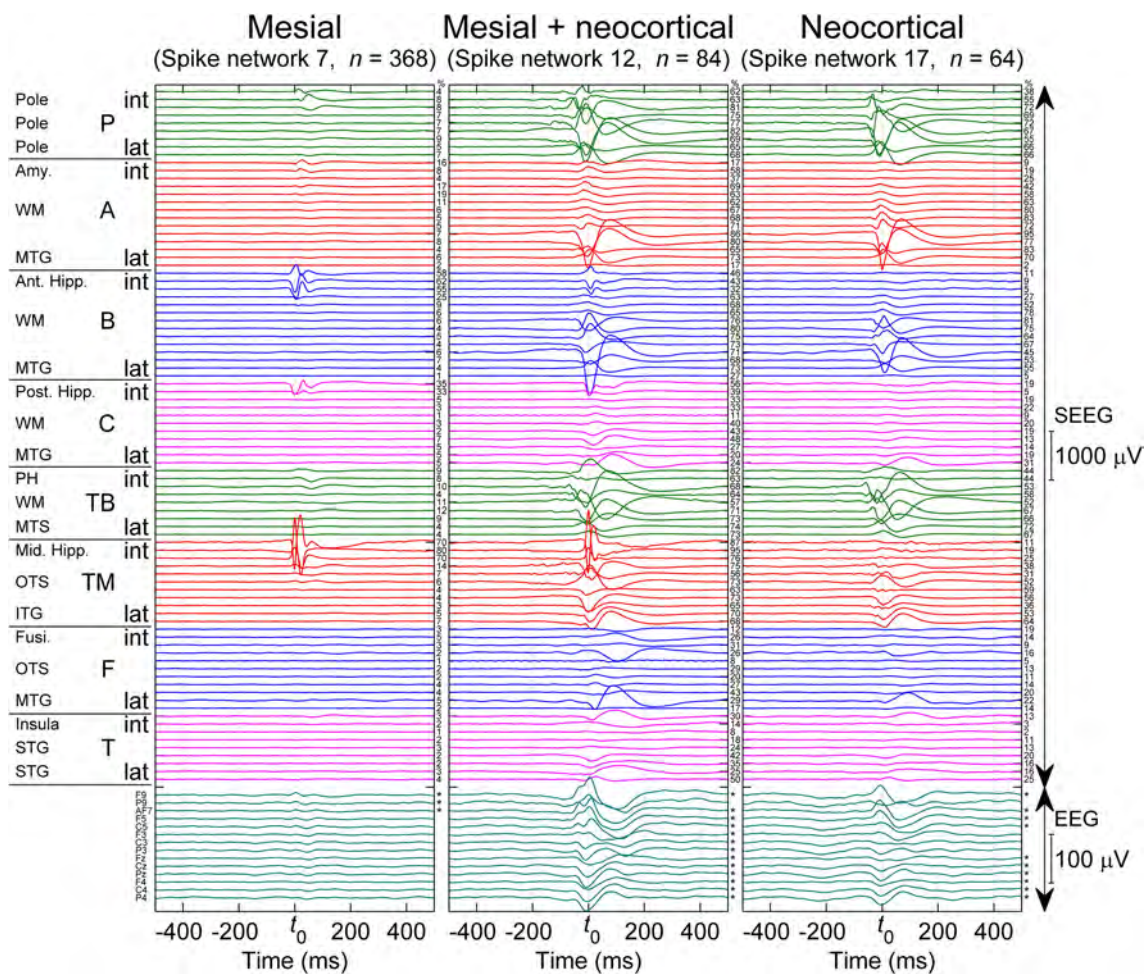


Fig. 3 Averaged simultaneous SEEG and EEG spikes corresponding to the three different spike networks in patient 5 and the percentage of significant responses (negative or positive; Walsh's test) at t_0 , compared to the background activity, for each intracerebral derivation using un-averaged signals. The stars on the right of averaged EEG signals indicate that these signals were statistically significant (Walsh's test) at t_0 . The spike networks 7, 12 and 17 were classified into: M network (anterior and mid hippocampus: B_{int} and TM_{int}); M + NC network (hippocampus: B_{int}, TM_{int}; PH: TB_{int}, temporal

pole: P_{int/lat}, anterior MTG: A_{lat}, ITG and Fusiform gyrus: B_{mid}, TB_{mid}, TM_{mid}); and NC network (temporal pole: P_{lat}; MTG: A_{lat}; ITG and fusiform gyrus: B_{mid}, TB_{mid}, TM_{mid}). Amy. Amygdala, WM white matter, MTG middle temporal gyrus, Ant. Hipp. anterior hippocampus, Post. Hipp. posterior hippocampus, PH para-hippocampal cortex, MTS middle temporal sulcus, Mid. Hipp. middle hippocampus, OTS occipito-temporal sulcus, ITG inferior temporal gyrus, Fusi. fusiform gyrus, OTS occipito-temporal sulcus, STG superior temporal gyrus; t_0 : trigger instant)

represented with the highest negativity in the left hemispheric scalp electrodes.

Statistical Analysis of Averaged EEG and Validation of ISSs

For each network, we performed a *qualitative* assessment of averaged ISS as to the morphology, amplitude and duration of the visually detected peak and the background activity. Furthermore, we also performed a *quantitative* validation of averaged ISS compared to background activity in every scalp electrode by the same statistical test used for IIS i.e. a test of outlier rejection under the null hypothesis that the averaged amplitude of the peak did not

significantly ($\alpha = 0.05$) differ from the averaged amplitude of the background activity. Combination of qualitative and quantitative assessments was used to determine if averaged EEG signals corresponded to epileptic spikes or not.

Averaged ISS Characterization

For each validated averaged ISS, we calculated the amplitude and duration in the scalp electrode with the highest negativity using the same method as for IIS (Fig. 4a; supplementary figures). For SNR determination of averaged ISS, we proceeded as follows:

Let $y(t)$ be the value of the considered averaged ISS segment at time t , we had:

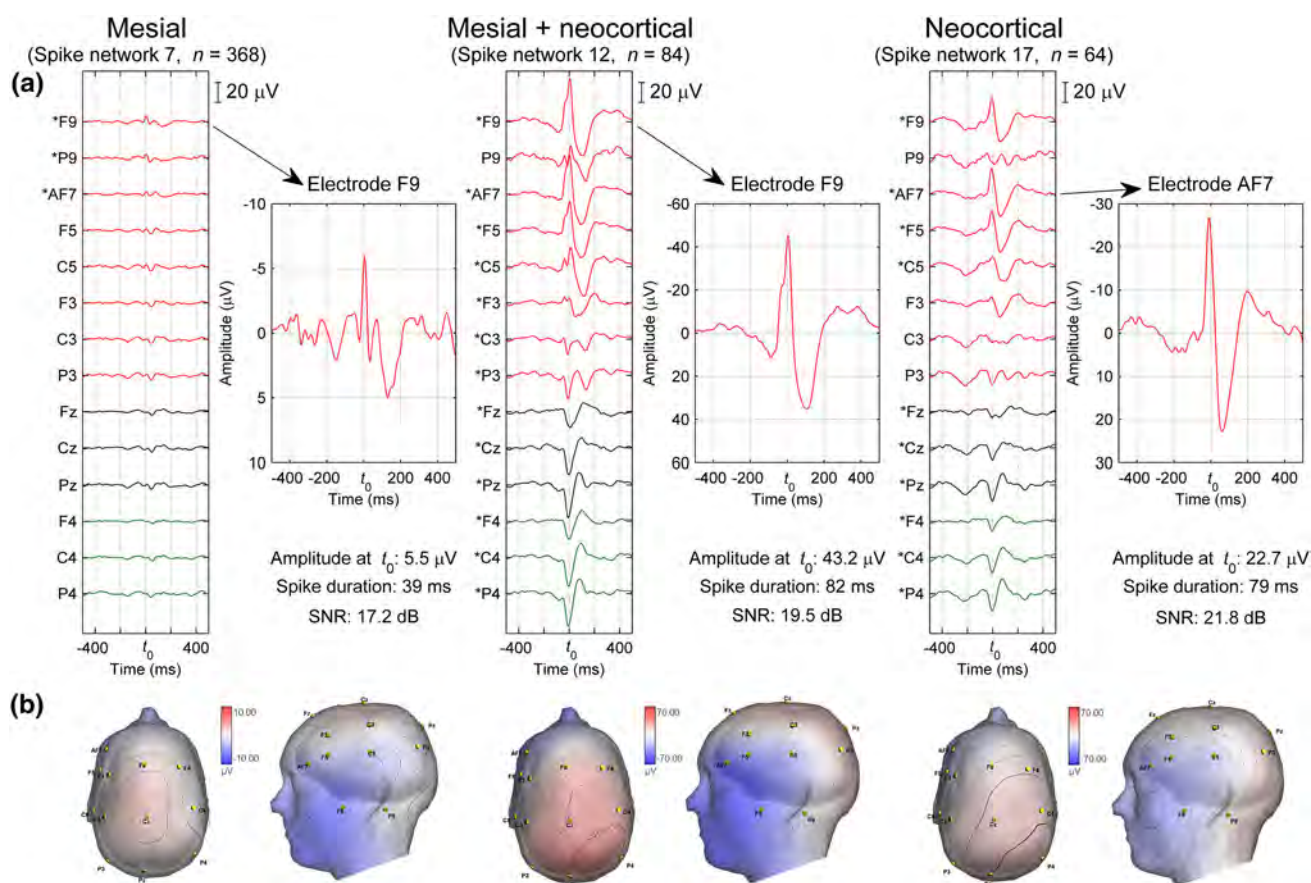


Fig. 4 a Averaged EEG signal and interictal scalp spike (ISS) characterization. The stars on the left of the electrode labels indicate that the corresponding averaged EEG signals at t_0 were statistically

significant (Walsh's test) and thus validated as ISS. **b** 3D amplitude maps for the three distinct spike networks in patient 5. Additional figures for the other patients are given in supplementary figures

$$y(t_0) = u + w(t_0)$$

where u represents the spike value at t_0 and $w(t)$ the background activity. We assumed that $w(t)$ was a random variable with a zero mean and a variance equal to σ_w^2 . Then, we defined the SNR as:

$$\text{SNR(dB)} = 10 \log_{10} \left(\frac{u^2}{\sigma_w^2} \right)$$

The estimation of σ_w^2 was made using the averaged ISS segment values corresponding to $[-500, -250] \cup [250, 500]$ ms.

In addition, the SNR of un-averaged EEG signals were computed in the same way as for the averaged EEG signals to obtain the mean SNR of each network.

Topographic Consistency Test

In order to look for ISS distribution consistency, we used the topographic consistency test (Koenig and Melie-García 2010) on all networks. We computed the Global Field Power, time-instant by time-instant, within a time window

corresponding to $[-500, 500]$ ms around t_0 with a number of observations varying between 48 and 668, a number of sensors varying between 8 and 25, depending of the considered network, and with 500 randomization runs. A false discovery rate (FDR) criterion of 5 % was applied.

Averaged ISS Clustering

We applied hierarchical clustering to verify in an automatic way (i.e. independent from expert visual analysis) the classification of averaged ISS distributions obtained by visual analysis (Van 't Ent et al. 2003). The automatic and expert classifications were expected to match if IIS networks (1) were physiologically relevant, and (2) corresponded to distinct and reproducible averaged scalp electrical fields.

To overcome the issue of inter- and intra-subject spike variability, we considered only the presence or absence of a spike on averaged EEG signals. Walsh's test results were used as an indicator of spike presence. Thus, the input data for hierarchical clustering was a matrix \mathbf{H} of r rows (the network number for all patients) and e columns (the total

number of different electrodes for all patients). In each cell of the matrix, the presence or absence of spike was coded as following: “+1” for the spike positivity; “-1” for the spike negativity; “0” for the absence of a significant spike. The partially irregular positioning of EEG electrodes resulted in missing values, especially among those contralateral to the presumed epileptogenic zone. In order to reduce the ratio of missing values, we normalized the lateralization of epileptic foci: the left side was chosen as a reference and all right-sided foci were permuted to the left. The data of patient 1 (M networks 1 and 2) were not included in the analysis due to the limited scalp electrode coverage ($n = 8$) and the missing values in the data matrix. Consequently, the matrix was built with 18 IIS networks (rows) and 11 groups of EEG electrodes (columns).

Hierarchical clustering aimed at sorting spike networks into groups so that the degree of association between two networks would be maximal if they belonged to the same group and minimal otherwise. The first step consisted in estimating the similarity or dissimilarity between every pair of rows in the data matrix, quantified as a distance variable. We selected the *city-block* distance that is especially relevant for discrete data sets. Spike networks were further grouped into a hierarchical tree, i.e. dendrogram. We chose the unweighted average distance as a linkage function: the lower the distance, the higher the similarity between two ISS distributions. The final ISS distributions were classified according to the visual analysis of the dendrogram.

Results

Interictal Intracerebral Spike (IIS) Characterization

A total of 4,048 IIS were selected in all seven patients, corresponding to 578 IIS/patient or 193 IIS/network. Twenty-one IIS networks were validated and classified into (1) nine M networks encompassing 1,949 IIS, (2) five M + NC networks with 628 IIS, and (3) seven NC networks with 1,471 IIS (Table 2). All nine M networks comprised sources localized in the anterior hippocampus, six included sources localized in the middle and/or posterior hippocampus, seven in the amygdala, and five in the para-hippocampal gyrus. Interestingly, mesial temporal epileptic sources were not fully synchronous, presenting a 2–10 ms latency between the maximum amplitudes of co-occurring mesial temporal spikes (Fig. 2). In non-mesial contacts, only 6.7 % had amplitudes at t_0 that significantly differ from the amplitude of the background activity using Walsh’s test. Mean amplitude in non-mesial contacts was about 7.4 μV . These significant responses were visually inspected by three experienced neurophysiologists (LK,

LGM and JPV) and none of them were considered as epileptic spikes (Patient 5, Fig. 3).

NC networks comprised five sources localized in the temporal pole, three sources localized in the middle temporal gyrus, nine basal temporal sources, including eight in the fusiform and one in the inferior temporal gyrus, and one in the superior temporal gyrus. All five M + NC networks comprised sources localized in the anterior hippocampus, the temporo-polar and basal temporal regions, three included sources localized in the para-hippocampal regions, and three additional MTL sources.

Across all 21 networks, IIS serving as triggers presented a mean amplitude at t_0 of $895 \pm 310 \mu\text{V}$ and a duration of 44 ± 10 ms. Their mean SNR was 18.2 dB, ranging from 11.6 to 26 dB. For each type of network, IIS amplitude and duration were: M $729 \pm 279 \mu\text{V}$ and 38 ± 11 ms; M + NC $1,236 \pm 414 \mu\text{V}$ and 43 ± 10 ms; NC $969 \pm 306 \mu\text{V}$ and 54 ± 9 ms (Figs. 2, 3, patient 5).

Visual Analysis of Averaged EEG 3D Amplitude Maps

The visual analysis of the averaged ISS 3D amplitude maps revealed two distinct patterns.

The first pattern was characterized by a low amplitude negativity in the ipsilateral anterior basal temporal electrodes (F9–FT9 or F10–FT10) and a low amplitude positivity in the midline electrodes (Cz). Amplitude interpolation localized the maximum negativity in a more anterior and inferior position corresponding to the cheekbone. This pattern was specific for M networks (Fig. 4b; supplementary figures).

The second pattern was characterized by a higher amplitude with a more widespread negativity in the left temporal electrodes. The highest negativity was recorded in the ipsilateral anterior basal temporal electrodes (F9–FT9 or F10–FT10). This pattern was additionally characterized by a widespread positivity in the vertex with a contralateral fronto-centro-parietal predominance (F4, C4, P4). This pattern corresponded to the M + NC and to the NC networks (Fig. 4b; supplementary figures).

Only a single amplitude map, corresponding to a NC network ($n = 21$), was discordant with the typical pattern of its category. This 3D amplitude map comprised a focal negativity in the fronto-central midline (Fz and Cz) electrodes and two positivities in the ipsilateral anterior basal and parietal electrodes (F9 and P3). The corresponding intracerebral source was localized in the superior bank of the left superior temporal gyrus.

Consistency Validation of Amplitude Maps

Averaged ISS distributions consistency was evaluated using topographic consistency test. When an FDR criterion of 5 % was applied to control for multiple testing, the

Table 2 Anatomical distribution of IIS for each spike network

Patients	IIS networks	Types	Numbers of IIS	Temporal pole			Amy-MTG			Ant. Hipp-ant. MTG			Post. Hipp-post. MTG			Parahipp.-basal T			Mid. hipp.-basal T			Insula-STG		
				int	mid	lat	int	mid	lat	int	mid	lat	int	mid	lat	int	mid	lat	int	mid	lat	int	mid	lat
P1	1	M	272				×																	
P1	2	M	149				×																	
P2	3	M	440				×																	
P3	4	M	171				×																	
P3	5	M	94				×																	
P4	6	M	159				×																	
P5	7	M	368				×																	
P6	8	M	248				×																	
P7	9	M	48				×																	
P2	10	M + NC	117				×																	
P3	11	M + NC	166				×																	
P5	12	M + NC	84				×																	
P6	13	M + NC	213				×																	
P7	14	M + NC	48				×																	
P1	15	NC	130				×																	
P4	16	NC	668				×																	
P5	17	NC	64				×																	
P6	18	NC	122				×																	
P6	19	NC	202				×																	
P7	20	NC	112				×																	
P7	21	NC	173				×																	

“×” indicates the presence of epileptic spikes with $SNR \geq 2$ and **bold circles** indicate for the spikes serving as triggers for averaging. *Amy* amygdala, *Hipp* hippocampus, *ITG* inferior temporal gyrus, *MTG* middle temporal gyrus, *STG* superior temporal gyrus, *Parahipp* para-hippocampal, *M* mesial, *NC* neocortical, *M + NC* mesial plus neocortical, *int* internal, *mid* middle, *lat* lateral, *T* temporal, Basal temporal corresponded to fusiform gyrus or inferior temporal gyrus

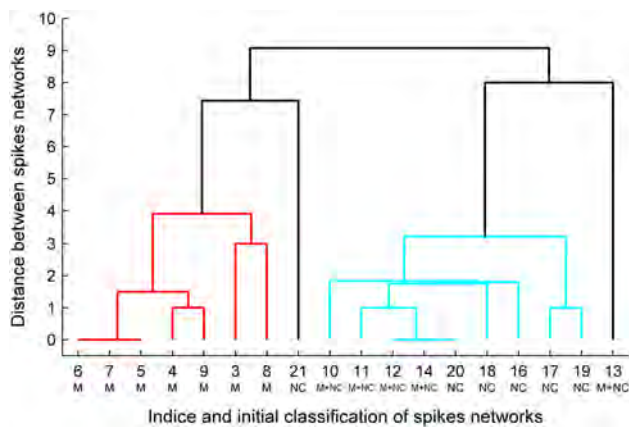


Fig. 5 Topographic consistency test (TCT), applied time-instant by time-instant to the EEG recordings, for the three different spike networks in patient 5. In the upper graphs, the dark line shows the global field power (GFP) computed for all EEG signals ($n = 14$) and for all observations ($n = 368, 84, 64$), the grey lines show the GFP of randomly shuffled EEG signals obtained with 500 randomization runs. In the lower graphs, the dark line shows the obtained p value, the dotted line shows the threshold of a false discovery rate (FDR) of 5%. Around t_0 , the GFP of real data is increasing and the p value is under the threshold indicating the presence of a consistent topography (Color figure online)

threshold of p varied between 0.010 and 0.044 (Table 4). At t_0 , topographic consistency tests were always successful and global field powers always higher than these of randomly ($n = 500$) shuffled EEG signals (Fig. 5).

Statistical Analysis of Averaged EEG and Validation of ISS

Most importantly, scalp spikes were recorded in every M network, with a significant negativity in the anterior basal temporal electrode (F9-FT9) that was, however, not specific to M networks (Table 3; Figs. 3, 4). Spikes with a significant negativity in the anterior and basal temporal electrodes were recorded in 20 networks: 90% in F9-FT9, 82% in AF7, 80% in T7 and 67% in F7. These rates did not significantly differ between the M, M + NC and NC networks. In contrast, a significant concomitant positivity was recorded in the vertex region (Fz, Pz, F3, F4, P4, P3) only in the M + NC and NC networks (Figs. 3, 4). The electrical field of this positivity involved the electrodes F4, C4 or P4 in 50–61% of cases, Fz, Cz and/or Pz in 38–48% of cases and C3 or P3 in 38–44% of cases. Only a single NC network (n21) was discordant with this 3D amplitude map as described in the previous paragraph (Table 3).

Averaged ISS Characteristics

Overall, ISS had an average amplitude of 15 μV in absolute value, a duration of 81 ms and a SNR of 18.0 dB

(Table 4). ISS generated by M networks had an average amplitude of 7.1 μV , a duration of 78 ms, and a SNR of 16.1 dB. In contrast, ISS generated by M + NC networks had an average amplitude of 36.1 μV , a duration of 78 ms, and a SNR of 22 dB. Finally, ISS generated by NC networks had an average amplitude of 10 μV , a duration of 87 ms and a SNR of 17.7 dB.

Mean SNR of un-averaged EEG signals varied from -4.9 to 14.4 dB (mean 2.0 dB). ISS generated by M networks had a mean SNR of -2.1 dB, M + NC networks of 8.7 dB and NC networks of 2.4 dB (Table 4). For a network, a negative value of mean SNR indicates that un-averaged amplitudes at t_0 did not differ from the background activity.

Averaged ISS Clusters: Automatic Classification of Amplitude Maps

Two main clusters were obtained from the automatic classification and analysis of the resulting dendrogram (Table 3; Fig. 6). The first cluster included all seven averaged ISS of the M networks and the second cluster included 9 of 11 averaged ISS of the M + NC and NC networks. Two outliers were observed: M + NC network 13 that was characterized by a more widespread positivity involving ipsilateral fronto-central electrodes, and network 21 that was characterized by a fronto-central midline negativity.

Discussion

In this study, we aimed to address the issues of (1) the contribution in scalp EEG of epileptic sources confined to mesial temporal structures, and (2) the distinction of their scalp EEG correlates from those of mesial plus neocortical and neocortical networks.

IIS Networks in Temporal Lobe Epilepsy Comprise Spatially Distributed Sources

In our study, based on SEEG recordings, we first characterized the intracerebral interictal networks that contributed to concomitant scalp EEG signals. A previous study with a similar objective primarily relied on intracranial (foramen ovale) as opposed to intracerebral recordings, without additional subdural electrodes, to characterize medial temporal lobe sources (Merlet et al. 1998). Foramen ovale electrodes, however, placed between the brainstem and the medial temporal lobe, capture the electrophysiological activity generated by both medial and basal temporal generators, thus precluding a differentiation of their respective contribution (Wieser et al. 1985; Eisenschenk

Table 3 Data matrix used for hierarchical clustering and threshold of p for topographic consistency test

Patients	IIS network	Types	Ipsilateral electrodes					Midline electrodes			Contralateral electrodes			FDR criterion: threshold of p	
			F9–FT9	AF7–F7	–FP1	F3–F5	C3	P3	Fz	Cz	Pz	P4	C4		F4
P2	3	M	–1	–1	–1	–1	–1	0	0	0	0	0	0	0	0.030
P3	4	M	–1	–1	0	0	0	0	0	0	0	0	0	1	0.020
P3	5	M	–1	–1	0	0	0	0	0	0	0	0	0	0	0.016
P4	6	M	–1	–1	0	0	0	0	0	0	0	0	0	0	0.034
P5	7	M	–1	–1	0	0	0	0	0	0	0	0	0	0	0.010
P6	8	M	–1	–1	0	–1	–1	0	0	–1	–1	0	0	0	0.024
P7	9	M	–1	–1	–1	0	0	0	0	0	0	0	0	1	0.022
P2	10	M + NC	–1	–1	0	1	0	1	1	1	1	1	1	1	0.036
P3	11	M + NC	–1	–1	0	1	1	1	1	1	1	1	1	1	0.038
P5	12	M + NC	–1	–1	–1	1	1	1	1	1	1	1	1	1	0.036
P6	13	M + NC	–1	1	1	1	1	0	0	1	1	0	0	0	0.034
P7	14	M + NC	–1	–1	–1	1	1	1	1	1	1	1	1	1	0.028
P4	16	NC	–1	–1	1	1	1	1	1	1	1	1	1	1	0.038
P5	17	NC	–1	–1	–1	0	0	1	1	1	1	1	1	1	0.036
P6	18	NC	0	–1	0	1	1	1	1	1	1	1	1	1	0.010
P6	19	NC	–1	–1	–1	0	0	0	1	1	1	1	1	1	0.044
P7	20	NC	–1	–1	–1	1	1	1	1	1	1	1	1	1	0.026
P7	21	NC	1	0	0	0	1	–1	–1	0	0	0	0	0	0.026

–1 and 1 were indicated respectively the presence at t_0 of negativity or positivity of ISS in the averaged EEG signals using Walsh's statistical test. Zero indicated that no spike was statistically detected at t_0 . Thresholds of p were obtained for topographic consistency test with a FDR of 5 % and with 500 randomization runs. *M* mesial, *M + NC* mesial plus neocortical, *NC* neocortical, *SNR* signal to noise ratio, *IIS* interictal intracerebral network, *FDR* false discovery rate

et al. 2001). Moreover, foramen ovale electrodes may miss the contribution of more lateral temporal generators to the concomitant scalp EEG spike. In contrast, SEEG provides a most appropriate methodology in investigating the spatial distribution of epileptic temporal lobe sources since: (1) SEEG allows for the simultaneous recording of all structures from the lateral to mesial aspect of the temporal lobe, including infolded sulcal cortex, with a good spatial resolution (Kahane et al. 2006); (2) SEEG constitutes the only available methodology permitting to record electrophysiological activity directly within cortical sources, as reflected by a phase reversal between contiguous contacts (Jonas et al. 2012) (Fig. 2); (3) SEEG facilitates the distinction of the different sources constituting a given network, as reflected in the common observation of slightly delayed multiple phase reversals between co-occurring intracerebral spikes. SEEG further allows to identify the leader source, generating the earliest and highest amplitude intracerebral spike, within a given network. Thus, in medial temporal networks, the leader source localized either in the anterior hippocampus, the para-hippocampal gyrus, the middle or the posterior hippocampus. These structures have been previously shown to be involved in medial temporal epileptic networks to a different extent (Spencer and Spencer 1994; Bragin et al. 2000; Bartolomei et al. 2008;

Bettus et al. 2008). The appreciation of these properties was crucial to correctly identify the leading structure serving as a trigger for each network and thus avoid attributing an intracerebral spike generated by the co-activation of both mesial and neocortical sources solely to a mesial source. Purity of M networks was demonstrated in this study using statistical test and expert analysis that confirmed that non-mesial contacts were not co-activated at t_0 : in average less than 7 % of significant responses in non-mesial contacts with a mean amplitude of 7.4 μ V.

IIS networks were categorized into one of three predefined categories: mesial, mesial plus neocortical and neocortical. The clinical and neurophysiological relevance of this epileptic network classification in TLE has been previously established (Maillard et al. 2004; Bartolomei et al. 2008). This is the first simultaneous SEEG and EEG study addressing the issue of mesial temporal lobe source contribution to scalp EEG that derives from a precise characterization of the underlying M, M + NC and NC networks.

Mesial Sources Significantly Contribute to Scalp EEG

The contribution of mesial temporal sources to scalp EEG has been under debate ever since the advent of EEG and SEEG recordings (Abraham and Ajmone-Marsan 1958),

Table 4 Averaged ISS characteristics

Patients	IIS networks	Types	Electrodes	Amplitude (μV)	SNR of averaged signals (dB)	Duration (ms)	Nb. spikes	Mean SNR of un-averaged signals (dB)
P1	1	M	FT9	-2.2	9.7	96	272	-4.8
P1	2	M	FT9	-4.2	9.1	108	149	-2.9
P2	3	M	T7	-8.6	21.6	78	440	-0.7
P3	4	M	FT9	-17.8	22.8	93	171	0.5
P3	5	M	FT9	-11.0	15.2	93	94	-1.0
P4	6	M	FT9	-3.8	13.1	63	159	-4.9
P5	7	M	F9	-5.5	17.2	39	368	-3.5
P6	8	M	P9	-7.0	19.4	45	248	-2.2
P7	9	M	FT9	-3.7	16.6	87	48	0.8
P2	10	M + NC	FT9	-15.6	8.1	95	117	-0.1
P3	11	M + NC	FT9	-64.2	24.1	84	166	13.5
P5	12	M + NC	F9	-43.2	19.5	82	84	6.4
P6	13	M + NC	FT9	-25.6	30.4	63	213	9.1
P7	14	M + NC	FT9	-31.9	27.7	66	48	14.4
P1	15	NC	AF7	-4.8	13.7	103	130	-0.7
P4	16	NC	FT9	-11.1	14.0	95	668	-0.4
P5	17	NC	AF7	-22.7	21.8	79	64	4.7
P6	18	NC	F7	-3.8	17.4	102	122	0.5
P6	19	NC	F7	-11.9	19.8	105	202	7.4
P7	20	NC	FT9	-14.0	25.6	70	112	7.9
P7	21	NC	FZ	-1.5	11.6	55	173	-2.7
			Mean	-15.0	18.0	81	193	2.0

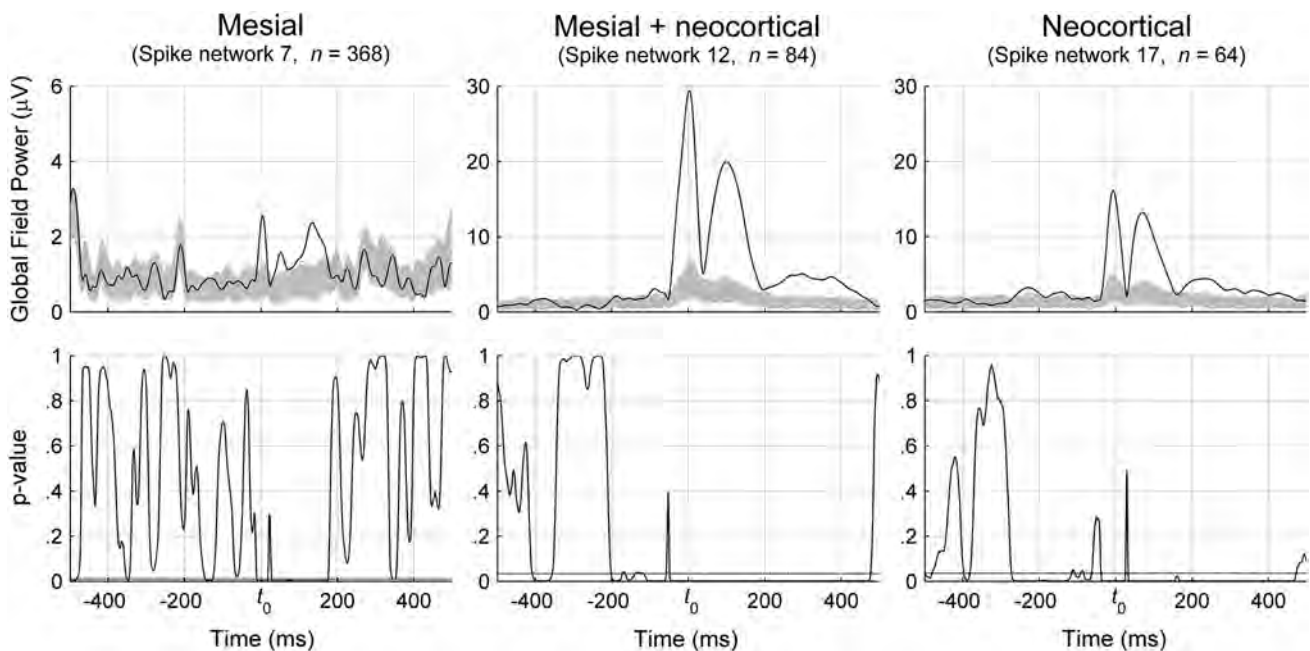


Fig. 6 Hierarchical clustering dendrogram of averaged ISS. All M ISS networks were classified in a same cluster whereas M + NC and NC ISS networks were classified together in another cluster. Two

outliers were observed in network 13, patient 6, (M + NC network) and in network 21, patient 7 (NC network)

yet remaining unresolved. This might be attributed to: (1) the technical challenge in simultaneously recording SEEG and scalp EEG; (2) the neurophysiological challenge in precisely disentangling the contribution of mesial from neocortical sources to scalp EEG signals.

In our study, we demonstrated that all nine M networks significantly contributed to scalp EEG. The corresponding scalp EEG spikes of M networks always presented a significant negativity recorded in the ipsilateral anterior basal temporal electrodes with an average amplitude of 7.1 μV , but no significant positivity. This contribution demonstrates that mesial temporal structures do not generate closed electrical fields despite the folding of the hippocampus and the opposite orientation of the subiculum and parahippocampal gyrus (Jayakar et al. 1991). It further supports that volume conduction also applies to electrical activity generated by deep cortical sources, distant from scalp EEG electrodes.

Regarding closed electrical fields within M networks, it should be noted that epileptic sources were never fully synchronous, as reflected by the 2–10 ms latency between the maximum amplitude of co-occurring mesial temporal spikes. This asynchronous mesial activation may also have contributed to prevent electrical cancellation. This lack of electrical field cancellation in M networks was observed regardless of an additional parahippocampal activation. This parahippocampal co-activation is often overlooked by routine visual interpretation of bipolar SEEG recordings, but has clearly emerged in the condensed amplitude and latency cartographies characterizing the IIS networks. Finally, within M networks, the amplitude of epileptic spikes recorded in the different co-activated structures presented with a great variability (Figs. 2, 3). Therefore, even in cases of synchronous sources localized in geometrically symmetrical structures, such as the opposite banks of a sulcus, the amplitude difference of the resulting electrical fields prevents cancellation.

The average amplitude of ISS generated by M networks, amounting to 7.1 μV , is below the amplitude range of common un-averaged scalp background EEG activity that reportedly ranges from 10 to 50 μV (Chang et al. 2011b). Mean SNR of un-averaged EEG signals of purely M networks (–2.1 dB; max 0.8 dB) also contribute to explain the poor observability of these networks in routine visual interpretation (Gavaret et al. 2004).

Our study is the first in vivo demonstration of sources confined to mesial temporal structures contributing to scalp EEG despite their lack of visibility in routine interpretation. In contrast, spikes generated by M + NC networks had a higher average amplitude of 36.1 μV that is consistent with their superior observability in routine visual interpretation of scalp EEG. The co-activation of mesial and neocortical sources in M + NC networks (e.g. anterior hippocampus, temporal pole, basal temporal area) could

render mesial sources detectable in routine visual interpretation. The slightly asynchronous activation of these mesial and neocortical sources facilitates their distinction and delineation by source localization derived from high-resolution EEG (Baumgartner et al. 1995). In our study, we refrained from applying source localization methods on the resulting scalp EEG spikes, due of the limited number of scalp electrodes applied simultaneous to SEEG (Lantz et al. 2003). However, our results suggest that the mesial component of widespread M + NC networks could be accessible to source localization.

MTL Sources Generate Scalp Amplitude Maps Distinct from Those Generated By Neocortical Sources

The negativity of averaged scalp spikes was recorded with the highest amplitude in ipsilateral anterior basal temporal electrodes in 90 % of cases, regardless of the underlying intracerebral temporal network. Therefore, the observation of a scalp EEG negativity in this region cannot be appreciated as a specific marker differentiating mesial from neocortical temporal sources. However, it emphasizes the utility of additional basal-temporal electrodes beyond the commonly applied 10–20 mounting system (Homan et al. 1988) in characterizing interictal networks within the temporal lobe. The more widespread temporal negativity and the midline fronto-parietal positivity of scalp spikes generated by NC and M + NC networks apparently reflected the activation of basal and lateral neocortical areas. At t_0 , the topographic consistency test, with a false discovery rate criterion of 5 %, was always successful for every network. Visual inspection of averaged EEG maps was confirmed by this effective method which determines the presence of averaged event-related field using randomization tests (Grouiller et al. 2011).

The hierarchical clustering method allowed to differentiate the scalp electrical fields generated by M networks from those generated by NC and M + NC networks, independent from expert visual evaluation.

The main characteristic of NC and M + NC networks concerned the presence of a significant fronto-centro-parietal positivity. This emphasizes the importance of considering the entire electrical field in a given scalp recording in order to infer the source localization corresponding to an observable spike. This vertex positivity is consistent with the previously reported electrical field in scalp EEG that results from cortical spikes arising from mesial temporal lobe structures as well as adjacent basal and lateral cortical areas (Ebersole and Wade 1991). However, our study further shows that exclusively mesial temporal networks contribute to scalp EEG and generate a distinct electrical field without a significant vertex positivity that clearly differs from networks involving both mesial and basal neocortical areas.

These results can also contribute to the appreciation and delineation of the respective contribution of mesial and basal temporal sources to cognitive scalp potentials evoked by visual categorization and recognition (Maillard et al. 2011). The vertex positivity of M + NC and NC spikes is consistent with the so-called « vertex positive component » of the N170 generated in the ventral temporal areas. On the other hand, the lack of vertex positivity of M spikes renders improbable the contribution of MTL generators to the so-called parietal P600 associated with visual recognition memory (Maillard et al. 2011).

Finally, the demarcation of mesial temporal source contribution to scalp EEG supports the notion that specific biomarkers of these mesial sources could be characterized and detected in the future with signal processing methods without requiring simultaneous invasive recordings and subsequent averaging. These detection methods would rely on the characterization of a mesial interictal scalp spike spatio-temporal template, derived from the current and further simultaneous SEEG and scalp EEG studies.

Conclusion

Mesial temporal sources contribute to scalp EEG despite their deep localization, their curved spatial configuration, and the blurring resulting from the superimposed neocortical activity. Although their contribution is weak, it is detectable by extraction from the respective background activity. Scalp EEG correlates of mesial temporal sources were only detectable in our study with a negativity in the ipsilateral anterior basal temporal electrodes, whereas mesial plus/or neocortical sources were associated with an additional fronto-centro-parietal positivity. This difference was clearly corroborated by the hierarchical clustering method. Our findings prompt further research towards the identification of scalp EEG biomarkers of mesial temporal sources in order to potentially avoid intracerebral recordings in the presurgical evaluation of refractory epilepsy and to serve as a framework for further neurological and cognitive neuroscience applications.

Acknowledgments The Authors would like to thank Cécile Popko (Université de Lorraine) for EEG-SEEG data management. This study was supported by the French Ministry of Health (PHRC 17-05, 2009) and the Regional Council of Lorraine.

References

- Abraham K, Ajmone-Marsan CA (1958) Patterns of cortical discharges and their relation to routine scalp electroencephalography. *Electroencephalogr Clin Neurophysiol* 10:447–461
- Alarcon G, Guy CN, Binnie CD, Walker SR, Elwes RD, Polkey CE (1994) Intracerebral propagation of interictal activity in partial activity: implications for source localisation. *J Neurol Neurosurg Psychiatry* 57:435–449
- Alarcon G, Garcia Seoane JJ, Binnie CD, Martin Miguel MC, Juler J, Polkey CE et al (1997) Origin and propagation of interictal discharges in the acute electrocorticogram. Implications for pathophysiology and surgical treatment of temporal lobe epilepsy. *Brain* 120:2259–2282
- Barba C, Barbati G, Minotti L, Hoffmann D, Kahane P (2007) Ictal clinical and scalp-EEG findings differentiating temporal lobe epilepsies from temporal ‘plus’ epilepsies. *Brain* 130:1957–1967
- Bartolomei F, Wendling F, Bellanger JJ, Régis J, Chauvel P (2001) Neural networks involving the medial temporal structures in temporal lobe epilepsy. *Clin Neurophysiol* 112:1746–1760
- Bartolomei F, Chauvel P, Wendling F (2008) Epileptogenicity of brain structures in human temporal lobe epilepsy: a quantified study from intracerebral EEG. *Brain* 131:1818–1830
- Baumgartner C, Lindinger G, Ebner A, Aull S, Serles W, Olbrich A et al (1995) Propagation of interictal epileptic activity in temporal lobe epilepsy. *Neurology* 45:118–122
- Bettus G, Wendling F, Guye M, Valton L, Régis J, Chauvel P, Bartolomei F (2008) Enhanced EEG functional connectivity in mesial temporal lobe epilepsy. *Epilepsy Res* 81:58–68
- Bragin A, Wilson CL, Engel J Jr (2000) Chronic epileptogenesis requires development of a network of pathologically interconnected neuron clusters: a hypothesis. *Epilepsia* 41(Suppl 6):S144–S152
- Chang BS, Schomer D, Niedermeyer E (2011a) Epilepsy in adults and the elderly. In: Schomer D, Lopes da Silva F (eds) *Niedermeyer’s electroencephalography: basic principles, clinical applications, and related fields*, MD: Wolters-Kluwer Lippincott Williams Wilkins, Baltimore, p 541–562
- Chang BS, Schomer D, Niedermeyer E (2011b) Normal EEG and sleep: adults and elderly. In: Schomer D, Lopes da Silva F (eds) *Niedermeyer’s electroencephalography: basic principles, clinical applications, and related fields*. MD: Wolters-Kluwer Lippincott Williams & Wilkins, Baltimore, p 183–214
- Chassoux F, Semah F, Bouillieret V, Landre E, Devaux B, Turak B et al (2004) Metabolic changes and electro-clinical patterns in mesio-temporal lobe epilepsy: a correlative study. *Brain* 127:164–174
- Ebersole JS (2000) Sublobar localization of temporal neocortical epileptogenic foci by source modeling. *Adv Neurol* 84:353–363
- Ebersole JS, Wade PB (1991) Spike voltage topography identifies two types of fronto-temporal epileptic foci. *Neurology* 41:1425–1431
- Eisenschenk S, Gilmore RL, Cibula JE, Roper SN (2001) Lateralization of temporal lobe foci: depth versus subdural electrodes. *Clin Neurophysiol* 112:836–844
- Gavaret M, Badier JM, Marquis P, Bartolomei F, Chauvel P (2004) Electric source imaging in temporal lobe epilepsy. *J Clin Neurophysiol* 21:267–282
- Gil-Nagel A, Risinger MW (1997) Ictal semiology in hippocampal versus extra hippocampal temporal lobe epilepsy. *Brain* 120:183–192
- Grouiller F, Thornton RC, Groening K, Spinelli L, Duncan JS, Schaller K et al (2011) With or without spikes: localization of focal epileptic activity by simultaneous electroencephalography and functional magnetic resonance imaging. *Brain* 134:2867–2886
- Harroud A, Bouthillier A, Weil AG, Nguyen DK (2012) Temporal lobe epilepsy surgery failures: a review. *Epilepsy Res Treat* 2012:201651
- Homan RW, Jones MC, Tawat S (1988) Anterior temporal electrodes in complex partial seizures. *Electroencephalogr Clin Neurophysiol* 70:105–109
- Jayakar P, Duchowny M, Resnick TJ, Alvarez LA (1991) Localization of seizure foci: pitfalls and caveats. *J Clin Neurophysiol* 8:414–431
- Jonas J, Descoins M, Koessler L, Colnat-Coulbois S, Sauvée M, Guye M et al (2012) Focal electrical intracerebral stimulation of a

- face-sensitive area causes transient prosopagnosia. *Neuroscience* 222:281–288
- Kahane P, Landré E, Minotti L, Francione S, Ryvlin P (2006) The Bancaud and Talairach view on the epileptogenic zone: a working hypothesis. *Epileptic Disord* 8:S16–S26
- Koenig T, Melie-García L (2010) A method to determine the presence of averaged event-related fields using randomization tests. *Brain Topogr* 23:233–242
- Koessler L, Maillard L, Benhadid A, Vignal JP, Felblinger J, Vespignani H et al (2009) Automated cortical projection of EEG sensors: anatomical correlation via the international 10-10 system. *Neuroimage* 46:64–72
- Koessler L, Benar C, Maillard L, Badier JM, Vignal JP, Bartolomei F et al (2010) Source localization of ictal epileptic activity investigated by high resolution EEG and validated by SEEG. *Neuroimage* 51:642–653
- Lantz G, Holub M, Ryding E, Rosén I (1996) Simultaneous intracranial and extracranial recording of interictal epileptiform activity in patients with drug resistant partial epilepsy: patterns of conduction and results from dipole reconstructions. *Electroencephalogr Clin Neurophysiol* 99:69–78
- Lantz G, Grave de Peralta R, Spinelli L, Seeck M, Michel CM (2003) Epileptic source localization with high density EEG: how many electrodes are needed? *Clin Neurophysiol* 114:63–69
- Lieb JP, Walsh GO, Babb TL, Walter RD, Crandall PH (1976) A comparison of EEG seizure patterns recorded with surface and depth electrodes in patients with temporal lobe epilepsy. *Epilepsia* 17:137–160
- Lopes da Silva, Van Rotterdam A (1993) Biophysical aspects of EEG and magnetoencephalogram generation. In: Niedermeyer E, Lopes da Silva F (edn) *Electroencephalography: basic principles, clinical applications, and related fields*. MD: Williams and Wilkins, Baltimore, p 93–109
- Maillard L, Vignal JP, Gavaret M, Guye M, Biraben A, McGonigal A et al (2004) Semiologic and electrophysiologic correlations in temporal lobe seizure subtypes. *Epilepsia* 45:1590–1599
- Maillard L, Koessler L, Colnat-Coulbois S, Vignal JP, Louis-Dorr V, Marie PY (2009) Combined SEEG and source localization study of temporal lobe schizencephaly and polymicrogyria. *Clin Neurophysiol* 120:1628–1636
- Maillard L, Barbeau EJ, Baumann C, Koessler L, Benar C, Chauvel P et al (2011) From perception to recognition memory: time course and lateralization of neural substrates of word and abstract picture processing. *J Cogn Neurosci* 23:782–800
- Merlet I, Gotman J (1999) Reliability of dipole models of epileptic spikes. *Clin Neurophysiol* 110:1013–1028
- Merlet I, Garcia-Larrea L, Ryvlin P, Isnard J, Sindou M, Mauguier F (1998) Topographical reliability of mesio-temporal sources of interictal spikes in temporal lobe epilepsy. *Electroencephalogr Clin Neurophysiol* 107:206–212
- Mikuni N, Nagamine T, Ikeda A, Terada K, Taki W, Kimura J et al (1997) Simultaneous recording of epileptiform discharges by MEG and subdural electrodes in temporal lobe epilepsy. *Neuroimage* 5:298–306
- Nayak D, Valentín A, Alarcón G, García Seoane JJ, Brunnhuber F, Juler J et al (2004) Characteristics of scalp electrical fields associated with deep medial temporal epileptiform discharges. *Clin Neurophysiol* 115(6):1423–1435
- Ramantani G, Koessler L, Colnat-Coulbois S, Vignal JP, Isnard J, Catenox H et al (2013) Intracranial evaluation of the epileptogenic zone in regional infrasyllian polymicrogyria. *Epilepsia* 54:296–304
- Sedat J, Duvernoy H (1990) Anatomical study of the temporal lobe. Correlations with nuclear magnetic resonance. *J Neuroradiol* 17:26–49
- Spencer S, Spencer D (1994) Entorhinal-hippocampal interactions in medial temporal lobe epilepsy. *Epilepsia* 35:721–727
- Van 't Ent D, Manshanden I, Ossenblok P, Velis DN, Verbunt JP et al (2003) Spike cluster analysis in neocortical localization related epilepsy yields clinically significant equivalent source localization results in magnetoencephalogram (MEG). *Clin Neurophysiol* 114(10):1948–1962
- Walsh JE (1959) Large sample nonparametric rejection of outlying observations. *Ann Inst Stat Math* 10:223–232
- Wennberg R, Cheyne D (2014) EEG source imaging of anterior temporal lobe spikes: validity and reliability. *Clin Neurophysiol* 125(5):886–902
- Wieser HG (2004) ILAE Commission on Neurosurgery of Epilepsy. ILAE Commission Report. Mesial temporal lobe epilepsy with hippocampal sclerosis. *Epilepsia* 45:695–714
- Wieser HG, Elger CE, Stodieck SR (1985) The 'foramen ovale electrode': a new recording method for the preoperative evaluation of patients suffering from mesio-basal temporal lobe epilepsy. *Electroencephalogr Clin Neurophysiol* 61:314–322
- Williamson PD, Thadani VM, French JA, Darcey TM, Mattson RH, Spencer SS et al (1998) Medial temporal lobe epilepsy: videotape analysis of objective clinical seizure characteristics. *Epilepsia* 39:1182–1188
- Yamazaki M, Tucker DM, Fujimoto A, Yamazoe T, Okanishi T, Yokota T, Enoki H, Yamamoto T (2012) Comparison of dense array EEG with simultaneous intracranial EEG for interictal spike detection and localization. *Epilepsy Res* 98(2–3):166–173

C. DISCUSSION & PERSPECTIVES

By analyzing simultaneous scalp and intracerebral EEG recordings, we have undertaken experimental work that contributes substantially to address the issues outlined in the introduction and stimulates further progress in the field by raising relevant perspectives and questions for future research. These novel findings and future perspectives include:

1. Our methodology, with the development of a detailed and highly sophisticated pipeline combining both statistical tests and expert review for the analysis of averaged interictal spikes and their corresponding networks that can be readily applied to address further questions regarding multiscale EEG signal correlations.
2. The evidence that epileptic discharges arising from mesial temporal sources are not spontaneously visible in scalp EEG, but can become detectable after averaging. Mesial temporal sources, contrary to common belief, contribute to scalp EEG despite their deep localization, their curved spatial configuration, and the blurring resulting from the superimposed neocortical activity. Although their contribution is weak, it is detectable by extraction from the respective background activity. This finding facilitates resolving a question that goes back to the advent of EEG and SEEG recordings¹.
3. The evidence for a contribution of mesial temporal networks to scalp EEG, demonstrating that mesial temporal structures do not generate closed electrical fields despite the folding of the hippocampus and the opposite orientation of the subiculum and parahippocampal gyrus⁴⁵. Our finding further supports that volume conduction also applies to electrical activity generated by deep cortical sources, distant from scalp EEG electrodes.
4. The differentiation of scalp EEG correlates of mesial vs. mesial plus/or neocortical temporal sources according to source orientation. Mesial temporal sources were only detectable in our study with a negativity in the ipsilateral anterior basal temporal electrodes, whereas mesial plus or neocortical sources were associated with an

additional fronto-centro-parietal positivity. This observation emphasizes the importance of considering the entire electrical field in a given scalp EEG to infer the source reconstruction corresponding to an observable spike.

5. The identification of scalp EEG biomarkers of mesial temporal sources could be the key to avoid invasive recordings in the presurgical evaluation of refractory temporal lobe epilepsy, the most common localization in adult patients, and serve as a solid framework for further neurological and cognitive neuroscience applications in the future.

2.2 SOURCE LOCALIZATION IN THE STUDY OF FRONTAL LOBE SOURCES AND THEIR SUBDURAL CORRELATES

A. INTRODUCTION

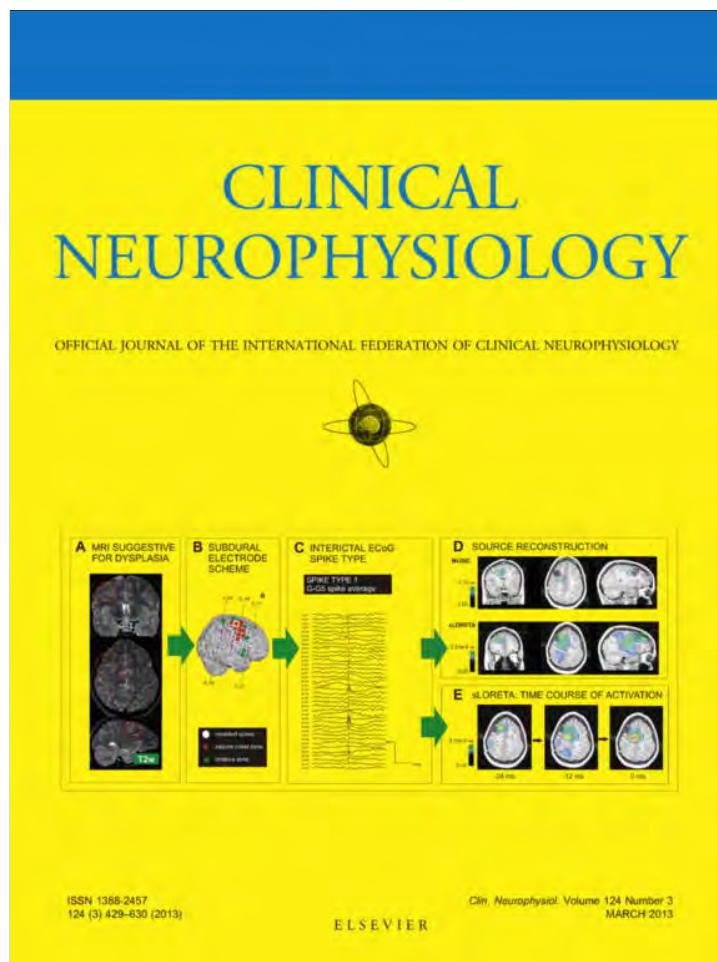
ESL derived from scalp EEG constitutes an established method nowadays and can provide a reliable 3D reconstruction of epileptic generators^{46,47}. However, despite recent advances and promising results^{48,49}, ESL has not replaced intracranial EEG investigations that have a superior spatial resolution in selected regions. The application of source localization methods to subdural EEG recordings could provide a suitable tool to improve the 3D demarcation of epileptic generators. In this study, we analyzed the simultaneous subdural and scalp EEG recordings of patients with refractory frontal lobe epilepsy undergoing presurgical evaluation. We applied ESL methods aiming to compare: (i) the source reconstructions deriving from interictal spikes in subdural recordings with the conventional electro-clinical delineation of the seizure onset zone and the irritative zone²³, and (ii) the postsurgical seizure outcome in cases where inverse solutions were included in the resection volume with cases where inverse solutions were partly/not included in the resection volume. For this purpose, we used MUSIC and sLORETA, two established and complementary source reconstruction algorithms that were shown to provide meaningful results in subdural EEG recordings in both simulations and case studies^{50,51}.

This approach is both novel and relevant in several ways. First of all, we applied the source localization methodology to subdural as opposed to scalp EEG tracings⁴⁷, thus extending the implementation of source localization to another recording scale. This is the first study to validate the applicability and accuracy and, most importantly, the clinical relevance of these novel source localization tools that were developed based on simulation and single case studies. A major benefit of this approach lies in overcoming the sampling limitations of subdural recordings that offer extensive cortical coverage, but may overlook deep sources, in contrast to SEEG that provides more accurate information for selected deep structures^{25,52}, but is plagued by sampling limitations due to incomplete and irregular cortical

coverage. The application of ESL has the potential to compensate for the shortcomings of both subdural and depth recordings, improving the 3D demarcation of epileptic generators, while retaining the benefit of broad cortical coverage.

Frontal lobe epilepsy constitutes the second most frequent type of localization-related refractory epilepsy that presents, however, lower rates of surgical success than temporal lobe epilepsy. The advances that can be attained by this novel approach could considerably improve the rates of postsurgical seizure freedom in frontal lobe epilepsy surgery.

B. SOURCE RECONSTRUCTION BASED ON SUBDURAL EEG RECORDINGS ADDS TO THE PRESURGICAL EVALUATION IN REFRACTORY FRONTAL LOBE EPILEPSY



This article appeared in a journal published by Elsevier. The attached copy is furnished to the author for internal non-commercial research and education use, including for instruction at the authors institution and sharing with colleagues.

Other uses, including reproduction and distribution, or selling or licensing copies, or posting to personal, institutional or third party websites are prohibited.

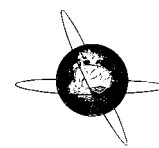
In most cases authors are permitted to post their version of the article (e.g. in Word or Tex form) to their personal website or institutional repository. Authors requiring further information regarding Elsevier's archiving and manuscript policies are encouraged to visit:

<http://www.elsevier.com/copyright>



Contents lists available at SciVerse ScienceDirect

Clinical Neurophysiology

journal homepage: www.elsevier.com/locate/clinph

Source reconstruction based on subdural EEG recordings adds to the presurgical evaluation in refractory frontal lobe epilepsy

Georgia Ramantani^{a,*}, Delphine Cosandier-Rimélé^b, Andreas Schulze-Bonhage^{a,b}, Louis Maillard^{c,d}, Josef Zentner^e, Matthias Dümpelmann^a

^a Epilepsy Center, University of Freiburg, Breisacher Str. 64, 79106 Freiburg, Germany

^b Bernstein Center, University of Freiburg, Hansastr. 9a, 79104 Freiburg, Germany

^c Service de Neurologie, Hôpital Central, CHU de Nancy, Nancy, France

^d Centre de Recherche en Automatique de Nancy (CRAN), Université de Lorraine, CNRS, UMR 7039, Vandoeuvre, France

^e Department of Neurosurgery, University of Freiburg, Breisacher Str. 64, 79106 Freiburg, Germany

ARTICLE INFO

Article history:

Accepted 2 September 2012

Available online 30 September 2012

Keywords:

Epilepsy surgery
Source localization
Intracranial
FCD
Subdural

HIGHLIGHTS

- This study shows that Electrical Source Localization derived from subdural recordings provides clinically relevant 3D localization of deep sources in refractory frontal lobe epilepsy due to focal cortical dysplasia.
- The inclusion of modeled sources in the resection strongly correlated with seizure freedom.
- Source localization from subdural EEG could improve tailored resection and surgical outcomes in refractory frontal lobe epilepsy due to focal cortical dysplasia.

ABSTRACT

Objective: In presurgical investigations of refractory frontal lobe epilepsy, subdural EEG recordings offer extensive cortical coverage, but may overlook deep sources. Electrical Source Localization (ESL) from subdural recordings could overcome this sampling limitation. This study aims to assess the clinical relevance of this new method in refractory frontal lobe epilepsy associated with focal cortical dysplasia.

Methods: In 14 consecutive patients, we retrospectively compared: (i) the ESL of interictal spikes to the conventional irritative and *seizure onset zones*; (ii) the surgical outcome of cases with congruent ESL and resection volume to cases with incongruent ESL and resection volume. Each spike type was averaged to serve as a template for ESL by the MUSIC and sLORETA algorithms. Results were superimposed on the corresponding pre and post-surgical MRI.

Results: Both ESL methods were congruent and consistent with conventional electroclinical analysis in all patients. In 7 cases, ESL identified a common deep source for spikes of different 2D localizations. The inclusion of ESL in the resection volume correlated with seizure freedom.

Conclusions: ESL from subdural recordings provided clinically relevant results in patients with refractory frontal lobe epilepsy.

Significance: ESL complements the conventional analysis of subdural recordings. Its potential in improving tailored resections and surgical outcomes should be prospectively assessed.

© 2012 International Federation of Clinical Neurophysiology. Published by Elsevier Ireland Ltd. All rights reserved.

1. Introduction

In the context of epilepsy surgery, intracranial recordings constitute the gold standard for defining the localization and extent

of the *epileptogenic zone* (Lüders et al., 2006). This is particularly relevant in complex cases with inconclusive imaging or contradictory electroclinical findings (Nair et al., 2008). Intracranial recordings serve to identify the “*seizure onset zone*” as a subset of the *epileptogenic zone* as well as of the more extensive “*irritative zone*” (Lüders et al., 2006). Understanding the intricate interrelations between the *irritative zone*, the *seizure onset zone* and the *epileptogenic zone* in the context of an “*epileptogenic lesion*”, constitutes a highly complex task, crucial for success in epilepsy surgery (Lüders et al., 2006).

* Corresponding author. Address: Epilepsy Center, University Medical Center Freiburg, Breisacher Str. 64, 79106 Freiburg, Germany. Tel.: +49 761 270 50610; fax: +49 761 270 50030.

E-mail address: georgia.ramantani@uniklinik-freiburg.de (G. Ramantani).

Subdural recordings offer extensive cortical coverage (Lüders et al., 2006), but are prone to sampling limitations for deep sources such as sulcal generators (Ebersole and Pedley, 2003). Recordings from depth electrodes provide information for selected deep structures (Kahane et al., 2006), but are plagued from sampling limitations due to incomplete and irregular cortical coverage. Thus, there is an urgent need for additional methods to compensate for the shortcomings of both subdural and depth recordings. Ideally, these new methods would improve the 3D demarcation of epileptic generators while retaining the benefit of broad cortical coverage.

Electrical Source Localization (ESL) derived from scalp EEG constitutes an established method nowadays and can provide reliable 3D reconstruction of epileptic generators (Michel et al., 2004; Plummer et al., 2008). However, despite recent advances and promising results (Koessler et al., 2010; Brodbeck et al., 2011), ESL has not replaced intracranial EEG investigations that have a superior spatial resolution in selected regions. The application of ESL methods to subdural EEG recordings could provide a suitable tool to improve the 3D demarcation of epileptic generators. The findings of several recent simulation (Chang et al., 2005; Dümpelmann et al., 2009, 2012; Fuchs et al., 2007; Zhang et al., 2008) and case studies (Dümpelmann et al., 2009, 2012; Fuchs et al., 2007; Rullmann et al., 2009; Kim et al., 2010) have provided evidence of the feasibility and reliability of source reconstruction based on intracranial recordings. In one of these studies (Kim et al., 2010) ESL modeled ictal discharges and results were compared with the resection volume in 6 patients with excellent surgical outcome. However, the localization of the *epileptogenic zone* in these patients was heterogeneous (4 temporal, 1 frontal, 1 parieto-occipital) and no information was provided as to histopathological findings. Therefore, the clinical relevance of these analytical tools has not been assessed in the presurgical investigation of patients with homogeneous localization and histopathology so far.

Frontal Lobe Epilepsy (FLE) constitutes the second most frequent type of localization related refractory epilepsy that is, however, plagued by lower rates of surgical success than temporal lobe epilepsy (Jeha et al., 2007; Spencer and Huh, 2008). Focal Cortical Dysplasia (FCD), the prevailing etiology in FLE, is a common substrate for surgically remediable epilepsy with proven intrinsic epileptogenicity (Chassoux et al., 2000) that can evade detection in conventional neuroimaging (Duncan, 2010). The present study aimed to assess the clinical relevance of source localization from subdural EEG recordings in patients with FLE related to FCD in the context of presurgical investigation.

To this purpose, we retrospectively analyzed the subdural EEG recordings of 14 patients with refractory FLE associated with FCD and compared: (i) the source reconstructions derived from interictal spikes in subdural recordings with the conventional electroclinical delineation of the *seizure onset zone* and the *irritative zone*; (ii) the surgical outcome in cases where inverse solutions were included in the resection volume with cases where inverse solutions were partly/not included in the resection volume. In this study, we used MUSIC and sLORETA, two established and complementary source reconstruction algorithms that were recently shown to provide meaningful results in subdural EEG recordings (Dümpelmann et al., 2009, 2012).

2. Patients and methods

2.1. Patients

A total of 252 patients underwent invasive VIDEO-EEG recordings with subdural electrodes in the context of presurgical workup for refractory epilepsy in the Epilepsy Center Freiburg between 1999 and 2009. Fourteen patients suspected of FLE based on the

sults of scalp video-EEG, MRI and FDG PET that presented: (a) long term subdural EEG recordings with extensive intracranial coverage of the frontal lobe with grid and strip electrodes, (b) epilepsy surgery based on the findings of this investigation, (c) diagnosis of FCD based on pathological assessment in 12/14 patients and MRI as well as EEG patterns suggestive of FCD in 2/14 patients were included in the present study.

The patient group comprised 5 males and 9 females aged 14–50 years (mean age 30 years). We retrospectively reviewed the medical history, the presurgical workup – including neuroimaging (MRI, FDG-PET), neuropsychological evaluations, long-term non-invasive investigations and invasive VIDEO-EEG recordings with subdural electrodes – the surgical procedures and their outcomes (Table 1). MRI was positive for FCD in 8 cases. In 2 further cases post-processing pointed to FCD-suspicious cortical areas, while the remaining 4 patients were considered MRI-negative. In all 14 cases, the results of non-invasive presurgical evaluation in the cooperating Epilepsy Centers of Freiburg, Heidelberg and Kork were inconclusive, so that intracranial EEG investigations were called for to allow for a precise delineation of the *epileptogenic zone* and demarcation of eloquent cortex. The consecutive invasive recordings and the resulting epilepsy surgery were performed in the Epilepsy Center Freiburg. Surgical procedures comprised a resection in 12 cases with additional multiple subpial transections (MSTs) in 2 cases. No resection was performed rather only MSTs in 2 cases, due to overlap of the *epileptogenic zone* with motor cortex. The study was granted approval by the institutional research ethics board. All patients gave their written informed consent.

2.2. Methods

2.2.1. Imaging data

The MRI scans were acquired either with a 1.5 Tesla scanner (Siemens Magnetom Vision or Siemens Magnetom Symphony) or with a 3 Tesla scanner (Siemens Magnetom TRIO) according to a standard protocol (Fauser and Schulze-Bonhage, 2006). MRI criteria suggestive for FCD were gyration anomalies, focal thickening of the cortex, blurring of the grey–white matter junction, and abnormal cortical and subcortical signal intensity.

2.2.2. EEG recordings

All patients were explored with a grid electrode array over the lateral convexity (8 × 8 contacts in 11 and 6 × 8 contacts in 3 cases) that extensively sampled the premotor and precentral areas, in order to allow for a delineation of motor cortex. The prefrontal areas, including the dorso-lateral prefrontal cortex, the orbito-frontal cortex, and Broca's area were sampled with additional subdural strip electrodes (4 6-contact-strips) in 14, 8, and 6 patients respectively. In 9 patients, medial frontal lobe structures including the medial prefrontal area, the anterior cingulate, the medial premotor area and the medial precentral area were also explored with strip electrodes. Grid and strip electrodes consisted of 4–64 stainless steel contacts embedded in silastic (Ad-Tech®, Racine, WI), with intercontact distances of 10 and 15 mm respectively. For grid placement, craniotomy with opening of the dura was performed over the designated cortical area, while subdural strip electrodes were inserted through burr holes. The total number of subdural contacts varied between 48 and 96, with an average of 78 contacts offering an extensive neurophysiological sampling of the area of interest in all cases. Subdural EEG recordings were obtained using a Neurofile NT® digital video-EEG system with 128 channels at a sampling rate of 1024 Hz, and a 16-bit A/D converter. A high-pass filter with a time constant of 1 s and a low-pass filter with a cutoff frequency of 344 Hz were applied to the signal in the recording system.

Table 1
 Characteristics of the patient group including demographics, results of non-invasive presurgical evaluation and subsequent invasive recordings with subdural electrodes, surgical procedures and seizure outcomes. The topography of scalp EEG interictal spikes is expressed by the electrode contacts (10–20 or 10–10 system) showing maximum amplitude.

Patients	Demographics		Findings of non-invasive presurgical evaluation				Findings of invasive presurgical evaluation				Surgery and outcomes				
	Age (y)	Gender	Initial ictal evaluation	VIDEO-EEG	Lat.	Scalp EEG spikes	MRI suggestive for FCD	FDG-PET interictal hypo-metabolism	Intra-cranial EEG spike types	SOZ localization	IZ localization	Surgical procedure	Resection of intracranially defined EZ	Histology	Final outcome Engel
<i>Fronto-lateral</i>															
1	16	f	Motor automatisms, L arm elevation, vocalization		R	F4-Fz	F2	Negative	1	LA 6	LA 4, 6, 8, 44/45	RE	Complete	FCD1b	Ia
2	33	f	B motor automatisms, L arm elevation, R manual automatisms, L eye version, L face clonic		R	F4	F3	B frontal	3	LA 6	LA 6, 44, 45	RE	Complete	FCD2a	Ia
3	50	f	L shoulder myoclonic, B pedalling, L leg/arm tonic, B motor automatisms		R	Negative	F2/F3, transamntle dysplasia	F2	6	LA 4	LA 1, 2, 3, 4, 6, 47	RE, MSTs	Partial	FCD2a	Ia
4	40	m	Vague experiential aura, LOC, R shoulder tonic, R head/trunk version, R arm elevation		L	FC1-Cz	Negative	Negative	2	LA 8	ME 4, 6	RE	Complete	FCD2b	Ia
5	27	m	R trunk/thigh tingling, R thigh flexion, R arm elevation, R thigh clonic, B thigh clonic, vocalization		L	Negative	Negative	Negative	2	LA 4, 8	LA 4, 6, 8	RE, MSTs	Partial	FCD1b	Ia
6	30	m	L hand tingling, spread of sensation to L shoulder, L arm elevation, R arm flexion, L arm clonic, vocalization		R	C2-CP2	Precentral, F1	Precentral, F1	2	LA 4	ME 4, 6, 8	MSTs	None	FCD (nc)	IVa
7	21	f	Ascending heat sensation, R head version, L arm elevation, L mouth corner tonic		R	F4	F1, F2	Negative	4	LA 4, 6, 8	LA 4, 6, 8, 1, 2, 3	RE	Partial	FCD2a	Ib
8	49	f	R head version, B arm elevation, urination		L	FC1, F3, C3	Negative	Precentral, F1	5	LA 4, 8	LA 4, 6, 8	RE, MSTs	Partial	FCD1b	I1b
<i>Fronto-medial</i>															
9	41	f	R knee twitching, L arm/head myoclonic, L arm elevation, B motor automatisms		L	Negative	Precentral, medial	Precentral, medial	2	ME 4	ME 4, 6	MSTs	None	FCD (nc)	I1a
10	16	f	L arm/leg tonic, L arm/leg clonic, vocalization		L	C3-CP1	F1, cingulate,	Cingulate	2	ME 4, 24	ME 4, 24	RE	Complete	FCD (nc)	Ib
11	20	m	Ascending heat sensation, pelvic thrusting, flush, R arm tonic, LOC, vocalization, oroalimentary automatisms, manual automatisms, thrashing of the extremities		L	FC1-F3-AF3-Fz	Cingulate (pp)	Cingulate	3	ME 32, 24, 31	ME 32, 24, 31, 23	RE	Partial	FCD (nc)	Ib
<i>Fronto-basal/-fronto-polar</i>															
12	25	m	Bimanual automatisms, LOC, R head version, pedaling, L nose rubbing		L	F3	Orbito-frontal, F3	Orbito-frontal, F3	3	BA 11, 47	BA 10, 11, 47	RE	Complete	FCD1a	Ia
13	14	f	R manual automatisms, B manual automatisms, vocalization, B leg thrusting, B leg clonic, B head clonic		R	FC2	Fronto-polar (pp)	Fronto-polar	3	LA 9, 46	LA 9, 46, 6, 8	RE	Complete	FCD1b	Ia
14	39	f	Expresses fear, retrosternal tightness, tachycardia, speech arrest, B arm elevation, L hand elevation, B leg thrusting, L manual automatisms		L	F3, FP1	Negative	Negative	4	BA 11	LA 6, 9, 46	RE	Partial	FCD1a	I11a

The localization of neuroimaging pathology is expressed according to the involvement of the superior frontal gyrus (F1), middle frontal gyrus (F2) and inferior frontal gyrus (F3). The localizations of the seizure onset zone (SOZ) and the irritative zone (IZ) are expressed by means of Brodmann areas and their exact topography; LA: lateral, BA: basal; ME: medial, Y: years; m: male; f: female; age: age in years (y) at the time of invasive presurgical evaluation with subdural electrodes; L: left; R: right; B: bilateral; LOC: loss of consciousness; lat.: lateralization; pp: post-processing; RE: cortical resection; MSTs: multiple subpial transections; nc: histologically verified, albeit not further classifiable cortical dysplasia.

2.2.3. Interictal spike detection and averaging

Subdural EEG segments of >30 min in calm wakefulness were carefully chosen to include an adequate number of interictal spikes and avoid ictal events or preictal changes. Sharp transients that appeared <3 times in selected 30 min segments were excluded from further analysis. Furthermore, segments of polyspikes (>2 spikes per 200 ms) and activity in the beta or gamma range were visually detected and excluded, so that interictal epileptiform events other than single spikes were excluded from consideration.

The resulting segments were reviewed using both bipolar and referential montages. Signals were recorded against a reference electrode placed on the forehead and eventually re-referenced to a common average reference. All patterns in ECoG were identified and selected according to the general principles recommended by the International Federation of Clinical Neurophysiology (1983) and used in standard EEG interpretation: sharp transients clearly distinguished from background activity with “epileptiform” morphology and a logical spatial distribution. The interictal spikes were marked at the time point of their highest amplitude using Neurofile NT[®]. Epochs of 1000 ms were extracted (500 ms before and after the highest amplitude of the event) and transferred for averaging with the Advanced Signal Analysis (ASA) software (A.N.T. Software B.V., Enschede, The Netherlands) (Supplementary Fig. S1A).

2.2.4. Interictal spike characterization

Visually detected interictal ECoG spikes were then classified according to their affiliation with the *seizure onset zone* or the *irritative zone* as defined by conventional electroclinical evaluation. In view of the multitude of identified interictal spikes, *spike types* were defined to describe spikes of similar spatio-temporal distribution that were presumed to correspond to activity from a single generator. Each spike type in subdural recordings was topographically characterized by the dominant contact (electrode contact with maximum amplitude) as defined in a referential montage. If the dominant contact was congruent with the cortical area delineated by the initial ictal discharge it was allocated to the *seizure onset zone*. Otherwise it was allocated to the *irritative zone*.

2.2.5. Realistic head model

The realistic boundary element (BEM) head model derived from the segmentation of the 3D T1-weighted normalized MRI dataset performed prior to electrode implantation (Supplementary Fig. S1B). The normalization was performed with respect to the standard brain of the Montreal Neurologic Institute (MNI) included in SPM99 and brain region identified for further processing steps (Kovalev et al., 2005). The BEM model was created using the ASA[®] package (A.N.T. Software B.V., Enschede, The Netherlands) (Zanow and Knösche, 2004) and consisted of a single homogeneous compartment representing the brain. In the 8 cases where medial contacts were considered for source localization, the brain compartment comprised of a single hemisphere. Regardless of the configuration (one or two hemispheres), the brain compartment consisted of 3446 vertices and 6888 triangles. The volume conduction effect outside the inner skull boundary was ignored in this study due to the very low electrical conductivity of the human skull layer (Fuchs et al., 2007; Kim et al., 2010).

2.2.6. Electrode positions

The electrode positions were determined from the normalized 3D T1-weighted MRI dataset with 1 mm isotropic resolution acquired after electrode implantation on the same scanner system as the pre-implantation MRI (Supplementary Fig. S1B). Individual stainless steel electrodes with ferromagnetic properties cause a local magnetic field inhomogeneity, which produces a signal void or “black hole artifact”. These circumscribed susceptibility artifacts

were used to determine the individual electrode positions. To this purpose, the center of each susceptibility artifact was manually marked using self-developed 3D visualization software (Kovalev et al., 2005).

2.2.7. Source localization of averaged spikes

The two algorithms applied were selected as representative either for *focal* source reconstruction methods (MUSIC) or for *distributed* source models (sLORETA) (Supplementary Fig. S1C).

MUSIC (MUltiple Signal Classification) facilitates the identification of intracranial generators with independent time courses (Mosher et al., 1992, 1999). The probe source for the scanning procedures is a point-like current source as in *dipole fit*. MUSIC enables the localization of several independent sources, including deep sources, but the focal nature of the algorithm prohibits extrapolations as to their spatial extent. The applicability and reliability of MUSIC in source reconstruction derived from ECoG was introduced and supported in earlier studies on simulated and real data (Chang et al., 2005; Dümpelmann et al., 2009).

sLORETA (standardized low-resolution brain electromagnetic tomography) relies on a *distributed source model* (Hämäläinen and Ilmoniemi, 1994; Pascual-Marqui, 2002) to provide a 3D activity distribution, including deep sources, and depict activation over time. Results correspond to a single value for a time interval. In our figures, this corresponds to the mean value of the distribution in the analysis interval, unless explicitly stated otherwise. sLORETA showed promising results in a recent simulation study with ECoG recordings (Dümpelmann et al., 2012).

The interval used for both localization algorithms was determined by the minima around the peak of the spike average. The same scan points distributed on a regular 3D lattice inside the brain with an edge length of 7 mm were used for both methods.

It should be noted that activation volumes given by each of the algorithms are not directly comparable. In particular, MUSIC provides focal solutions (Dümpelmann et al., 2009) while the spatial extent of sLORETA solutions is variable and depends on signal-to-noise ratio and distance to electrodes (Dümpelmann et al., 2012), with results corresponding to statistical estimates in both cases. Thus, the topography of the activation maximum rather than the activation volume was considered in comparisons between source reconstructions and resection volumes.

2.2.8. Visualization of sources in MRI

Source localization results are demonstrated as overlaid to the T1-weighted individual pre-implantation or post-resection spatially normalized MRI (Supplementary Fig. S1). This allows the comparison of the MRI-identifiable resection volume in the 12 patients who subsequently underwent resective surgery with the source reconstruction results.

2.2.9. Intracranial investigation and postoperative validation

The distinct anatomic-functional properties of different frontal lobe regions define the extent of subdural electrode sampling as well as the patterns of propagation. Therefore, patients were grouped according to the localization of their respective *seizure onset zone* in the fronto-lateral (LA), the fronto-medial (ME) or the fronto-basal (BA) structures. Thus, 8 patients were assigned to the lateral, 3 to the medial, and 3 to the fronto-basal group (Tables 1 and 2).

The different spike types were analyzed separately by source reconstruction methods and the results were compared with the localization of the dominant contact of the respective interictal ECoG spike, as expressed in Brodmann areas. Inverse solutions were further analyzed according to their allocation to the *seizure onset zone* or *irritative zone*.

Table 2
 Interictal ECoG spike types with distinct topography allocated to the seizure onset zone (SOZ) or the irritative zone (IZ), localization of the respective MUSIC and sLORETA inverse solutions, inclusion of inverse solutions in resection volume, agreement between source localization algorithms and surgical outcomes. The localization of the dominant contacts for each spike type (electrode contacts with the highest amplitude) and of the respective inverse solutions is expressed by means of Brodmann areas and their topography.

Patient	Interictal ecog spike types	MUSIC		sLORETA		Correlation of ESL methods	FINAL OUTCOME ENGEL
		Localization of dominant contact	Localization of inverse solution	Localization of inverse solution	Inclusion in resection		
<i>Fronto-lateral</i>							
1	SOZ	21	LA 6	LA 6, 46	○	○	Ia
2	SOZ	183	LA 6	LA 6	○	○	Ia
	IZ	30	LA 4	LA 4	○	○	
	SOZ	111	BA 11	BA 11	○	○	Ia
3	SOZ	143	ME 4	ME 4, 6	○	○	
	IZ	177	BA 11	BA 11	○	○	
	IZ	158	LA 47	LA 47	○	○	
	SOZ	15	LA 4	LA 4, 6	○	○	
	IZ	3	LA 6	LA 6	○	○	
	IZ	8	LA 1,2,3	LA 4	○	○	
4	SOZ	331	LA 8	ME/LA 8	○	○	Ia
	IZ	3	ME 6	ME/LA 8	○	○	
5	SOZ	97	LA 8	LA/ME 8	○	○	Ia
	IZ	97	ME 6	LA/ME 6	○	○	
6	SOZ	175	LA 4	LA 4	●	○	IVa
	IZ	172	LA 4, 8	LA 4	○	○	
7	SOZ	18	LA 6	LA 6	○	○	Ib
	SOZ	5	LA 6 LA 4 LA 1,2,3	LA 4	○	○	
	IZ	55	LA 8	LA 1,2,3	●	○	IIB
8*	SOZ	18	LA 4	LA 8	○	○	
	SOZ	40	LA 4	LA 4	○	○	
	SOZ	32	LA 8	LA 8	○	○	
	IZ	16	ME 4	ME 4	○	○	
	IZ	18	ME 4	ME 4	○	○	
<i>Fronto-medial</i>							
9	SOZ	463	ME 4	ME 4	●	○	Ila
	IZ	10	LA 4	LA 4	○	○	
10	SOZ	141	ME 4, 24	ME 4, 24	○	○	Ib
	IZ	8	LA 6	LA 6	○	○	
11	SOZ	117	ME 24, 32	ME 24, 32	○	○	Ib
	SOZ	44	ME 24, 32	ME 24, 32	○	○	
	IZ	32	LA 6	ME 24, 32	○	○	
<i>Fronto-basal/-fronto-polar</i>							
12	SOZ	70	BA 11	BA 11	○	○	Ia
	IZ	22	BA 47	BA 47	○	○	
	IZ	4	LA 46	LA 46	○	○	
13	SOZ	161	LA 9, 46	LA 9, 46	○	○	Ia
	IZ	395	LA 46	LA 46	○	○	
	IZ	20	LA 9	LA 9	○	○	
14	SOZ	1574	BA 11	LA/ME 6, 8	○	○	IIIa
	IZ	28	LA 9	LA 8, 9	○	○	
	SOZ	138	ME 6	LA 6	●	○	
	IZ		LA 46	LA 46, 6	○	○	

LA: lateral; BA: basal; ME: medial. The inclusion of inverse solutions in the resection and the correlation between the two source localization methods is given in symbols: ○: complete; ●: partial; ●: none. Nr: number; *: seizure onset zone included cortical areas producing low voltage rapid discharges, but no spikes.

To validate the clinical relevance of the ESL-defined epileptic generators we compared the post-surgical outcome between cases with inverse solutions corresponding to the *seizure onset zone* included in the resection volume (complete concordance) and cases with inverse solutions corresponding to the *seizure onset zone* partly included in the resection volume (partial concordance) or altogether excluded from resection volume (discordance).

3. Results

Results of representative cases for the fronto-lateral, fronto-medial and fronto-basal group, chosen to demonstrate different localizations of the *seizure onset zone* and *irritative zone* are illustrated in Figs. 1–3.

3.1. Interictal spike detection

Three to 463 (median 91) interictal ECoG spikes were identified and averaged to facilitate source reconstruction for each of 41 different spike types in 14 patients. With the exception of patient 1 that had a single spike type (Fig. 4), all patients presented 2–6 (median 3) interictal spike types, with 8 patients presenting >2 distinct spike types (Table 2).

3.2. Concordance between conventional analysis of spikes and their modeled sources

Thirty-seven inverse solutions localized within the depth of the Brodmann area delineated by conventional evaluation (Fig. 1–3) and 4 fully allocated to a different, adjacent Brodmann area. Out of the 37 congruent inverse solutions, 33 were confined within the respective Brodmann area (Fig. 2) and 4 additionally involved an adjacent Brodmann area (Fig. 4). Moreover, 7 out of these inverse solutions localized at equal distance to the medial and lateral surface of the respective Brodmann area (Fig. 1), although solely derived from a lateral, medial or basal dominant contact (Table 2).

The 3D inverse solutions defined by their maximum of activation corresponded with the topography of the *irritative zone* or the *seizure onset zone* as delineated in conventional evaluation (Table 2) including areas at the margin of subdural grids (Figs. 1–4) or areas sampled by irregularly spaced subdural strips (Figs. 2 and 3). Source reconstruction provided meaningful results despite the limited subdural coverage of the presumed generator (Tables 1 and 2).

3.3. Concordance between source localization algorithms

MUSIC and sLORETA provided congruent results for 39/41 modeled spike populations regardless of the localization of the respective dominant contact (Table 2). Two cases of partial incongruence were observed in the inverse solutions of patients 1 and 10 respectively.

In the case of patient 1 (Tables 1 and 2) MRI raised suspicion for a transmantle FCD in the premotor/prefrontal region (Fig. 4A), with the *seizure onset zone* identified in the premotor area, as a subset of a more extensive *irritative zone* that included parts of the premotor and prefrontal cortex (Fig. 4B). MUSIC provided a single inverse solution that localized within the posterior border of the resection, corresponding to the posterior margin of the lesion (Fig. 4D). The sLORETA source reconstruction is shown for three different time points, with the reconstruction maximum shifting from the *seizure onset zone* in the anterior margin of the lesion at –24 ms to the *irritative zone* at the posterior margin of the lesion at 0 ms (Fig. 4E). The reconstruction maximum of sLORETA at 0 ms corresponded with the MUSIC inverse solution (Fig. 4D). The complete resection of the *seizure onset zone* – including the reconstruction maximum

of sLORETA at –24 ms – but not the full extent of the *irritative zone* – including the reconstruction maximum of sLORETA at 0 ms and the MUSIC solution – led to seizure freedom (Fig. 4D). According to the different characteristics of the two methods, these results could correspond to an analytic visualization of spatio-temporally diverse activation patterns by sLORETA that were summed up to provide a single focal solution by MUSIC.

In the case of patient 10 (Table 2), the partial discrepancy between MUSIC and sLORETA inverse solutions for a spike population allocated to the *irritative zone* can be readily attributed to increased noise due to a superimposed interfering rhythmic activity with similar distribution. The presence of noise led to increased activation volume and less reliable results, especially for sLORETA, as previously reported (Dümpelmann et al., 2012).

3.4. Validation against epilepsy surgery outcomes

In all 6 patients with complete concordance of the modeled source corresponding to the *seizure onset zone* with the resected volume, the surgical treatment resulted in seizure freedom. In 4 out of 6, the resected volume also included the modeled sources corresponding to the *irritative zone* (pt. 4, 11, 12, 13) (Tables 1 and 2). In the remaining 2 patients (pt. 2, 5) the resected volume included the modeled sources corresponding to the *seizure onset zone* but not the *irritative zone* (Fig. 1). In the 6 cases of partial concordance, 4 patients (pt. 1, 3, 7, 10) were seizure free following surgery (Fig. 4) and 2 patients (pt. 8, 14) had rare seizures or a worthwhile improvement (Tables 1 and 2). In the 2 cases of discordance (pt. 6, 9) (Fig. 2), there was no worthwhile improvement (Tables 1 and 2).

4. Discussion

To our knowledge, this study represents the first effort to assess the clinical relevance of source localization from subdural EEG recordings in patients with homogeneous localization related epileptic substrates in the context of presurgical investigation.

4.1. Concordance of source reconstruction with intracranial investigation

In this study, 3D source reconstruction provided anatomically meaningful results conform to the conventional analysis of the corresponding spikes. Furthermore, source reconstruction refined localization regarding deep sources. This property was especially relevant in cases where the 3D visualization of a deep source reconciled different 2D localizations of spike types (Table 2). This finding suggests that the additional use of source localization algorithms may outbalance the shortcomings of a grid evaluation regarding deep sources, introducing a surrogate for additional investigations with intracerebral depth electrodes.

In terms of source localization based on intracranial recordings, reliable results can only be achieved for brain regions adequately sampled by subdural electrode contacts (Dümpelmann et al., 2009, 2012). However, subdural coverage is carefully chosen to sample the area of interest as defined by the non-invasive electro-clinical, and neuroimaging data. Furthermore, source reconstruction provided electro-clinically valid results in all cases, including those where sampling was less extensive or meticulous, as in the medial (Fig. 2) and orbito-frontal (Fig. 3) regions.

4.2. Concordance between source localization algorithms

In all but two cases, inverse solutions by MUSIC and sLORETA were congruent. MUSIC provided spatially limited solutions while

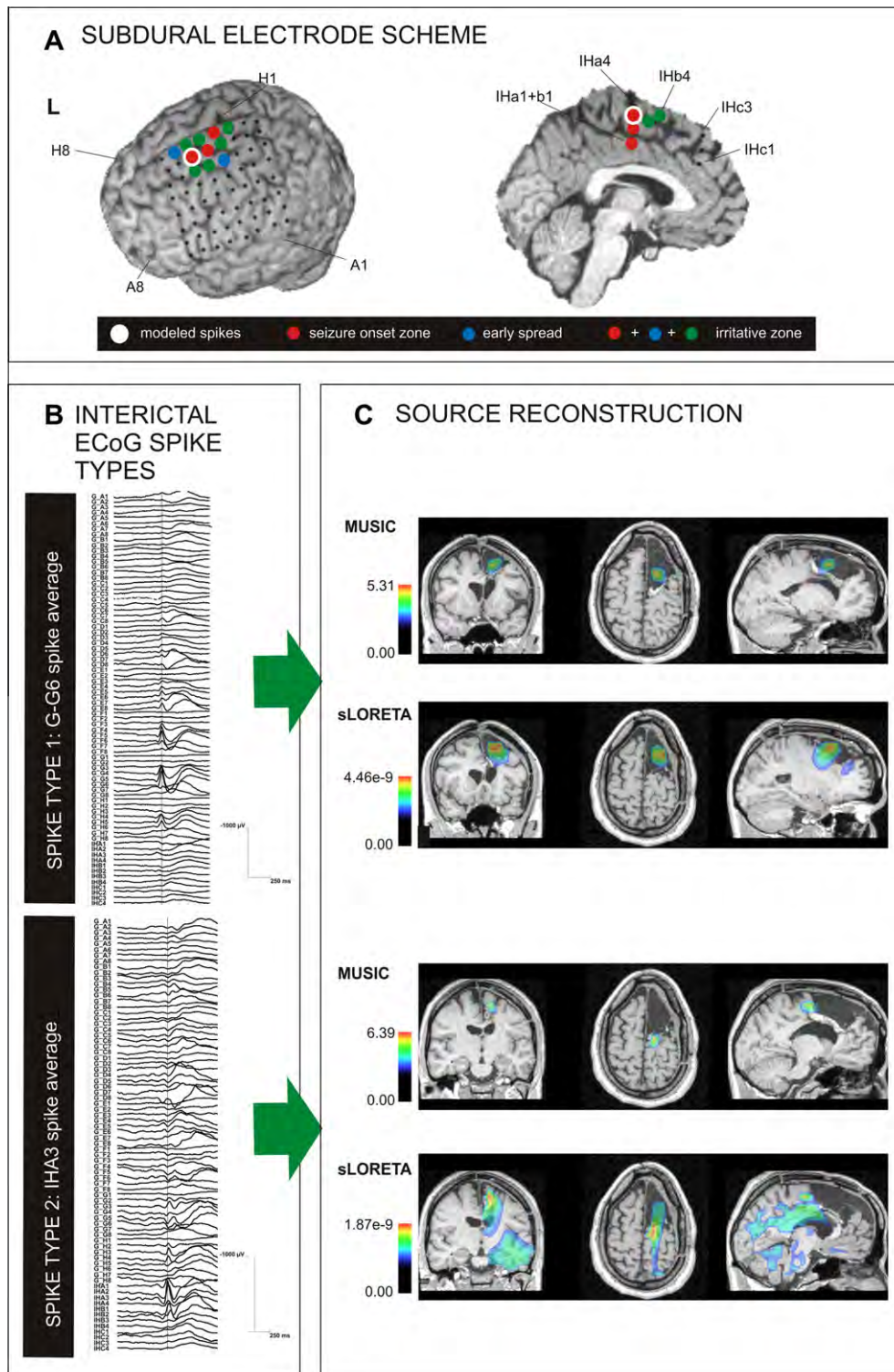


Fig. 1. Fronto-lateral and fronto-medial seizure onset zone. Subdural electrode scheme, interictal ECoG spike types and source reconstruction for patient 5, representing the fronto-lateral group. (A) Subdural electrode scheme superimposed on the individual MRI including a 8×8 contact grid electrode with full coverage of the motor and premotor cortex and 3 4-contact electrode strips sampling the medial aspect of the motor, premotor and prefrontal cortex. The seizure onset zone in this non-lesional patient was delineated in the paramedian lateral and medial premotor cortex, extending to the anterior border of the motor cortex. (B) Two interictal ECoG spike types were analyzed, both allocated to the seizure onset zone, with the cortical area producing spike type 1 more frequently involved in seizure onset. Spike type 1 showed maximum amplitude in the lateral aspect of the premotor cortex (G-G6) while spike type 2 was registered with a maximum in the medial strip (IHA3) contacts (monopolar montage against a common average reference). (C) Source reconstruction by MUSIC and sLORETA provided congruent inverse solutions: (1) the inverse solution for spike type 1 localized within the supplementary motor area, correlated with the seizure onset zone, and was fully included in the resection, as illustrated superimposed on the post-resection individual MRI and (2) the solution for spike type 2 corresponded to a generator in the depth of the superior frontal sulcus that localized at the posterior margin of resection and within the area treated with MSTs. The full inclusion of the inverse solution for spike type 1 and partial inclusion of the inverse solution for spike type 2 (less frequently involved in seizure onset) in the resection correlated with seizure freedom. MSTs: multiple subpial transections.

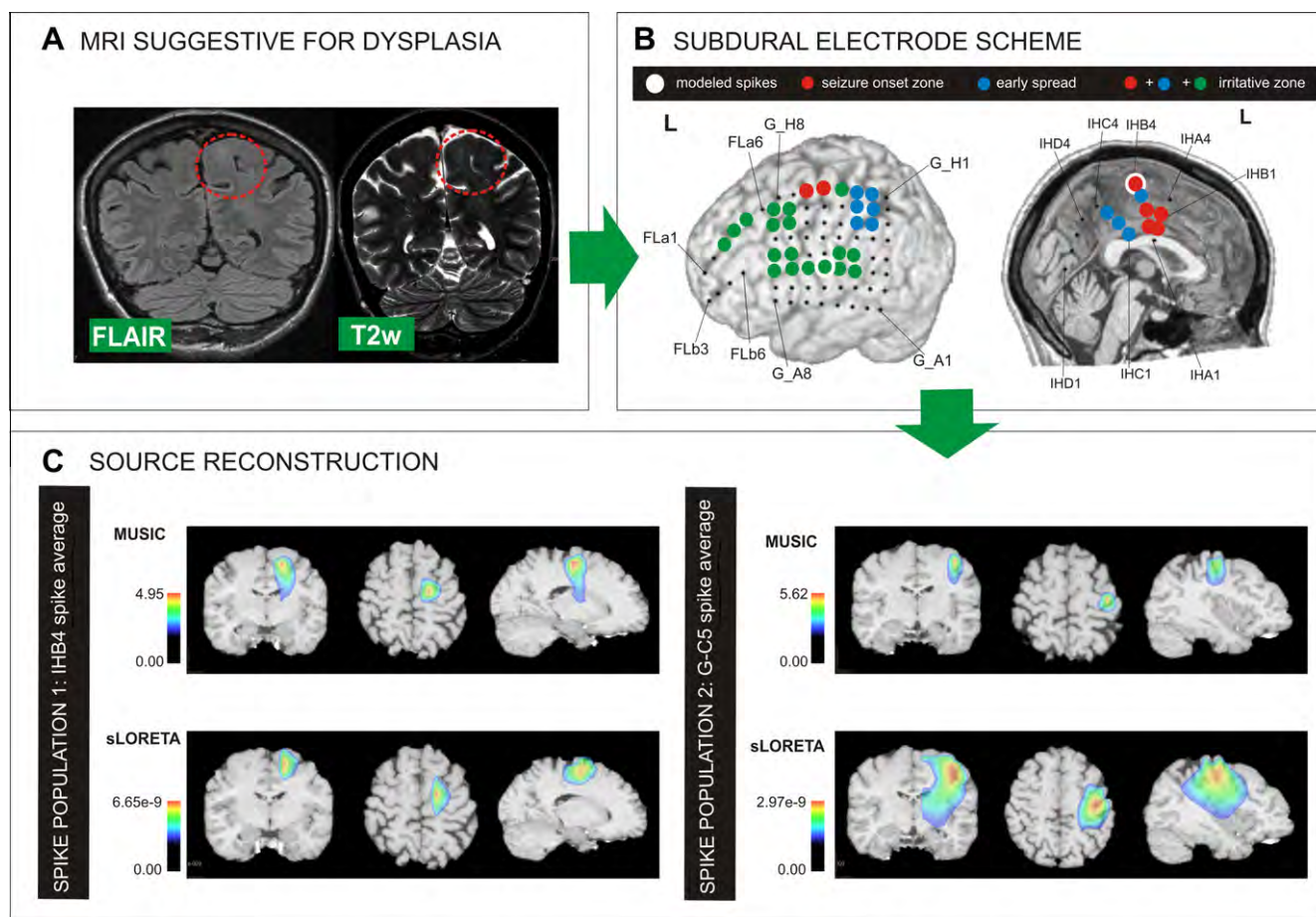


Fig. 2. Fronto-medial seizure onset zone. MRI findings suggestive for dysplasia, subdural electrode scheme and source reconstruction in patient 9, representing the fronto-medial group. (A) MRI findings suggestive for FCD in the depth of the motor cortex (paramedian, leg area) including blurring of the grey–white matter junction and abnormal cortical and subcortical signal intensity, as depicted in coronal FLAIR and T2-weighted imaging (included in red dotted circle). (B) Subdural electrode scheme superimposed on the individual MRI including a 8×8 contact grid electrode with full coverage of the motor and premotor cortex and 4 4-contact electrode strips sampling the medial aspect of the motor, premotor and prefrontal cortex. The seizure onset zone was delineated in the medial and paramedian motor cortex, with the irritative zone extending to the lateral premotor and prefrontal areas. Two spatiotemporally distinct interictal ECoG spike types allocated to the seizure onset zone (IHB4) and the irritative zone (G-C5) were analyzed. (C) source reconstruction by MUSIC and sLORETA (EEG data not shown) provided two distinct inverse solutions, as superimposed on pre-implantation MRI: (1) the inverse solution for spike type 1 localized within the paramedian aspect of the motor cortex and correlated with the seizure onset zone and (2) the inverse solution for spike type 2 localized within the lateral convexity and was allocated to the irritative zone. In this case, resective surgery was not feasible, due to overlapping of the seizure onset zone with the motor cortex. MSTs led to a temporary alleviation from seizure burden, followed by relapse 9 months after surgery. FCD: focal cortical dysplasia; MSTs: multiple subpial transections.

sLORETA source reconstruction consisted of a more widespread activation (Figs. 3 and 4), consistent with previous studies (Fuchs et al., 2007; Michel et al., 2004). Furthermore, the application of MUSIC in our study resulted in single-value and thus focal solutions for a set time interval (Michel et al., 2004), while sLORETA facilitated the illustration of activation over time by employing a “physiological” constraint that presumes a high correlation of neuron activity in neighboring cortical areas (Dümpelmann et al., Dümpelmann et al., 2012). The understanding of these properties is crucial in elucidating apparently incongruent results. This is particularly the case in spatio-temporally complex activation patterns that are visualized as a sequence of time-dependent activation distributions by sLORETA but are presented as a single focal solution for the full time interval by MUSIC, as in patient 1 (Fig. 4).

Finally, it is important to emphasize that activation volumes should be appreciated as an approximation of the true extent of the cortical generator and thus cannot be directly compared either with the volume of resection or between the two source reconstruction algorithms applied. Novel computational approaches including a model that combines a spatio-temporal representation of EEG generators (neocortical neuronal populations) with a

biophysically pertinent account of cortical activity transmission to the recording electrodes (Cosandier-Riméle et al., 2010) are expected to shed new light on this very crucial aspect.

4.3. Validation against epilepsy surgery outcomes

In this study, we analyzed interictal spikes from ECoG recordings to model cortical generators and subsequently compared inverse solutions with the gold standard of seizure outcome after the resection of the presumed epileptogenic tissue. Thus, source localization results correlated with the seizure onset zone and the irritative zone as defined in standard electro-clinical evaluation. Consequently, the complete resection of the inverse solutions allocated to the seizure onset zone with/without further inverse solutions allocated to the irritative zone led to seizure freedom in all cases. This emphasizes the importance of seizure onset zone compared to that of irritative zone, in accordance with the results of a previous study (Asano et al., 2009). In our study we opted out statistical analyses because of an insufficient number of subjects. Seizure freedom was also achieved in 4/6 patients where part of the inverse solution allocated to the seizure onset zone localized at

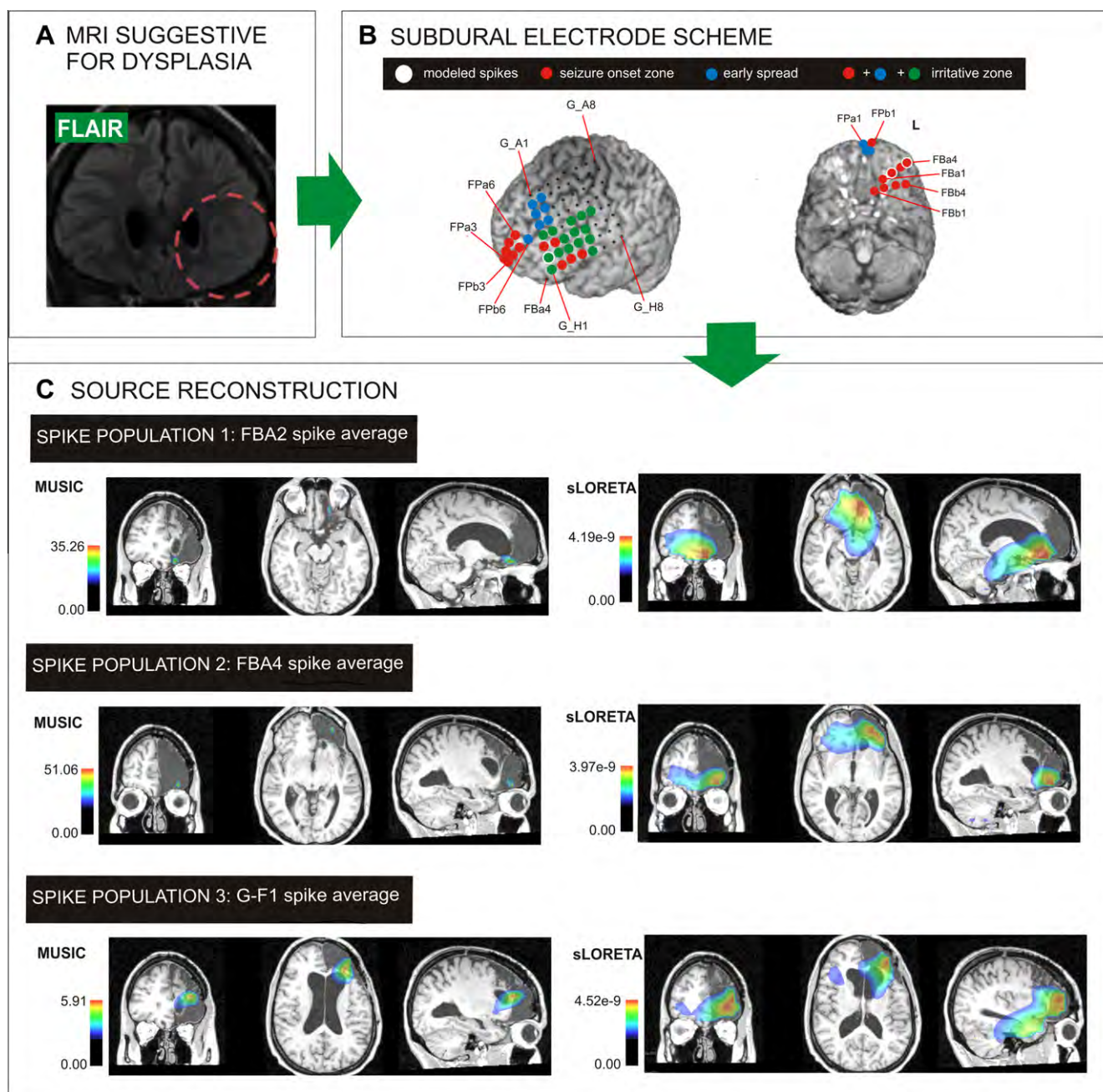


Fig. 3. Fronto-basal and fronto-polar seizure onset zone. MRI findings suggestive for dysplasia, subdural electrode scheme and source reconstruction in patient 12, representing the fronto-basal/fronto-polar group. (A) MRI findings suggestive for FCD in the orbito-frontal cortex including blurring of the grey-white matter junction and abnormal cortical and subcortical signal intensity, as depicted in coronal FLAIR weighted imaging (included in red dotted circle). (B) Subdural electrode scheme superimposed on the individual MRI including a 8×8 contact grid electrode over the lateral convexity with full coverage of the motor, premotor and prefrontal cortex, 2 6-contact electrode strips sampling the fronto-polar, lateral region and 2 4-contact electrode strips sampling the orbito-frontal cortex. The seizure onset zone in this patient was delineated within the orbito-frontal epileptogenic lesion, while the irritative zone extended to the dorso-lateral prefrontal cortex. Three spatiotemporally distinct spike types with maximum amplitude within the seizure onset zone in the basal aspect of the orbito-frontal cortex (FBA2, FBA4) and in the irritative zone extending to the dorso-lateral prefrontal cortex (G-F1) were analyzed. (C) Source reconstruction by MUSIC and sLORETA (EEG data not shown) provided congruent inverse solutions, as superimposed on post-resection MRI: (1) the inverse solution for spike types 1 and 2 localized within the paramedian and lateral aspect of the orbito-frontal cortex respectively and correlated with the seizure onset zone and (2) the inverse solution for spike type 3 localized at the superior margin of the seizure onset zone and corresponded with the irritative zone. Seizure freedom was achieved as a result of a resection that included all 3 inverse solutions. FCD: focal cortical dysplasia.

the margin of the resection volume. This might be an effect of a partial disconnection of the epileptogenic network or of a slight brain shift resulting from the surgical procedure.

However, it should be noted that the delineation of the epileptogenic zone does not derive solely from spikes as a marker of epileptogenicity. Further surrogate markers derive from electrophysiological

approaches to localize scalp EEG ictal discharges (Koessler et al., 2010), detect rapid discharges (Cosandier-Rimélé et al., 2011) and high-frequency oscillations (Jacobs et al., 2010). In our study, we applied ESL to interictal spikes because of the superior signal to noise ratio compared to ictal discharges (Koessler et al., 2010) and obtained relevant results in the particular context of FLE associated with FCD.

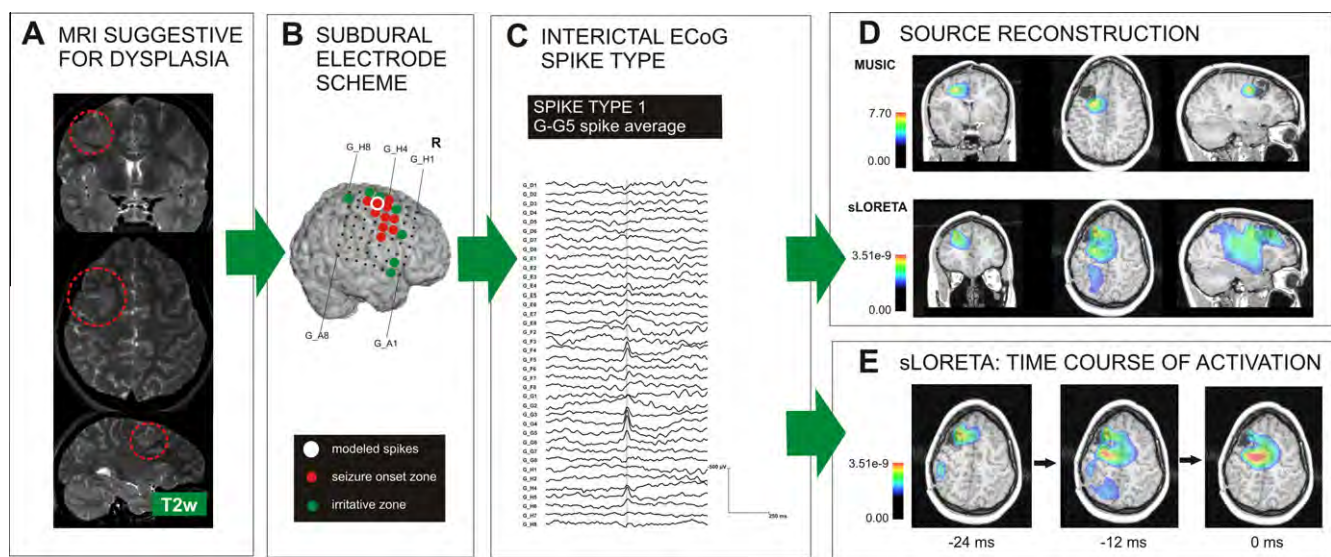


Fig. 4. Partial incongruence between inverse solutions by MUSIC and sLORETA. MRI findings suggestive for transmantle dysplasia, interictal ECoG spikes (single spike type) visually identified and analyzed and source reconstruction for patient 1, including the time course of activation for sLORETA. (A) MRI findings suggestive for FCD in the depth of the premotor cortex including blurring of the grey–white matter junction, focal thickening of the cortex, abnormal cortical and subcortical signal intensity, as depicted in T2-weighted imaging (included in red dotted circle). (B) Subdural electrode scheme superimposed on the individual MRI including a 8×8 contact grid electrode with full coverage of the motor and premotor cortex. (C) Spike type 1 with maximum amplitude at contact G-C5 (monopolar montage, common average reference), corresponding to the seizure onset zone within the epileptogenic lesion in the lateral premotor cortex. D: source reconstruction by MUSIC and sLORETA provided partially incongruent inverse solutions, as superimposed on post-resection MRI. MUSIC provided a single inverse solution within the posterior border of the resection, corresponding to the posterior margin of the epileptogenic lesion. The sLORETA source reconstruction is shown for three different time points, with the reconstruction maximum shifting from anterior to posterior over time. The reconstruction maximum of sLORETA at -24 ms localized within the seizure onset zone that corresponded to the anterior margin of the MRI-detectable lesion and at 0 ms it localized within the posterior border of the irritative zone that corresponded with the MUSIC inverse solution. The complete resection of the seizure onset zone – including the source reconstruction maximum of sLORETA at -24 ms – but not the full extent of the irritative zone – including the source reconstruction maximum of sLORETA at 0 ms and the MUSIC inverse solution – led to seizure freedom. FCD: focal cortical dysplasia.

The next steps will be to apply this new method to ictal discharges and perform a prospective comparison with the conventional analysis in a wider clinical context.

5. Conclusion

In this study, we have shown that source localization methods applied to intracranial recordings provide complementary information that facilitates the identification and accurate delineation of the epileptogenic zone and thus improves the presurgical evaluation of FLE patients. Analytical approaches of ESL could add both depth and extent to the localization accuracy of visual interpretation in subdural EEG recordings and could thus constitute a surrogate of intracerebral depth investigations while retaining the superior spatial coverage of subdural grid electrodes.

Appendix A. Supplementary data

Supplementary data associated with this article can be found, in the online version, at <http://dx.doi.org/10.1016/j.clinph.2012.09.001>.

References

Asano E, Juhász C, Shah A, Sood S, Chugani HT. Role of subdural electrocorticography in prediction of long-term seizure outcome in epilepsy surgery. *Brain* 2009;132(Pt 4):1038–47.

Brodbeck V, Spinelli L, Lascano AM, Wissmeier M, Vargas MI, Vulliemoz S, et al. Electroencephalographic source imaging: a prospective study of 152 operated epileptic patients. *Brain* 2011;134:2887–97.

Chang N, Gulrajani R, Gotman J. Dipole localization using simulated intracerebral EEG. *Clin Neurophysiol* 2005;116:2707–16.

Chassoux F, Devaux B, Landré E, Turak B, Nataf F, Varlet P, et al. Stereoelectroencephalography in focal cortical dysplasia: a 3D approach to delineating the dysplastic cortex. *Brain* 2000;123:1733–51.

Cosandier-Rimélé D, Merlet I, Bartolomei F, Badier JM, Wendling F. Computational modeling of epileptic activity: from cortical sources to EEG signals. *J Clin Neurophysiol* 2010;27:465–70.

Cosandier-Rimélé D, Bartolomei F, Merlet I, Chauvel P, Wendling F. Recording of fast activity at the onset of partial seizures: depth EEG vs. scalp EEG. *Neuroimage* 2011;59:3474–87.

Duncan JS. Imaging in the surgical treatment of epilepsy. *Nat Rev Neurol* 2010;6:537–50.

Dümpelmann M, Fell J, Wellmer J, Urbach H, Elger CE. 3D source localization derived from subdural strip and grid electrodes: a simulation study. *Clin Neurophysiol* 2009;120:1061–9.

Dümpelmann M, Ball T, Schulze-Bonhage A. sLORETA allows reliable distributed source reconstruction based on subdural strip and grid recordings. *Hum Brain Mapp* 2012;33:1172–88.

Ebersole JS, Pedley TA. Current practice of clinical electroencephalography. 3rd ed. Lippincott Williams and Wilkins; 2003.

Fauser S, Schulze-Bonhage A. Epileptogenicity of cortical dysplasia in temporal lobe dual pathology: an electrophysiological study with invasive recordings. *Brain* 2006;129:82–95.

Fuchs M, Wagner M, Kastner J. Development of volume conductor and source models to localize epileptic foci. *J Clin Neurophysiol* 2007;24:101–19.

Hämäläinen MS, Ilmoniemi RJ. Interpreting magnetic fields of the brain: minimum norm estimates. *Med Biol Eng Comput* 1994;32:35–42.

Jacobs J, Zijlmans M, Zelmans R, Chatillon CE, Hall J, Olivier A, et al. High frequency electroencephalographic oscillations correlate with outcome of epilepsy surgery. *Ann Neurol* 2010;67:209–20.

Jeha LE, Najm I, Bingaman W, Dinner D, Widdess-Walsh P, Lüders H. Surgical outcome and prognostic factors of frontal lobe epilepsy surgery. *Brain* 2007;130:574–84.

Kahane P, Landré E, Minotti L, Francione S, Ryvlin P. The Bancaud and Talairach view on the epileptogenic zone: a working hypothesis. *Epileptic Disord* 2006;8(Suppl. 2):S16–26.

Kim JS, Im CH, Jung YJ, Kim EY, Lee SK, Chung CK. Localization and propagation analysis of ictal source rhythm by electrocorticography. *Neuroimage* 2010;52:1279–88.

Koessler L, Benar C, Maillard L, Badier JM, Vignal JP, Bartolomei F, et al. Source localization of ictal epileptic activity investigated by high resolution EEG and validated by SEEG. *Neuroimage* 2010;51:642–53.

Kovalev D, Spreer J, Honegger J, Zentner J, Schulze-Bonhage A, Huppertz HJ. Rapid and fully automated visualization of subdural electrodes in the presurgical evaluation of epilepsy patients. *AJNR Am J Neuroradiol* 2005;26:1078–83.

Lüders HO, Najm I, Nair D, Widdess-Walsh P, Bingaman W. The epileptogenic zone: general principles. *Epileptic Disord* 2006;8(Suppl. 2):S1–9.

- Michel CM, Murray MM, Lantz G, Gonzalez S, Spinelli L, Grave de Peralta R. EEG source imaging. *Clin Neurophysiol* 2004;115:2195–222.
- Mosher JC, Lewis PS, Leahy RM. Multiple dipole modeling and localization from spatio-temporal MEG data. *IEEE Trans Biomed Eng* 1992;39:541–57.
- Mosher JC, Baillet S, Leahy RM. EEG source localization and imaging using multiple signal classification approaches. *J Clin Neurophysiol* 1999;16:225–38.
- Nair DR, Burgess R, McIntyre CC, Lüders H. Chronic subdural electrodes in the management of epilepsy. *Clin Neurophysiol* 2008;119:11–28.
- Pascual-Marqui RD. Standardized low-resolution brain electromagnetic tomography (sLORETA): technical details. *Methods Find Exp Clin Pharmacol* 2002;24(Suppl. D):5–12.
- Plummer C, Harvey AS, Cook M. EEG source localization in focal epilepsy: where are we now? *Epilepsia* 2008;49:201–18.
- Rullmann M, Anwänder A, Dannhauer M, Warfield SK, Duffy FH, Wolters CH. EEG source analysis of epileptiform activity using a 1 mm anisotropic hexahedra finite element head model. *Neuroimage* 2009;44:399–410.
- Spencer S, Huh L. Outcomes of epilepsy surgery in adults and children. *Lancet Neurol* 2008;7:525–37.
- Zanow F, Knösche TR. ASA-Advanced Source Analysis of continuous and event-related EEG/MEG signals. *Brain Topogr* 2004;16:287–90.
- Zhang Y, van Drongelen W, Kohrman M, He B. Three-dimensional brain current source reconstruction from intra-cranial ECoG recordings. *Neuroimage* 2008;42:683–95.

C. DISCUSSION & PERSPECTIVES

Several outcomes of this experimental work are relevant in the context of this thesis:

1. The further development and refinement of ESL deriving from subdural EEG recordings, a groundbreaking methodology that will serve as an additional tool in the presurgical evaluation of demanding epilepsy surgery cases.
2. The application of source reconstruction in our study delivered anatomically meaningful results that were conform to the conventional analysis of the corresponding spikes, but offered a superior localization regarding deep sources (Figure 6). This observation suggests that the additional use of source localization algorithms may outbalance the shortcomings of a grid evaluation regarding deep sources, thus introducing a surrogate for adjunctive investigations with intracerebral depth electrodes.
3. Although source reconstruction provided electro-clinically valid results in all cases, including those where sampling was less extensive or meticulous, as in the medial and orbitofrontal regions, it is apparent that reliable results are only attainable for brain regions adequately sampled by subdural electrode contacts. The limitation posed to this novel ESL method is, however, counterbalanced by the fact that subdural coverage is carefully chosen to sample the area of interest, as defined by the non-invasive electro-clinical and neuroimaging data.
4. The application of sLORETA to subdural EEG recordings in our study resulted in more widespread activations, whereas MUSIC provided spatially limited solutions. Furthermore, the use of MUSIC resulted in single-value and thus focal solutions for a set time interval, while sLORETA facilitated the illustration of activation over time. The understanding of these properties of our ESL methods is crucial in elucidating incongruent results.
5. The activation volumes resulting from source reconstruction should be appreciated as an approximation of the true extent of the cortical generator and thus cannot be

directly compared either with the volume of resection or between the two source reconstruction algorithms. This is an important aspect of ESL studies that has been addressed in a recent work using a realistic multimodal modeling approach for the evaluation of distributed source analysis, as performed by sLORETA³⁷. This simulation study pointed to an overestimation of source volume by distributed source localization, as applied to both scalp and subdural EEG recordings, particularly for more extensive sources. The choice of the optimal source localization method for this particular setting should be further investigated in the future.

6. The inclusion of modeled sources in the resection strongly correlated with postsurgical seizure freedom, underlining that ESL from subdural EEG could improve tailored resection and surgical outcomes in refractory frontal lobe epilepsy and thus offering the clinical validation of this novel tool. The added value of ESL from subdural EEG will have to be further validated in prospective studies, including variable source extents and localizations.
7. Considering that the delineation of the epileptogenic zone does not derive solely from spikes as a marker of epileptogenicity, the next step will be to apply this new method to ictal discharges and perform a prospective comparison with the conventional analysis in a broader clinical context.

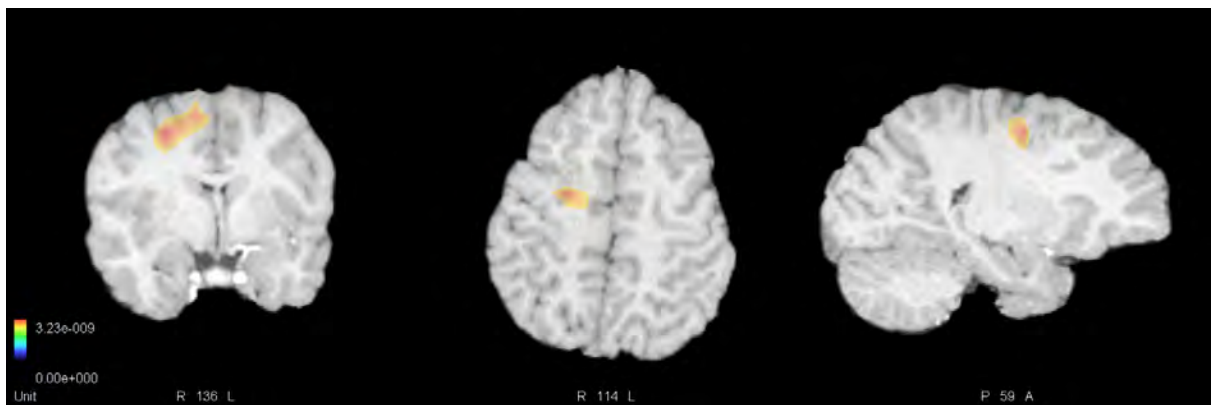


Figure 6: Source localization by SLORETA deriving from subdural EEG recordings, pointing to a cortical source located at the bottom of a sulcus.

2.3 SIMULTANEOUS SUBDURAL AND SCALP EEG CORRELATES OF FRONTAL LOBE EPILEPTIC SOURCES

A. INTRODUCTION

All previous studies in simultaneous intracranial and scalp EEG recordings, both historical and contemporary, have been conducted exclusively in temporal lobe epilepsy. However, extratemporal sources are equally prevalent as temporal sources in pediatric epilepsy surgery and constitute a significant challenge regarding electro-clinical correlations and postsurgical outcomes^{18,19,53}. In particular, frontal lobe epilepsy studies have reported 12–37% of patients without any scalp EEG spikes at all, and a predominance of widespread unilateral or even bilateral spikes in the remaining cases^{54–57}. Focal interictal spikes have been observed in scalp EEG mainly in association with dorsolateral frontal sources, whereas medial and orbitofrontal sources have been reported to give rise to bifrontal spikes, if any, with unilateral, albeit often falsely lateralizing, predominance^{54,57}. Factors contributing to the disparity between scalp EEG spikes and their cortical substrates include the inaccessibility of large parts of the frontal lobe to scalp electrodes, the extent of intralobar and interlobar connections, and the presence of secondary bilateral synchrony. These disparities often render invasive EEG recordings necessary to delineate the epileptogenic zone in refractory frontal lobe epilepsy.

In this study, we aimed to assess the scalp EEG detectability of cortical sources in frontal lobe epilepsy as delineated by subdural EEG recordings. We investigated how the localization, extent, and amplitude of cortical activation affect the presence of simultaneous scalp EEG correlates. We used the same patient group as in study 2¹³, undergoing simultaneous scalp and intracranial EEG recordings, and featuring cortical sources well-characterized through ESL and postsurgical outcomes (Figure 7). Simultaneous scalp and intracranial EEG recordings combined with ESL provide a unique opportunity to study the interrelations between cortical generators and their subdural and scalp correlates. This study is innovative in more than one ways: 1) this is the first study to analyze simultaneous

subdural and scalp EEG recordings in frontal lobe epilepsy to address the issue of cortical substrates for scalp spikes, and 2) this represents the first attempt to use both visual analysis and ESL deriving from subdural EEG recordings in refining the localization and adding a 3D perception of cortical substrates.

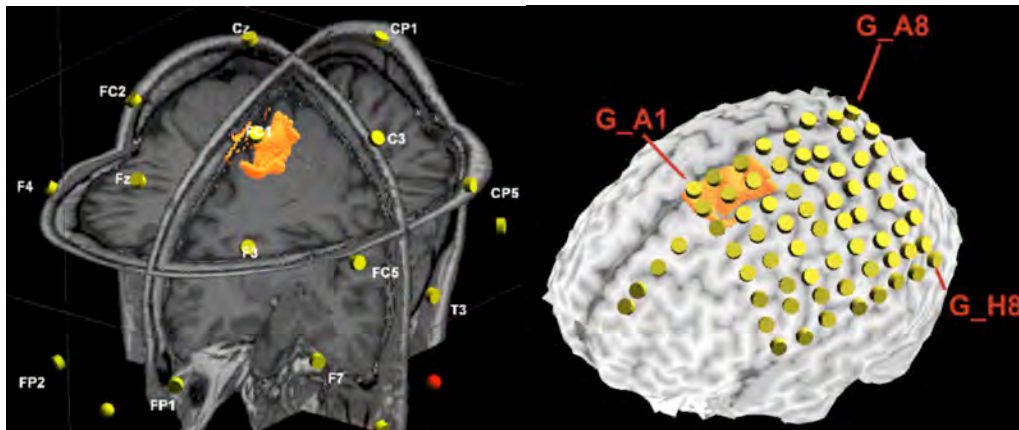


Figure 7: Source reconstruction deriving from subdural recordings and placed in a realistic head model of the patient with superimposed scalp EEG (left) and subdural grid electrode positions (right).

B. SIMULTANEOUS SUBDURAL AND SCALP EEG CORRELATES OF FRONTAL LOBE EPILEPTIC SOURCES

Simultaneous subdural and scalp EEG correlates of frontal lobe epileptic sources

*Georgia Ramantani, *Matthias Dümpelmann, †Laurent Koessler, *Armin Brandt, ‡§Delphine Cosandier-Rimélé, ¶Josef Zentner, *Andreas Schulze-Bonhage, and †#**Louis Georges Maillard

Epilepsia, **(*)1–11, 2014
doi: 10.1111/epi.12512

SUMMARY

Objective: To assess the visibility and detectability in scalp electroencephalography (EEG) of cortical sources in frontal lobe epilepsy (FLE) as to their localization, and the extent and amplitude of activation.

Methods: We analyzed the simultaneous subdural and scalp interictal EEG recordings of 14 patients with refractory frontal lobe epilepsy (FLE) associated with focal cortical dysplasia. Subdural spike types were identified and averaged for source localization and detection of their scalp EEG correlates. Both raw and averaged scalp EEG segments were reviewed for spikes, blinded to subdural segments. We further analyzed the correlation of spike-to-background amplitude ratios in subdural and scalp EEG.

Results: We identified 36 spike types in subdural EEG, corresponding to 29 distinct sources. Four of 29 sources were visible by visual evaluation of scalp EEG and six additional sources were detectable after averaging: four in the medial frontal, two in the dorsolateral gyri, two in the depth of dorsolateral sulci, and two in the basal frontal region. Cortical sources generating scalp-detectable spikes presented a median of 6 cm² of activated cortical convexity surface and a subdural spike-to-background-amplitude ratio >8. These sources were associated with a higher number of activated subdural grid contacts and a higher subdural spike-to-background amplitude ratio than sources generating non-scalp-detectable spikes.

Significance: Not only dorsolateral but also basal and medial sources can be detectable in FLE. This is the first in vivo demonstration derived from simultaneous subdural and scalp EEG recordings of the complementary significance of extensive source activation and higher subdural spike-to-background amplitude ratio in the detection of cortical sources in FLE.

KEY WORDS: Source localization, Intracranial recordings, Refractory epilepsy.



Dr. Georgia Ramantani is a child neurologist at the Epilepsy Center, University Hospital Freiburg, Germany.

Several in vitro, in vivo, and simulation studies have been conducted to clarify the interrelations of scalp and intracranial electroencephalography (EEG) findings (Abraham &

Marsan, 1958; Cooper et al., 1965; Ebersole, 1997; Kobayashi et al., 2005; Tao et al., 2005, 2007; Cosandier-Rimélé et al., 2008). This issue is of cardinal importance in epilepsy management, with scalp EEG constituting a major localizing tool from the primary diagnosis and epilepsy classification to the planning of an intracranial investigation or of a resection in a refractory course. It is noteworthy that previous in vivo studies, both historic and contemporary, have been conducted exclusively in temporal lobe epilepsy (TLE; Abraham & Marsan, 1958; Tao et al., 2005; Ray et al., 2007; Tao et al., 2007). Therefore, there is an imperative need to extend these observations to extratemporal and particularly to frontal lobe epilepsy (FLE), which constitutes a challenge regarding both electroclinical correlations

Accepted November 14, 2013.

*Epilepsy Center, University Hospital Freiburg, Freiburg, Germany; †Research Center for Automatic Control (CRAN), University of Lorraine, CNRS, UMR 7039, Vandoeuvre, France; ‡INSERM UMR 1099, Rennes, France; §University of Rennes 1, LTSI, Rennes, France; ¶Department of Neurosurgery, University Hospital Freiburg, Freiburg, Germany; #Department of Neurology, Central University Hospital, CHU de Nancy, Nancy, France; and **Medical Faculty, University of Lorraine, Nancy, France

Address correspondence to Georgia Ramantani, Epilepsy Center, University Hospital Freiburg, Breisacher Str. 64, 79106 Freiburg, Germany. E-mail: georgia.ramantani@uniklinik-freiburg.de

Wiley Periodicals, Inc.

© 2014 International League Against Epilepsy

(Quesney et al., 1992; Salanova et al., 1993; Bautista et al., 1998) and epilepsy surgery outcomes (Englot et al., 2012).

FLE studies have indeed reported 12–37% of patients without any interictal scalp EEG spikes at all, and a predominance of widespread unilateral or bilateral interictal spikes in the remaining cases (Quesney et al., 1992; Salanova et al., 1993; Bautista et al., 1998; Elsharkawy et al., 2008). Focal interictal spikes have been observed in scalp EEG recordings, mainly in association with dorsolateral frontal sources, whereas medial and orbitofrontal sources have been reported to give rise to bifrontal spikes, if any, with unilateral, albeit often falsely lateralizing, predominance (Quesney et al., 1992; Bautista et al., 1998; Smith et al., 2004). Factors contributing to the disparity between scalp EEG spikes and their cortical substrates include the inaccessibility of large parts of the frontal lobe to scalp electrodes, the extent of intralobar and interlobar connections, and the presence of secondary bilateral synchrony (Kellinghaus & Lüders, 2004).

As a result of this disparity, intracranial recordings still remain mandatory to localize the cortical sources of interictal and ictal discharges in refractory FLE (Englot et al., 2012). In a recent study, we showed that electrical source localization (ESL) derived from subdural interictal EEG spikes in FLE can improve the accuracy of cortical generator localization, both in terms of gyral and deep sulcal resolution (Ramantani et al., 2013b). Simultaneous scalp and intracranial EEG recordings combined with ESL provide a unique opportunity to study the interrelations between cortical generators and their subdural and scalp correlates.

In this study, we aimed to assess the scalp EEG detectability of cortical sources in FLE as delineated by subdural EEG recordings. For this purpose, we retrospectively compared the localization, extent, and amplitude of cortical activation as to the presence of simultaneous scalp EEG correlates. We chose to investigate patients with epilepsy associated with focal cortical dysplasia (FCD; Bast et al., 2006), the prevailing etiology in refractory FLE.

PATIENTS AND METHODS

Patients

Fourteen patients with refractory FLE associated with FCD and (1) extensive intracranial coverage of the frontal lobe with subdural grid and strip electrodes, (2) simultaneous scalp EEG recordings, (3) technically flawless interictal recording segments of >30 min in calm wakefulness, and (4) clinically validated ESL (Ramantani et al., 2013a), were included in this study. Patients with substantial intracranial hemorrhage or skull defect were excluded. The patient group comprised five male and nine female patients, aged 14–50 years (mean 30). The study was granted approval by the institutional research ethics board. All patients gave their written informed consent.

Methods

EEG recordings and electrode positions

Grid and strip electrode description, placement, and positions were previously reported (Ramantani et al., 2013b). The coverage and number as well as the gyral localization of subdural electrode contacts are given in Table 1.

Simultaneous scalp EEG recordings with electrodes placed according to the 10–20 system (Koessler et al., 2009) using sterile procedures were also available. Occasionally, 1–2 electrodes were slightly displaced from their standard positions to avoid the surgical scars and local edema, usually near the scalp incision in the frontocentral region.

Simultaneous scalp and subdural EEG recordings were obtained using a Neurofile NT digital video-EEG system (Ramantani et al., 2013b).

Interictal spike detection, selection, and analysis

Subdural EEG segments of >30 min in calm wakefulness were carefully chosen to include an adequate number of interictal spikes and avoid ictal events or preictal changes. Sharp transients that appeared less than three times in selected segments, as well as segments of polyspikes (>2 spikes in 200 msec) and activity in the beta or gamma range were visually detected and excluded.

The resulting segments were reviewed using both bipolar and referential montages, and interictal spikes were identified according to the International Federation of Societies for Electroencephalography and Clinical Neurophysiology (1983) recommendations and marked at the time point of their highest amplitude. In view of the multitude of identified interictal spikes, *spike types* were defined to describe spikes of similar spatiotemporal distribution that were presumed to correspond to a single generator. Each spike type was topographically characterized by (1) the dominant contact with maximum amplitude, as defined in a referential montage (Tables 1 and 2), and (2) the amplitude ratio between the spike peak and the mean background activity, calculated in an interval of (–500; –250) and (+250; +500) msec around the peak (Table 2). Subdural EEG spikes of the same type were subsequently averaged to serve for (1) ESL, and (2) detection of their scalp EEG correlates. ESL performed by MUSIC (MULTiple SIGNAL Classification; Mosher et al., 1992, 1999) and sLORETA (standardized low-resolution brain electromagnetic tomography; Hämäläinen and Ilmoniemi, 1994; Pascual-Marqui, 2002) was applied to refine the information obtained by visual analysis of subdural spikes and thus served as the reference for localizing their cortical sources, according to the topography of the activation maximum.

Simultaneous scalp and subdural EEG raw segments were separately and independently analyzed by two experienced epileptologists (GR, LGM). In a first step, interictal spikes were annotated in scalp and subdural EEG recordings. Overall, 21–576 spikes (median 194), corresponding to 3–463 (median 91) spikes of each designated spike type, were

Table 2. Characteristics of cortical sources in all 14 patients with frontal lobe epilepsy, including their anatomic localization, the localization of dominant contacts, the number of subdural contacts involved in the electrical field, the amplitude and spike-to-background amplitude ratio of subdural EEG spikes, the visibility of their scalp EEG correlates, the number of averaged subdural EEG spikes of each spike type, and the resulting detectability of their scalp EEG correlates as well as the amplitude and spike-to-background amplitude ratio of corresponding scalp EEG spikes. The numbers in column 1 refer to the corresponding patients, as presented in Table 1

Sources	Sublobar localization of dominant subdural contacts	Number of subdural contacts		Subdural EEG spike amplitude (μ V)	Subdural spike to background amplitude ratio	Raw scalp EEG visibility	Number of averaged subdural EEG spikes	AVG scalp EEG detectability	Simultaneous scalp EEG spike amplitude, μ V	Scalp EEG spike to background amplitude ratio
		Dorsolateral	Medial/basal							
Medial frontal sources										
3/R premotor medial SFG	Medial premotor	3	2	93	8.2	No events	143	No events	8	0.4
5/L premotor medial SFG	Medial premotor	4	6	197	9.8	No events	97	C4/Fz/Cz		
8/L premotor medial SFG	Medial premotor	6	2	226	20.3	No events	18	No events	5	1.9
9/L premotor medial SFG	Medial premotor	8	2	145	51.0	No events	463	C3/Cz/Pz/P3		
5/L prefrontal medial SFG	Lateral dorsal prefrontal	5	4	252	14.0	No events	97	No events	4	0.5
10/L motor cingulate gyrus	Medial prefrontal/anterior cingulate	3	3	150	15.6	No events	141	Cz		
11/L anterior cingulate gyrus	Anterior cingulate	4	4	257	17.1	No events	117	No events		
	Anterior cingulate	6	6	165	4.4	No events	44	No events		
	Lateral dorsal prefrontal	2	2	380	13.0	No events	32	Fp2/F4/C4/Fz/Cz/Pz	50	1.2
Basal/orbitofrontal sources										
2/R basal lateral/OF	Lateral ventral prefrontal/basal OF	2	2	154	8.3	No events	111	No events		
3/R basal lateral/OF	Basal OF	2	2	207	24.2	No events	177	No events		
	Lateral ventral prefrontal	3	3	269	19.1	No events	158	No events		
12/L lateral basal/polar/OF	Basal OF	4	4	274	21.5	No events	22	No events		
12/L medial basal/polar/OF	Basal OF	3	3	141	9.7	FPI/F7	70	FPI/F7/T3	6	0.4
14/L medial basal OF	Basal OF	4	4	143	7.8	No events	157	FPI/F7/T3	11	0.7
Dorsolateral sulcal sources										
9/L motor depth of central sulcus	Lateral primary motor	4	4	276	19.7	No events	10	No events		
7/R motor depth of central sulcus	Lateral primary motor	5	5	160	16.8	No events	55	No events		
1/R premotor depth of SFS	Lateral premotor	7	7	178	11.4	No events	21	No events		
7/R premotor depth of SFS	Lateral premotor	6	6	223	5.1	No events	5	No events		
8/L premotor depth of SFS	Lateral premotor	2	2	43	3.0	No events	18	No events		
	Lateral premotor	5	5	341	28.9	Cz/Pz/C3/P3	40	Pz/Cz/C3/P3/F3	19	2.0
4/R prefrontal depth of SFS	Medial premotor	4	4	203	18.9	No events	16	Cz/C3/Pz	12	1.4
	Lateral dorsal/medial prefrontal	2	2	187	4.7	No events	331	No events		
8/L prefrontal depth of SFS	Lateral dorsal prefrontal	7	7	268	12.1	No events	32	No events		
14/L prefrontal depth of SFS	Lateral ventral prefrontal	2	2	254	16.5	No events	138	No events		
	Medial prefrontal	2	2	115	3.9	No events	28	No events		

Continued

Table 2. Continued.

Sources	Sublobar localization of dominant subdural contacts	Number of subdural contacts		Subdural EEG		Raw scalp EEG visibility	Number of averaged subdural EEG spikes	AVG scalp EEG detectability	Simultaneous scalp EEG spike amplitude, μ V	Scalp EEG spike to background amplitude ratio
		Dorsolateral	Medial/basal	Subdural EEG spike amplitude (μ V)	Subdural EEG spike to background amplitude ratio					
13/R prefrontal dorsal lateral SFS	Medial prefrontal	8	4	116	39.4	No events	161	Fz	4	1.4
7/R prefrontal depth of IFS	Lateral dorsal prefrontal	5	3	616	27.2	Fz	395	Fz/Cz	5	0.3
Dorsolateral gyral sources	Lateral premotor	6		108	7.1	No events	18	No events		
2/R central operculum	Operculum	4		193	4.2	No events	30	No events		
3/R central operculum	Primary motor operculum	2		255	8.2	No events	15	No events		
2/R premotor operculum	Operculum	6		198	19.0	No events	183	No events		
6/R premotor lateral in MFG	Lateral premotor	8		162	20.0	No events	172	C4/C3/Cz/Pz/P3/P4	6	1.0
10/L prefrontal MFG	Lateral dorsal prefrontal	2		203	5.6	No events	8	No events		
12/L lateral/ventral/polar MFG	Lateral dorsal/ventral prefrontal	2		248	16.4	No events	4	No events		
13/R prefrontal dorsal lateral SFG	Lateral dorsal prefrontal	8	5	538	65.7	Fz/Cz	20	Fz	14	1.5

AVG, average; SFG, superior frontal gyrus; SFS, superior frontal sulcus; OF, orbito-frontal region; IFS, inferior frontal sulcus; MFG, middle frontal gyrus.

patient (range 1–5), corresponding to 29 distinct cortical sources (Table 2). All sources were localized within subdural electrode coverage. Seven sources were localized in the medial frontal gyri (Fig. 1), seven in dorsolateral gyri, 10 in the depth of dorsolateral sulci (Fig. 2), and five in the basal or orbitofrontal gyri (Fig. 3).

Twenty-eight of 29 sources were adjacent to the dominant subdural contact. However, 5 of these 28 sources also corresponded to an additional spike type with a dominant subdural contact remote to the source. Three of these five sources were localized in the depth of the superior frontal sulcus and generated spikes visible on both lateral and medial subdural contacts, one was localized in the orbitofrontal region and generated spikes visible on both basal and lateral ventral contacts, and one was located in the anterior cingulate gyrus and generated spikes visible on both medial and lateral contacts. The only source fully remote from the dominant contact was localized in the medial aspect of the superior frontal gyrus, whereas the dominant contact was lateral prefrontal (Table 2).

Source visibility and detectability in scalp EEG in relation to their localization

Only 4 of 29 cortical sources produced spikes *visible* by routine visual evaluation of simultaneous raw scalp EEG recordings (Table 2): two sources localized in the superior frontal sulcus, one in the superior frontal gyrus, and one in the orbitofrontal region (Figs. 2 and 3).

After averaging, 10 of 29 (six additional) sources were *detectable*: 4 of 7 in the medial frontal, 2 of 7 in the dorsolateral gyri, 2 of 10 in the depth of dorsolateral sulci, and 2 of 5 in the basal-frontal regions (Table 2). Two of four detectable medial frontal sources were localized in the premotor medial aspect of the superior frontal gyrus, and two in the cingulate gyrus (Fig. 1); none were visible before averaging. One of two detectable dorsolateral gyral sources was localized in the superior frontal gyrus and was visible before averaging, and one was localized in the middle frontal gyrus and was not visible before averaging. Both detectable dorsolateral sulcal sources were localized in the depth of the superior frontal sulcus (Fig. 2) and were visible before averaging. Both detectable frontobasal sources were localized in the medial polar orbitofrontal cortex, and one was visible before averaging (Fig. 3).

Source detectability in scalp EEG in relation to the extent and amplitude of dorsolateral cortical activation

Subdural EEG spikes detectable in simultaneous scalp EEG presented a 116–616 μ V amplitude and an 8–66 spike-to-background amplitude ratio. The number of subdural grid contacts involved in scalp-detectable cortical spikes were 0–14 (median 6), thus roughly corresponding to a cortical convexity activation of 0–14 cm². In contrast, subdural EEG spikes not detectable in scalp EEG presented a

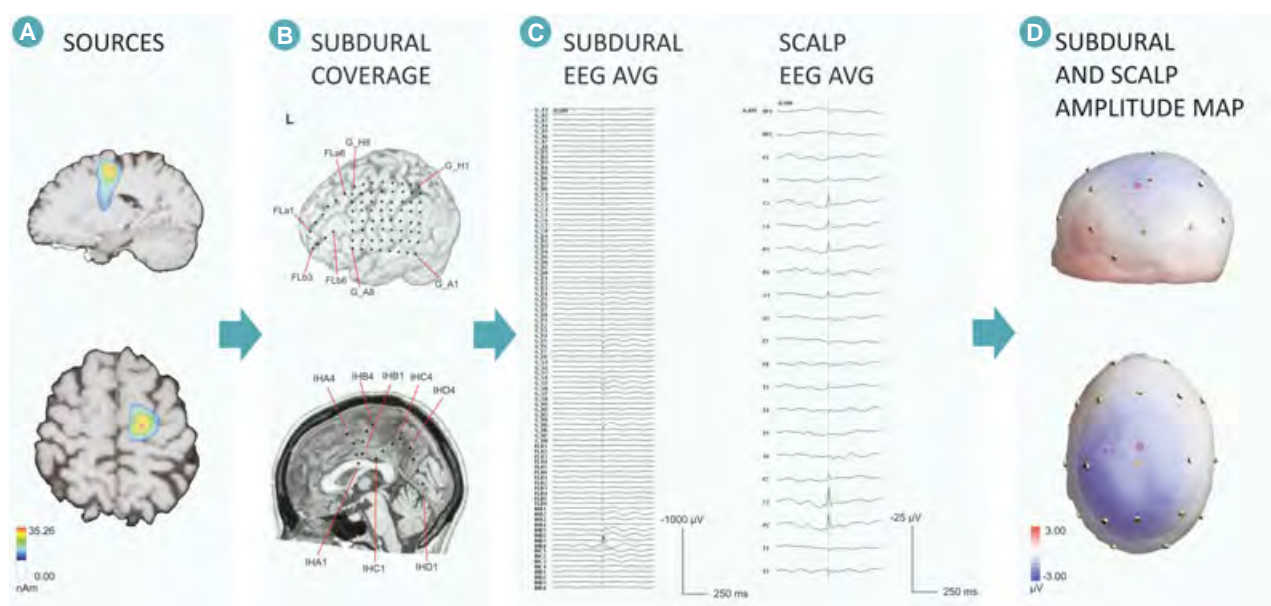


Figure 1.

Patient 9, with a premotor source localized in the medial part of the left superior frontal gyrus. Illustration of the source reconstruction by MUSIC (A), the subdural electrode coverage (B), subdural EEG and scalp EEG averaged spikes (C), and the 3D overlay of the subdural and scalp amplitude map (D), with the sphere diameters corresponding to the amplitude of the subdural EEG spike. The subdural EEG average, presenting an activation of six dorsolateral and two medial contacts, corresponds to a bilateral frontocentral averaged scalp EEG spike, with the highest amplitude in electrodes Cz/Pz/C3/P3.

Epilepsia © ILAE

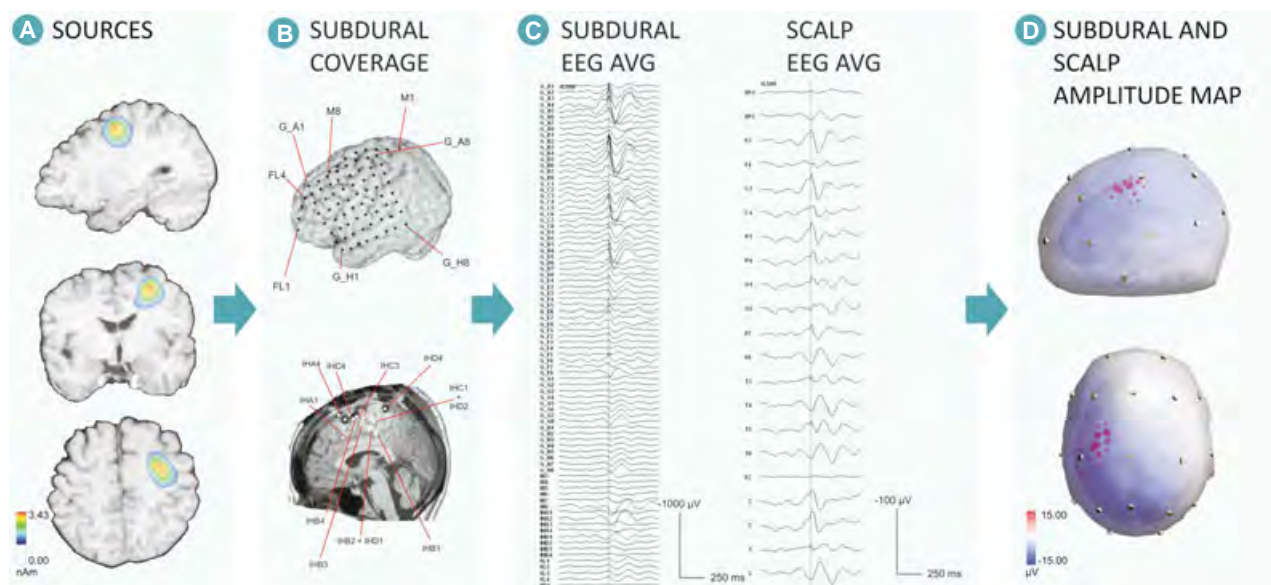


Figure 2.

Patient 8, with a dorsolateral premotor source localized in the depth of the left superior frontal sulcus. Illustration of the source reconstruction by MUSIC (A), the subdural electrode coverage (B), subdural EEG and scalp EEG averaged spikes (C), and the 3D overlay of the subdural and scalp amplitude map (D), with the sphere diameters corresponding to the amplitude of the subdural EEG spike. The subdural EEG average, presenting an activation of 11 dorsolateral subdural contacts, corresponds to a left and medial frontocentral and parietal averaged scalp EEG spike, with the highest amplitude in electrodes Cz/Pz/F3/C3/P3.

Epilepsia © ILAE

43–276 μV amplitude range and a 3–24 spike-to-background amplitude ratio and involved 0–8 subdural grid contacts (median 2).

The number of activated subdural grid contacts and the subdural spike-to-background amplitude ratio were significantly higher ($p < 0.001$ and $p = 0.002$, respectively) for

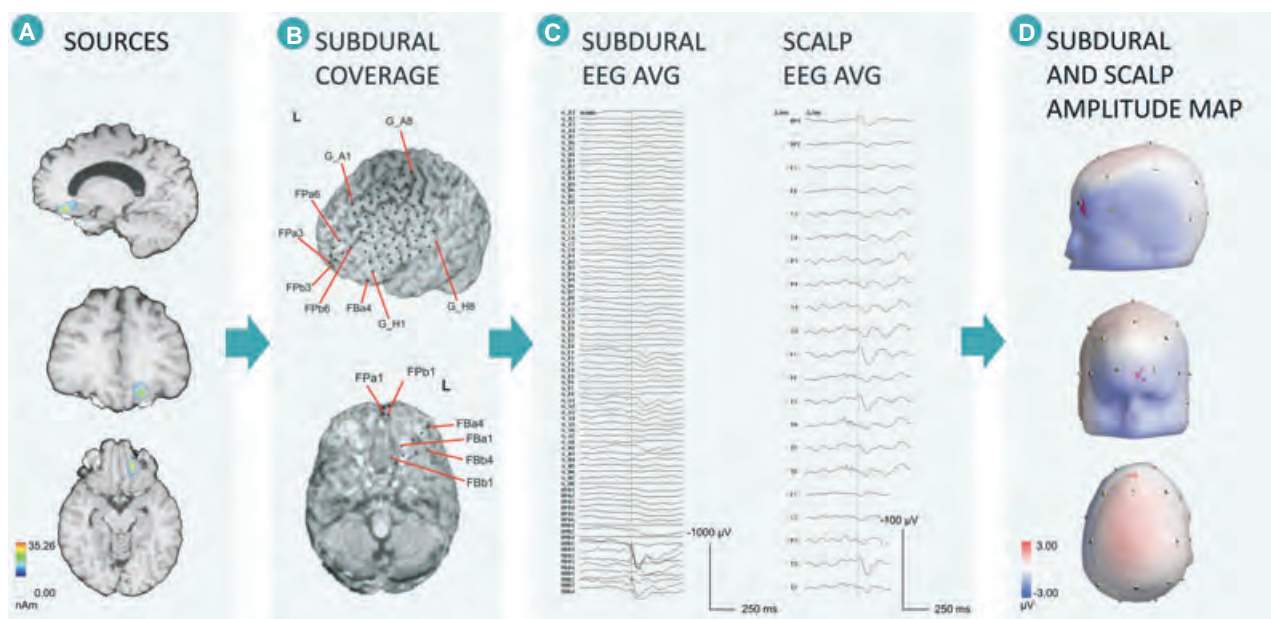


Figure 3.

Patient 12, with a mesial orbitofrontal source localized in the medial and polar part of the left orbitofrontal cortex. Illustration of the source reconstruction by MUSIC (A), the subdural electrode coverage (B), subdural EEG and scalp EEG averaged spikes (C), and the 3D overlay of the subdural and scalp amplitude map (D), with the sphere diameters corresponding to the amplitude of the subdural EEG spike. The subdural EEG average, presenting an activation of four frontobasal subdural contacts, corresponds to a bilateral left predominant frontopolar, basal and temporal scalp EEG average spike, with the highest amplitude in electrodes Fp1, F7, T3.

Epilepsia © ILAE

sources generating scalp-detectable spikes compared to sources generating no scalp-detectable spikes. The respective subdural and scalp spike-to-background amplitude ratios of scalp-detectable spikes were strongly correlated (Fig. S1; $p = 0.002$). Furthermore, the amplitude of averaged scalp-detectable spikes was related to the number of activated grid contacts ($p < 0.001$).

Spatial distribution of detectable cortical sources in scalp EEG

All four detectable medial frontal sources (two in the cingulate gyrus and two in the medial part of the superior frontal gyrus) projected to midline dominant scalp electrodes (Cz in four cases with additional Fz and Pz in two cases). Additional ipsilateral or contralateral frontocentral scalp electrodes were involved in one and two cases, respectively. Both orbitofrontal sources generating scalp-detectable spikes (Fig. 3) projected to ipsilateral frontopolar and temporal electrodes (Fp1, F7, T3). Moreover, detectable dorso-lateral sources localized in the superior frontal gyrus or in the superior frontal sulcus projected to midline electrodes (Fz, Cz, or Pz) in all three cases and involved additional ipsilateral frontal-centroparietal electrodes (F3, C3, P3) in one case (Fig. 2). The remaining detectable gyral dorso-lateral source localized in the middle frontal gyrus and projected to additional bilateral centroparietal scalp electrodes. In this last case, a careful analysis of the temporal dynamics of the scalp spike showed a 20 msec delay

between the spikes recorded on C3 and C4, thus suggesting that the right scalp spike was related to propagation rather than to volume conduction from the left middle frontal gyrus source to the contralateral scalp electrodes.

DISCUSSION

The identification of the cortical sources of EEG constitutes a fundamental issue in electrophysiology, and the matching of scalp signals to their cortical substrates is an important key in decoding these complex source-signal interrelations (Abraham & Marsan, 1958; Tao et al., 2005, 2007). To our knowledge, our study is the first to analyze simultaneous subdural and scalp EEG recordings in FLE to address the issue of cortical substrates for scalp spikes. Furthermore, this represents the first attempt to use both visual analysis and ESL of subdural EEG recordings in refining the localization and adding a three-dimensional (3D) perception of cortical substrates.

Visibility of sources in raw scalp EEG

In our study, we showed that most frontal lobe sources failed to generate scalp-visible spikes. Indeed, only 14% sources had scalp EEG correlates *visible* in routine analysis. This is much lower than the 63–88% rates previously reported in nonsimultaneous subdural- and scalp-EEG recordings (Quesney et al., 1992; Salanova et al., 1993; Bautista et al., 1998; Elsharkawy et al., 2008). This cannot

be attributed to the limited spatial 10–20 scalp-sampling that was also applicable to all previous studies. This discrepancy may be due to a selection bias related to the improved magnetic resonance imaging (MRI) detection of epileptogenic lesions such as FCD nowadays. These patients may present more spatially limited irritative zones, less likely to generate interictal EEG scalp spikes *visible* in routine interpretation. Moreover, this discrepancy is largely related to methodologic issues, since past studies compared the results of nonsimultaneous scalp- and subdural-EEG recordings, thus preventing accurate spatial correlations between the cortical substrates of scalp and subdural spikes, while increasing the probability of sampling interictal spikes. On the other hand, in simultaneous scalp- and subdural-EEG recordings, the attenuation effect of the silastic membrane of the grid may account for lower spike visibility (Lanfer et al., 2013). However, this effect has been minimized in our study by carefully inspecting and selecting scalp EEG segments for the absence of amplitude asymmetry.

In line with previous reports (Quesney et al., 1992; Salanova et al., 1993; Bautista et al., 1998), three of four scalp-visible interictal EEG spikes in our study corresponded to sources localized in the *lateral* convexity, particularly in the superior frontal sulcus or superior frontal gyrus. Only one case of a scalp-visible interictal EEG spike corresponded to a *medial* orbitofrontal and polar source.

Overall detectability of sources in averaged scalp EEG

After averaging of subdural interictal EEG spikes, six additional sources were rendered *detectable* in scalp-EEG. Averaging allows increasing the signal-to-noise ratio by attenuating the background activity and thus the contribution of nonpileptic cortical sources (Abraham & Marsan, 1958). This suggests that the very low visibility of FLE interictal sources is partly linked to cortical activity generated in adjacent regions (Ramantani et al., 2006). The significance of this was emphasized recently in a study using a realistic model of cortical and scalp EEG generation at seizure onset (Cosandier-Rim  l   et al., 2012). Our study is the first to quantitatively assess this parameter *in vivo*, in the context of FLE. The elimination of background activity revealed not only medial or basal frontal but also dorsolateral cortical sources that would otherwise be undetectable in scalp EEG. However, it should be noted that averaging did not enhance detectability when applied to <10 subdural EEG spikes, as was the case in three spike types corresponding to dorsolateral cortical sources.

It is important to note that in our study, there were no systematically detectable or undetectable cortical source localizations. Indeed, even spikes originating from sources adjacent to the convexity may be missed by scalp recordings. Conversely, 8 of 22 sources in the medial frontal gyri, in the depth of dorsolateral sulci, or in the orbitofrontal cortex were detectable, whereas these regions have been reported to generate spikes escaping routine scalp EEG

interpretation (Quesney et al., 1992; Salanova et al., 1993; Bautista et al., 1998; Smith et al., 2004). The detectability of mesial frontal as well as orbitofrontal sources may be partly attributed to the breach effect of the overlying craniotomy in simultaneous scalp- and subdural-EEG recordings. However, this still constitutes an important finding, especially since we have largely counteracted this effect by ruling out patients with substantial skull defects.

Detectability and scalp EEG correlates of medial frontal sources

Two of four medial detectable sources were located in the medial premotor aspect of the superior frontal gyrus, and two in the cingulate gyrus. Sources restricted to medial frontal lobe structures are believed to be less detectable due to the horizontal orientation of resulting neuronal currents and the distance to the frontocentral scalp electrodes (Bautista et al., 1998). In our study, however, these sources did not present a lower detectability compared to lateral convexity sources. Three medial detectable sources were located in the premotor areas, including the mid-cingulate motor cortex. The specific cytoarchitectonic characteristics of this agranular cortex—and especially of the mid-cingulate cortex, with a high density of pyramidal cells in layer V (Vogt et al., 2003), as well as its highly functional cortico-cortical connections facilitating the rapid spread of epileptic discharges, may account for this detectability (Matsumoto et al., 2007). All detectable medial sources had a common projection on midline electrodes, reflecting the fact that their spatial geometry was not purely vertical, but corresponded to a more complex 3D configuration involving the banks of medial sulci, such as the cingulate sulcus. These sources involved additional frontocentral scalp electrodes in three cases: these were either ipsilateral, or contralateral and falsely lateralized, in line with previous reports (Quesney et al., 1992; Salanova et al., 1993; Bautista et al., 1998; Smith et al., 2004; Elsharkawy et al., 2008).

Detectability and scalp EEG correlates of orbitofrontal sources

Another two detectable sources were orbitofrontal, of altogether five sources localized in this region. Sources restricted to medial orbitofrontal structures have been presumed undetectable in scalp EEG recordings, due to the vertical orientation of the neuronal currents and the resulting equivalent dipole, the distance to the overlying frontal scalp electrodes, and the absence of recording contacts below the orbitofrontal plane (Gavaret et al., 2006). However, this latter study derived from nonsimultaneous scalp and intracerebral EEG recordings. In our study, subdural EEG spikes corresponding to both detectable orbitofrontal sources were restricted to basal strip electrodes, lacking concomitant grid activation, and thus rendering propagation to the lateral convexity improbable. This observation strongly suggests that sources restricted to the medial

orbitofrontal cortex can be detectable in scalp EEG, in line with a previously reported case of orbitofrontal spikes recorded by depth-electrode contacts occurring simultaneously with scalp-visible spikes (Merlet & Gotman, 1999). Of interest, both detectable orbitofrontal sources had a common projection to ipsilateral frontotemporal electrodes (Fp1, F7, T3), as reported for two of four patients with orbitofrontal epilepsy in a previous study (Smith et al., 2004). The previously described bifrontal pattern in relation to orbitofrontal sources (Ludwig et al., 1975; Merlet & Gotman, 1999; Smith et al., 2004) was not observed in our study.

Detectability and scalp EEG correlates of dorsolateral sulcal or gyral sources

Overall, 4 of 17 dorsolateral sources generated scalp-detectable spikes, including 2 of 7 gyral and 2 of 10 sulcal sources. The comparable detectability of gyral and sulcal dorsolateral sources in our study is in contrast to the perception that gyral sources with their predominantly radial voltage fields present optimal scalp EEG detectability, whereas sulcal sources with their predominantly tangential voltage fields are less detectable in scalp EEG. This lack of predominance of gyral sources in terms of scalp EEG detectability may be partly attributed to their more pronounced attenuation by the silastic membrane of the grid, compared to deeper sources (Lanfer et al., 2013). Therefore, considering the gyral dorsolateral sources, the only source localized in the superior frontal gyrus and one of three sources in the middle frontal gyrus, but none of the opercular sources, were detectable. Considering sulcal dorsolateral sources, both sources located in the superior frontal sulcus, but none in the inferior frontal and central sulcus, were detectable. Moreover, detectable sources localized in the superior frontal gyrus or in the superior frontal sulcus projected to dominant midline electrodes (Fz, Cz, Pz) in all three cases and involved additional lateralized frontal-centroparietal scalp electrodes in one case. The remaining detectable gyral dorsolateral sources were localized in the middle frontal gyrus and projected to additional bilateral centroparietal scalp electrodes. Altogether, sources lateral to the superior frontal gyrus projected to both midline and lateral scalp electrodes that were ipsilateral rather than falsely lateralizing, in contrast to medial sources. Finally, contrary to the common perception of predominantly widespread interictal spikes in FLE (Kellinghaus & Lüders, 2004), these were limited to three or fewer scalp electrodes in the majority of detectable sources. This may be attributed to the enhanced detectability of spatially limited sources after averaging. Indeed, these sources may have been overlooked in previous studies that relied on only routine visual interpretation.

Source visibility and detectability according to the extent and amplitude of dorsolateral cortical activation

In our study, the majority of interictal spikes recorded from subdural electrodes were not *detectable* in the simulta-

neous scalp EEG after averaging, regardless of source localization. This underscores the contribution of parameters other than source localization, including the extent and amplitude of cortical activation, to the interrelations between intracerebral sources and their scalp correlates. We specifically addressed the contribution of the extent and amplitude of cortical activation to the scalp EEG correlates of sources projecting to dorsolateral grid electrode contacts. No assessment of this particular contribution for the generation of scalp-EEG spikes has been undertaken in the context of FLE to date. The extent of cortical activation can be roughly estimated from the number of activated contacts, and the amplitude of cortical activation can be estimated from the subdural spike-to-background amplitude ratio, provided that a neocortical source is adjacent to and covered by the subdural grid electrodes (Abraham & Marsan, 1958; Tao et al., 2005). In the present study, we showed that both the number of activated subdural grid contacts and the spike-to-background amplitude ratio were significantly higher for sources generating scalp-detectable spikes. The median cortical activation extent of 6 cm² corresponding to scalp-detectable sources in our study is comparable to the seminal *in vitro* estimation in the absence of background activity (Cooper et al., 1965) that has been widely cited and partly corroborated by simulation studies (Kobayashi et al., 2005). It is, however, lower than the 10–20 cm² cortical activation extent derived from more recent *in vivo* and *in vitro* studies in TLE (Tao et al., 2005; Cosandier-Rimele et al., 2008). The discrepancy of our estimates to the latter values may be partly attributed to the variable lobar localization considered in each of the two *in vivo* studies (Cooper et al., 1965; Tao et al., 2005). However, it most probably underscores the difference between sources that are *visible* in routine visual interpretation and sources that are *detectable* only after averaging, resulting from the interaction between the cortical activation extent and the blurring effect of the surrounding cortical activity (Tao et al., 2005). In our study, averaging indeed attenuated the blurring effect of the background activity and thus probably enhanced the detectability of spatially limited cortical sources. We further showed that the subdural spike-to-background amplitude ratios were significantly higher for sources generating scalp-detectable spikes and established a strong correlation between the spike-to-background amplitude ratios of subdural and scalp spikes, thus demonstrating the significance of cortical spike amplitude on source detectability.

Limitations of the study

With the disparity between scalp and subdural EEG recordings partly accounted for by the impedance of the dura, skull, and scalp, there are two further technical issues constituting inherent limitations in establishing accurate correlations. Although the bone flap was carefully replaced following the implantation of the subdural grid electrodes, the craniotomy could produce a breach effect resulting in

higher amplitudes of scalp EEG potentials through the abolition of spatial filtering by skull bone. On the other hand, the silastic membrane of the subdural grid constitutes an additional layer over the cortical areas of interest that could result in further attenuation of scalp signals (Lanfer et al., 2013). Because both conditions would result in either enhancement or local attenuation of both epileptic interictal spikes and background activity in scalp EEG, segments were carefully inspected and selected for the absence of amplitude asymmetry. Furthermore, as mentioned in the Methods section, patients with significant skull defects or those with subdural or epidural hemorrhage interfering with the quality of the recordings were excluded. Nonetheless, despite inherent limitations, simultaneous scalp and subdural recordings offer a unique chance to study the correlations of scalp EEG spikes with their cortical substrates in epilepsy patients, taking advantage of the superior spatial resolution of subdural grids.

CONCLUSION

Our study showed that not only dorsolateral but also orbitofrontal and medial-frontal sources can be detectable in scalp EEG. This work constitutes the first in vivo demonstration based on simultaneous subdural and scalp EEG recordings and the first quantitative assessment of the complementary significance of extensive source activation and higher subdural spike-to-background amplitude ratio in the detection of epileptic generators in FLE. This contributes to the decoding of interrelations between cortical sources and their scalp EEG correlates. The appreciation of these interrelations is indeed of cardinal importance for the development and validation of new diagnostic tools such as electrical source localization derived from scalp EEG, magnetoencephalography (MEG), or EEG–functional MRI (fMRI) that may constitute a surrogate for invasive recordings in the future (Bast et al., 2005; Koessler et al., 2010; Jacobs et al., 2013). This is particularly relevant for FCD that represents the main substrate of surgically remediable neocortical partial epilepsy (Bast et al., 2006). Indeed, surgical outcomes in FCD-associated epilepsy, contrary to other cortical malformations (Ramantani et al., 2013a), are strongly related to the complete removal of the epileptogenic lesion that can be reliably localized by the analysis of its interictal activity.

ACKNOWLEDGMENTS

The authors would like to express their gratitude to the medical technicians of the Epilepsy Center Freiburg (Carolin Gierschner, Andre Haak, Christiane Lehmann, Anika Schinkel, Verena Schulte, and Mandy Wenzel) for their valuable assistance.

DISCLOSURE

None of the authors has any conflict of interest to disclose. We confirm that we have read the Journal's position on issues involved in ethical publication and affirm that this report is consistent with those guidelines.

REFERENCES

- Abraham K, Marsan CA. (1958) Patterns of cortical discharges and their relation to routine scalp electroencephalography. *Electroencephalogr Clin Neurophysiol* 10:447–461.
- Bast T, Ramantani G, Boppel T, Metzke T, Ozkan O, Stippich C, Seitz A, Rupp A, Rating D, Scherg M. (2005) Source analysis of interictal spikes in polymicrogyria: loss of relevant cortical fissures requires simultaneous EEG to avoid MEG misinterpretation. *Neuroimage* 25:1232–1241.
- Bast T, Ramantani G, Seitz A, Rating D. (2006) Focal cortical dysplasia: prevalence, clinical presentation and epilepsy in children and adults. *Acta Neurol Scand* 113:72–81.
- Bautista RE, Spencer DD, Spencer SS. (1998) EEG findings in frontal lobe epilepsies. *Neurology* 50:1765–1771.
- Cooper R, Winter AL, Crow HJ, Walter WG. (1965) Comparison of subcortical, cortical and scalp activity using chronically indwelling electrodes in man. *Electroencephalogr Clin Neurophysiol* 18:217–228.
- Cosandier-Rimélé D, Merlet I, Badier JM, Chauvel P, Wendling F. (2008) The neuronal sources of EEG: modeling of simultaneous scalp and intracerebral recordings in epilepsy. *Neuroimage* 42:135–146.
- Cosandier-Rimélé D, Bartolomei F, Merlet I, Chauvel P, Wendling F. (2012) Recording of fast activity at the onset of partial seizures: depth EEG vs. scalp EEG. *Neuroimage* 59:3474–3487.
- Ebersole JS. (1997) Defining epileptogenic foci: past, present, future. *J Clin Neurophysiol* 14:470–483.
- Elsharkawy AE, Alabbasi AH, Pannek H, Schulz R, Hoppe M, Pahs G, Nayel M, Issa A, Ebner A. (2008) Outcome of frontal lobe epilepsy surgery in adults. *Epilepsy Res* 81:97–106.
- Englot DJ, Wang DD, Rolston JD, Shih TT, Chang EF. (2012) Rates and predictors of long-term seizure freedom after frontal lobe epilepsy surgery: a systematic review and meta-analysis. *J Neurosurg* 116:1042–1048.
- Gavaret M, Badier JM, Marquis P, McGonigal A, Bartolomei F, Regis J, Chauvel P. (2006) Electric source imaging in frontal lobe epilepsy. *J Clin Neurophysiol* 23:358–370.
- Hämäläinen MS, Ilmoniemi RJ. (1994) Interpreting magnetic fields of the brain: minimum norm estimates. *Med Biol Eng Comput* 32:35–42.
- Jacobs J, Stich J, Zahneisen B, Assländer J, Ramantani G, Schulze-Bonhage A, Korinthenberg R, Hennig J, Levan P. (2013) Fast fMRI provides high statistical power in the analysis of epileptic networks. *Neuroimage* Oct 18 [Epub ahead of print].
- International Federation of Societies for Electroencephalography and Clinical Neurophysiology. (1983) *Recommendations for the Practice of Clinical Neurophysiology*. Elsevier, Amsterdam.
- Kellinghaus C, Lüders HO. (2004) Frontal lobe epilepsy. *Epileptic Disord* 6:223–239.
- Kobayashi K, Yoshinaga H, Ohtsuka Y, Gotman J. (2005) Dipole modeling of epileptic spikes can be accurate or misleading. *Epilepsia* 46:397–408.
- Koessler L, Maillard L, Benhadid A, Vignal JP, Felblinger J, Vespignani H, Braun M. (2009) Automated cortical projection of EEG sensors: anatomical correlation via the international 10–10 system. *Neuroimage* 46:64–72.
- Koessler L, Benar C, Maillard L, Badier JM, Vignal JP, Bartolomei F, Chauvel P, Gavaret M. (2010) Source localization of ictal epileptic activity investigated by high resolution EEG and validated by SEEG. *Neuroimage* 51:642–653.
- Lanfer B, Röer C, Scherg M, Rampp S, Kellinghaus C, Wolters C. (2013) Influence of a silastic ECoG grid on EEG/ECoG based source analysis. *Brain Topogr* 26:212–228.
- Ludwig B, Marsan CA, Van Buren J. (1975) Cerebral seizures of probable orbitofrontal origin. *Epilepsia* 16:141–158.
- Matsumoto R, Nair DR, LaPresto E, Bingham W, Shibasaki H, Lüders HO. (2007) Functional connectivity in human cortical motor system: a cortico-cortical evoked potential study. *Brain* 130:181–197.
- Merlet I, Gotman J. (1999) Reliability of dipole models of epileptic spikes. *Clin Neurophysiol* 110:1013–1028.
- Mosher JC, Lewis PS, Leahy RM. (1992) Multiple dipole modeling and localization from spatio-temporal MEG data. *IEEE Trans Biomed Eng* 39:541–557.

- Mosher JC, Baillet S, Leahy RM. (1999) EEG source localization and imaging using multiple signal classification approaches. *J Clin Neurophysiol* 16:225–238.
- Pascual-Marqui RD. (2002) Standardized low-resolution brain electromagnetic tomography (sLORETA): technical details. *Methods Find Exp Clin Pharmacol* 24(Suppl. D):5–12.
- Quesney LF, Constain M, Rasmussen T, Stefan H, Olivier A. (1992) How large are frontal lobe epileptogenic zones? EEG, ECoG, and SEEG evidence. *Adv Neurol* 57:311–323.
- Ramantani G, Boor R, Paetau R, Ille N, Feneberg R, Rupp A, Boppel T, Scherg M, Rating D, Bast T. (2006) MEG versus EEG: influence of background activity on interictal spike detection. *J Clin Neurophysiol* 23:498–508.
- Ramantani G, Koessler L, Colnat-Coulbois S, Vignal JP, Isnard J, Catenoix H, Jonas J, Zentner J, Schulze-Bonhage A, Maillard LG. (2013a) Intracranial evaluation of the epileptogenic zone in regional infrasyllvian polymicrogyria. *Epilepsia* 54:296–304.
- Ramantani G, Cosandier-Riméle D, Schulze-Bonhage A, Maillard L, Zentner J, Dümpelmann M. (2013b) Source reconstruction based on subdural EEG recordings adds to the presurgical evaluation in refractory frontal lobe epilepsy. *Clin Neurophysiol* 124:481–491.
- Ray A, Tao JX, Hawes-Ebersole SM, Ebersole JS. (2007) Localizing value of scalp EEG spikes: a simultaneous scalp and intracranial study. *Clin Neurophysiol* 118:69–79.
- Salanova V, Morris HH III, Van Ness PC, Lüders H, Dinner D, Wyllie E. (1993) Comparison of scalp electroencephalogram with subdural electrocorticogram recordings and functional mapping in frontal lobe epilepsy. *Arch Neurol* 50:294–299.
- Smith JR, Sillay K, Winkler P, King DW, Loring DW. (2004) Orbitofrontal epilepsy: electroclinical analysis of surgical cases and literature review. *Stereotact Funct Neurosurg* 82:20–25.
- Tao JX, Ray A, Hawes-Ebersole S, Ebersole JS. (2005) Intracranial EEG substrates of scalp EEG interictal spikes. *Epilepsia* 46:669–676.
- Tao JX, Baldwin M, Ray A, Hawes-Ebersole S, Ebersole JS. (2007) The impact of cerebral source area and synchrony on recording scalp electroencephalography ictal patterns. *Epilepsia* 48:2167–2176.
- Vogt BA, Berger GR, Derbyshire SW. (2003) Structural and functional dichotomy of human midcingulate cortex. *Eur J Neurosci* 18:3134–3144.

SUPPORTING INFORMATION

Additional Supporting Information may be found in the online version of this article:

Figure S1. Correlation between subdural and scalp spike-to-background-amplitude ratios of scalp-detectable sources (Wilcoxon test: $p = 0.002$).

C. DISCUSSION & PERSPECTIVES

Several outcomes of this experimental work are relevant in the context of this thesis, including:

1. The lack of scalp-visible spikes in the majority of frontal lobe sources: only 14% sources presented scalp EEG correlates visible in routine analysis. This figure is much lower than the 63–88% rates previously reported in non-simultaneous subdural- and scalp-EEG recordings^{54–57}, whereas this discrepancy can be readily attributed to methodological aspects. This finding is crucial for the clinical care of frontal lobe epilepsy patients, regarding both diagnosis and treatment monitoring.
2. The lack of scalp-visible spikes in the majority of sources located in basal or medial regions within the frontal lobe. Three of four scalp-visible interictal EEG spikes in our study corresponded to sources localized in the lateral convexity, particularly in the superior frontal sulcus or superior frontal gyrus. Only one case of a scalp-visible interictal EEG spike corresponded to a medial orbitofrontal and polar source. This observation corroborates previous findings from non-simultaneous subdural- and scalp-EEG recordings^{54,55,57}.
3. Background activity plays a crucial role in disguising the scalp EEG correlates of frontal lobe sources. After averaging of subdural interictal EEG spikes, thus increasing the signal-to-noise ratio by attenuating the background activity, six additional sources were rendered detectable in scalp-EEG. This finding suggests that the very low visibility of frontal lobe sources is partly linked to cortical activity generated in adjacent regions⁵⁸. Our study is the first to quantitatively assess this parameter in vivo, in the context of frontal lobe epilepsy. The elimination of background activity revealed not only medial or basal frontal but also dorsolateral cortical sources that would otherwise be undetectable in scalp EEG.
4. No systematically detectable or undetectable cortical source localizations were found in our study. Spikes originating from sources in the lateral convexity were missed,

whereas sources in the medial frontal gyri, in the depth of dorsolateral sulci, or in the orbitofrontal cortex were detectable after averaging, contrary to the perception that spikes generated in these regions escape detection in scalp EEG.

5. The extent of cortical activation – given by the number of activated contacts – and the subdural spike-to-background amplitude ratio determined the detection of dorsolateral cortical sources in our study. This is the first study to assess the contribution of the extent and amplitude of cortical activation to the detectability of scalp EEG correlates of frontal lobe sources. We applied the methodology previously conceived by Abraham & Marsan¹ and, up to now, only implemented in the study of temporal lobe sources^{1,42}.
6. The median cortical activation extent corresponding to scalp-detectable sources in our study amounts to 6 cm² and is thus comparable with the seminal in vitro measurement in the absence of background activity⁴ that has been widely cited and partly corroborated by simulation studies⁵⁹. It is, however, lower than the 10–20 cm² cortical activation extent derived from more recent in vivo and in vitro studies in temporal lobe epilepsy^{7,8}. This discrepancy may be attributed to the different lobar localization, as all other studies so far have been conducted in temporal lobe epilepsy. However, this divergence most probably underscores the difference between sources that are visible in routine visual interpretation and deep or small sources that are detectable only after averaging that attenuates the blurring effect of the overlying cortical background activity.
7. Considering the vast differences in coverage (depth, cortical extent) between explorations by subdural grid electrode arrays or by SEEG, we plan to analyze the interrelations between cortical sources and their scalp EEG correlates in frontal lobe epilepsy using simultaneous SEEG and scalp recordings. For this purpose, we intend to apply the sophisticated methodology used in our recent work on temporal lobe epilepsy²⁶.

CHAPTER 3: DISCUSSION

This thesis aimed to clarify the interrelations between cortical sources and their scalp EEG correlates in the setting of simultaneous multiscale EEG recordings performed for the presurgical evaluation of refractory focal epilepsy. For this purpose, we implemented novel methodological pipelines deriving from source localization.

The main findings of our study are summarized below:

1. Mesial temporal sources contribute to scalp EEG despite their deep localization, their curved spatial configuration, and the blurring resulting from the superimposed neocortical activity. Although their contribution is weak, it is detectable by extraction from the respective background activity. Scalp EEG correlates of mesial temporal sources were only detectable in our study with a negativity in the ipsilateral anterior basal temporal electrodes, whereas mesial plus/or neocortical sources were associated with an additional fronto-centro-parietal positivity. This difference was corroborated by the hierarchical clustering method. Our findings prompt further research towards the identification of scalp EEG biomarkers of mesial temporal sources to potentially evade intracerebral recordings in the presurgical evaluation of refractory epilepsy and to serve as a framework for further neurological and cognitive neuroscience applications.
2. We have shown that ESL applied to intracranial recordings provides complementary information that facilitates the identification and accurate delineation of the epileptogenic zone and thus improves the presurgical evaluation of patients with frontal lobe epilepsy. Analytical approaches of ESL could add both depth and extent to the localization accuracy of visual interpretation in subdural EEG recordings. These tools could thus constitute a surrogate of intracerebral depth investigations while retaining the superior spatial coverage of subdural grid electrodes.
3. Not only dorsolateral but also orbitofrontal and medial-frontal sources can be detectable in scalp EEG. This work constitutes the first in vivo demonstration based

on simultaneous subdural and scalp EEG recordings and the first quantitative assessment of the complementary significance of extensive source activation and higher subdural spike-to-background amplitude ratio in the detection of epileptic generators in FLE. This observation contributes to the decoding of interrelations between cortical sources and their scalp EEG correlates.

The appreciation of these interrelations is indeed of cardinal importance for the development and validation of new diagnostic tools such as ESL derived from scalp EEG, magnetoencephalography (MEG), or EEG–functional MRI (fMRI) that may constitute a surrogate for invasive recordings in the future^{10,12,15,48}.

PERSPECTIVES

Dense array recordings, increasingly used in presurgical workup in the last decade though yet unsuitable for long-term recordings, have the potential to significantly increase the sensitivity of scalp EEG. The studies of Yamazaki et al.^{60,61}, deriving from simultaneously recorded 256-channel dense array EEG and intracranial EEG provide 45% detection rates for mesial temporal and 56% for neocortical extratemporal spikes by visual inspection of the scalp EEG. Interestingly, mesial temporal lobe spikes detected in these dense array EEG recordings presented considerably higher amplitude compared with detected neocortical spikes. Simultaneous dense array scalp EEG and SEEG recordings can provide the optimal setting to analyze the scalp EEG correlates of cortical sources. The denser sampling on the scalp scale will match the superior sampling by depth electrodes and offer higher resolution results. This framework could find applications in the validation of source reconstruction results by different algorithms.

More than a half-century ago, Penfield and colleagues found that seizures in epileptic patients could be cured by removing the brain region giving rise to localized abnormal discharges on EEG⁶²⁻⁶⁴. Since then, identifying seizure onset on intracranial EEG has become the cornerstone for localizing epileptic foci. However, the value of ictal scalp EEG in presurgical epilepsy evaluation has long been the subject of considerable debate. False localization and even false lateralization are not uncommon, particularly in patients with extratemporal epilepsy^{65,66}. Scalp ictal rhythms may only reflect propagation from sources that are not recordable with scalp electrodes, rather than indicate the location of seizure onset zone^{41,42}. Additionally, different cerebral source configurations can generate a similar distribution of scalp voltage or magnetic fields. Thus, maximal activity at a certain electrode or sensor does not necessarily indicate that the generators are located in the area underlying it^{46,67}. Moreover, because the skull attenuates fast frequencies more than slow frequencies, high-frequency gamma rhythms at ictal onset simply cannot be recorded with conventional scalp EEG. So far, the ictal scalp EEG correlates of cortical sources have only

been addressed in the context of simultaneous scalp and subdural EEG recordings in temporal lobe epilepsy^{41,42}. These studies pointed to the cortical source area and synchrony at seizure onset as the most critical factors determining the generation of scalp-visible ictal EEG patterns.

Frontal lobe epilepsy constitutes a challenge both concerning EEG findings and postsurgical seizure outcomes. The next step in the context of frontal lobe epilepsy would be the analysis of scalp EEG correlates for deep sources, as sampled by SEEG, implementing the methodology already developed for mesial temporal lobe sources²⁶. The three studies comprising this thesis have addressed the issue of interictal scalp EEG correlates of cortical sources in frontal and temporal lobe epilepsy. Our methodology, however, both regarding source localization tools^{13,14} and network analysis²⁶ can be further developed for implementation in the analysis of ictal discharges, the most reliable biomarker for the epileptogenic zone. Furthermore, we could apply the pipeline developed for frontal and temporal lobe sources to further lobar –and sublobar – localizations.

To determine visibility and detectability of frontal lobe interictal epileptic sources, we used ESL derived from intracranial recordings to characterize the intracerebral source. In a recent study related to this thesis³⁷, we quantitatively compared the accuracy of ESL obtained from simultaneous intracranial and scalp recordings of epileptic spikes generated by a spatiotemporal source model. Interestingly, we showed that the larger the source, the less accurate the source reconstruction derived from intracranial recordings. This last study (Annex A) shows the limitations of the 3D characterization of intracerebral sources based on subdural grids and calls for further studies using depth electrodes as a reference method to delineate intracerebral epileptic sources. It also shows the potential of simulation studies to address the issues of visibility and detectability on the scalp of intracerebral sources.

CONCLUSION

Multiscale EEG recordings facilitate the analysis of interrelations between cortical sources and their scalp EEG correlates. Source localization methodology can further promote our efforts to decode these interrelations. Deep sources, such as mesial temporal or fronto-basal sources, are not visible, but they are detectable in scalp EEG. Scalp EEG spikes correlate with extensive cortical activation and high spike-to-background amplitude ratios. The spatiotemporal resolution of scalp EEG poses intrinsic limitations to the localization of its corresponding cortical sources. Studying the interrelations between invasive and scalp EEG is, however, of cardinal importance for the development and validation of novel diagnostic tools such as ESL, MEG, and fMRI that may constitute potent surrogates for invasive recordings in the future. Our observations can help to see more than just the tip of the iceberg in terms of cortical activity (Figure 8).

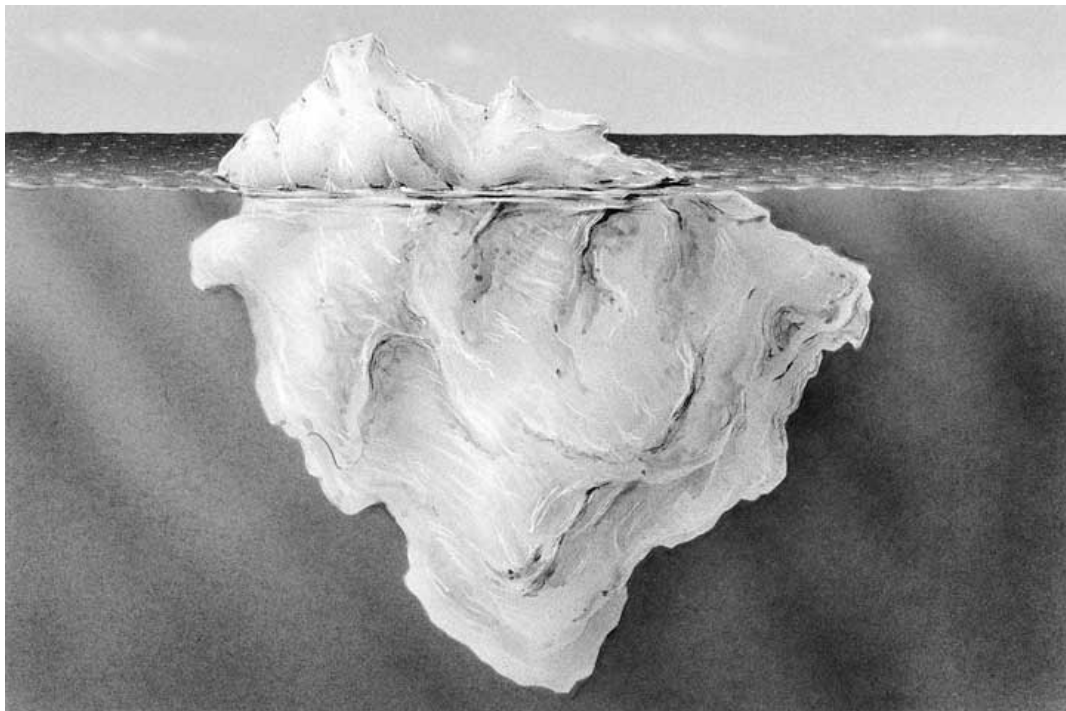


Figure 8: *Iceberg: A massive body of floating ice that has broken away from a glacier or ice field. Most of an iceberg lies underwater, but because ice is not as dense as water, about one ninth of it remains above the surface.*

BIBLIOGRAPHY

1. Abraham K, Marsan CA. Patterns of cortical discharges and their relation to routine scalp electroencephalography. *Electroencephalogr Clin Neurophysiol*. 1958;10:447–61.
2. Klass DW, Bickford RG. Reflections on the birth and early development of EEG at the Mayo Clinic. *J Clin Neurophysiol Off Publ Am Electroencephalogr Soc*. 1992;9:2–20.
3. Pillai J, Sperling MR. Interictal EEG and the diagnosis of epilepsy. *Epilepsia*. 2006;47 Suppl 1:14–22.
4. Cooper R, Winter AL, Crow HJ, Walter WG. Comparison of subcortical, cortical and scalp activity using chronically indwelling electrodes in man. *Electroencephalogr Clin Neurophysiol*. 1965;18:217–28.
5. Ebersole JS. Defining epileptogenic foci: past, present, future. *J Clin Neurophysiol Off Publ Am Electroencephalogr Soc*. 1997;14:470–83.
6. Kobayashi K, Yoshinaga H, Oka M, Ohtsuka Y, Gotman J. A simulation study of the error in dipole source localization for EEG spikes with a realistic head model. *Clin Neurophysiol Off J Int Fed Clin Neurophysiol*. 2003;114:1069–78.
7. Tao JX, Ray A, Hawes-Ebersole S, Ebersole JS. Intracranial EEG substrates of scalp EEG interictal spikes. *Epilepsia*. 2005;46:669–76.
8. Cosandier-Rimélé D, Merlet I, Badier JM, Chauvel P, Wendling F. The neuronal sources of EEG: modeling of simultaneous scalp and intracerebral recordings in epilepsy. *NeuroImage*. 2008;42:135–46.
9. Cuello-Oderiz C, von Ellenrieder N, Dubeau F, Gotman J. Influence of the location and type of epileptogenic lesion on scalp interictal epileptiform discharges and high-frequency oscillations. *Epilepsia*. 2017;
10. Jäger V, Dümpelmann M, LeVan P, Ramantani G, Mader I, Schulze-Bonhage A, et al. Concordance of Epileptic Networks Associated with Epileptic Spikes Measured by High-Density EEG and Fast fMRI. *PLoS One*. 2015;10:e0140537.
11. Rikir E, Koessler L, Gavaret M, Bartolomei F, Colnat-Coulbois S, Vignal J-P, et al. Electrical source imaging in cortical malformation-related epilepsy: a prospective EEG-SEEG concordance study. *Epilepsia*. 2014;55:918–32.
12. Bast T, Ramantani G, Boppel T, Metzke T, Ozkan O, Stippich C, et al. Source analysis of interictal spikes in polymicrogyria: loss of relevant cortical fissures requires simultaneous EEG to avoid MEG misinterpretation. *NeuroImage*. 2005;25:1232–41.
13. Ramantani G, Cosandier-Rimélé D, Schulze-Bonhage A, Maillard L, Zentner J, Dümpelmann M. Source reconstruction based on subdural EEG recordings adds to the presurgical evaluation in refractory frontal lobe epilepsy. *Clin Neurophysiol*. 2013;124:481–91.
14. Ramantani G, Dümpelmann M, Koessler L, Brandt A, Cosandier-Rimélé D, Zentner J, et al. Simultaneous subdural and scalp EEG correlates of frontal lobe epileptic sources. *Epilepsia*. 2014;55:278–88.

15. Jacobs J, Stich J, Zahneisen B, Assländer J, Ramantani G, Schulze-Bonhage A, et al. Fast fMRI provides high statistical power in the analysis of epileptic networks. *NeuroImage*. 2014;88:282–94.
16. Jacobs J, Menzel A, Ramantani G, Körbl K, Assländer J, Schulze-Bonhage A, et al. Negative BOLD in default-mode structures measured with EEG-MREG is larger in temporal than extra-temporal epileptic spikes. *Front Neurosci*. 2014;8:335.
17. Haas LF. Hans Berger (1873-1941), Richard Caton (1842-1926), and electroencephalography. *J Neurol Neurosurg Psychiatry*. 2003;74:9.
18. Ramantani G, Kadish NE, Strobl K, Brandt A, Stathi A, Mayer H, et al. Seizure and cognitive outcomes of epilepsy surgery in infancy and early childhood. *Eur J Paediatr Neurol*. 2013;17:498–506.
19. Ramantani G, Kadish NE, Anastasopoulos C, Brandt A, Wagner K, Strobl K, et al. Epilepsy surgery for glioneuronal tumors in childhood: avoid loss of time. *Neurosurgery*. 2014;74:648–57; discussion 657.
20. Ramantani G, Stathi A, Brandt A, Strobl K, Schubert-Bast S, Wiegand G, et al. Posterior cortex epilepsy surgery in childhood and adolescence: Predictors of long-term seizure outcome. *Epilepsia*. 2017;58:412–9.
21. Ramantani G, Kadish NE, Mayer H, Anastasopoulos C, Wagner K, Reuner G, et al. Frontal Lobe Epilepsy Surgery in Childhood and Adolescence: Predictors of Long-Term Seizure Freedom, Overall Cognitive and Adaptive Functioning. *Neurosurgery* [Internet]. 2017 [cited 2017 Jul 5]; Available from: <https://academic.oup.com/neurosurgery/article-abstract/doi/10.1093/neuros/nyx340/3924379/Frontal-Lobe-Epilepsy-Surgery-in-Childhood-and>
22. Ramantani G, Strobl K, Stathi A, Brandt A, Schubert-Bast S, Wiegand G, et al. Reoperation for refractory epilepsy in childhood: a second chance for selected patients. *Neurosurgery*. 2013;73:695–704.
23. Rosenow F, Lüders H. Presurgical evaluation of epilepsy. *Brain J Neurol*. 2001;124:1683–700.
24. Dumpelmann M, Cosandier-Rimele D, Ramantani G, Schulze-Bonhage A. A novel approach for multiscale source analysis and modeling of epileptic spikes. *Conf Proc Annu Int Conf IEEE Eng Med Biol Soc IEEE Eng Med Biol Soc Annu Conf*. 2015;2015:6634–7.
25. Ramantani G, Koessler L, Colnat-Coulbois S, Vignal J-P, Isnard J, Catenoix H, et al. Intracranial evaluation of the epileptogenic zone in regional infrasylvian polymicrogyria. *Epilepsia*. 2013;54:296–304.
26. Koessler L, Cecchin T, Colnat-Coulbois S, Vignal J-P, Jonas J, Vespignani H, et al. Catching the Invisible: Mesial Temporal Source Contribution to Simultaneous EEG and SEEG Recordings. *Brain Topogr*. 2015;28:5–20.
27. Cosandier-Rimélé D, Merlet I, Bartolomei F, Badier J-M, Wendling F. Computational modeling of epileptic activity: from cortical sources to EEG signals. *J Clin Neurophysiol Off Publ Am Electroencephalogr Soc*. 2010;27:465–70.

28. Lopes da Silva FH, van Rotterdam A. Biophysical aspects of EEG and magnetoencephalogram generation. In: Niedermeyer E, Lopes da Silva F (eds) *Electroencephalography: basic principles, clinical applications, and related fields*. Baltimore: MD: Williams and Wilkins; 1993. p. 93–109.
29. Koessler L, Colnat-Coulbois S, Cecchin T, Hofmanis J, Dmochowski JP, Norcia AM, et al. In-vivo measurements of human brain tissue conductivity using focal electrical current injection through intracerebral multicontact electrodes. *Hum Brain Mapp*. 2017;38:974–86.
30. Law SK, Nunez PL, Wijesinghe RS. High-resolution EEG using spline generated surface Laplacians on spherical and ellipsoidal surfaces. *IEEE Trans Biomed Eng*. 1993;40:145–53.
31. Cuffin BN. Effects of local variations in skull and scalp thickness on EEG's and MEG's. *IEEE Trans Biomed Eng*. 1993;40:42–8.
32. Eshel Y, Witman S, Rosenfeld M, Abboud S. Correlation between skull thickness asymmetry and scalp potential estimated by a numerical model of the head. *IEEE Trans Biomed Eng*. 1995;42:242–9.
33. Haueisen J, Ramon C, Czapski P, Eiselt M. On the influence of volume currents and extended sources on neuromagnetic fields: a simulation study. *Ann Biomed Eng*. 1995;23:728–39.
34. Gloor P. Neuronal generators and the problem of localization in electroencephalography: application of volume conductor theory to electroencephalography. *J Clin Neurophysiol Off Publ Am Electroencephalogr Soc*. 1985;2:327–54.
35. Merlet I, Gotman J. Reliability of dipole models of epileptic spikes. *Clin Neurophysiol Off J Int Fed Clin Neurophysiol*. 1999;110:1013–28.
36. Ramantani G, Maillard L, Koessler L. Correlation of invasive EEG and scalp EEG. *Seizure*. 2016;41:196–200.
37. Cosandier-Rimélé D, Ramantani G, Zentner J, Schulze-Bonhage A, Dümpelmann M. A realistic multimodal modeling approach for the evaluation of distributed source analysis: application to sLORETA. *J Neural Eng*. 2017;14:056008.
38. Penfield W G, Jasper H H. *Epilepsy and the Functional Anatomy of the Human Brain*. Boston, Mass, USA: Little Brown & Co; 1954.
39. Delucchi MR, Garoutte B, Aird RB. The scalp as an electroencephalographic averager. *Electroencephalogr Clin Neurophysiol*. 1962;14:191–6.
40. Geisler CD, Gerstein GL. The surface EEG in relation to its sources. *Electroencephalogr Clin Neurophysiol*. 1961;13:927–34.
41. Ray A, Tao JX, Hawes-Ebersole SM, Ebersole JS. Localizing value of scalp EEG spikes: a simultaneous scalp and intracranial study. *Clin Neurophysiol Off J Int Fed Clin Neurophysiol*. 2007;118:69–79.

42. Tao JX, Baldwin M, Ray A, Hawes-Ebersole S, Ebersole JS. The impact of cerebral source area and synchrony on recording scalp electroencephalography ictal patterns. *Epilepsia*. 2007;48:2167–76.
43. Zumsteg D, Friedman A, Wieser HG, Wennberg RA. Propagation of interictal discharges in temporal lobe epilepsy: correlation of spatiotemporal mapping with intracranial foramen ovale electrode recordings. *Clin Neurophysiol Off J Int Fed Clin Neurophysiol*. 2006;117:2615–26.
44. Kahane P, Landré E, Minotti L, Francione S, Ryvlin P. The Bancaud and Talairach view on the epileptogenic zone: a working hypothesis. *Epileptic Disord Int Epilepsy J Videotape*. 2006;8 Suppl 2:S16–26.
45. Jayakar P, Duchowny M, Resnick TJ, Alvarez LA. Localization of seizure foci: pitfalls and caveats. *J Clin Neurophysiol Off Publ Am Electroencephalogr Soc*. 1991;8:414–31.
46. Michel CM, Murray MM, Lantz G, Gonzalez S, Spinelli L, Grave de Peralta R. EEG source imaging. *Clin Neurophysiol Off J Int Fed Clin Neurophysiol*. 2004;115:2195–222.
47. Plummer C, Harvey AS, Cook M. EEG source localization in focal epilepsy: where are we now? *Epilepsia*. 2008;49:201–18.
48. Koessler L, Benar C, Maillard L, Badier J-M, Vignal JP, Bartolomei F, et al. Source localization of ictal epileptic activity investigated by high resolution EEG and validated by SEEG. *NeuroImage*. 2010;51:642–53.
49. Brodbeck V, Spinelli L, Lascano AM, Wissmeier M, Vargas M-I, Vulliemoz S, et al. Electroencephalographic source imaging: a prospective study of 152 operated epileptic patients. *Brain J Neurol*. 2011;134:2887–97.
50. Dümpelmann M, Fell J, Wellmer J, Urbach H, Elger CE. 3D source localization derived from subdural strip and grid electrodes: a simulation study. *Clin Neurophysiol Off J Int Fed Clin Neurophysiol*. 2009;120:1061–9.
51. Dümpelmann M, Ball T, Schulze-Bonhage A. sLORETA allows reliable distributed source reconstruction based on subdural strip and grid recordings. *Hum Brain Mapp*. 2012;33:1172–88.
52. Maillard LG, Tassi L, Bartolomei F, Catenoix H, Dubeau F, Szurhaj W, et al. Stereo-electroencephalography and surgical outcome in polymicrogyria-related epilepsy: A multi-centric study. *Ann Neurol*. 2017;
53. Harvey AS, Cross JH, Shinnar S, Mathern GW, Mathern BW, ILAE Pediatric Epilepsy Surgery Survey Taskforce. Defining the spectrum of international practice in pediatric epilepsy surgery patients. *Epilepsia*. 2008;49:146–55.
54. Quesney LF, Constain M, Rasmussen T, Stefan H, Olivier A. How large are frontal lobe epileptogenic zones? EEG, ECoG, and SEEG evidence. *Adv Neurol*. 1992;57:311–23.
55. Salanova V, Morris HH, Van Ness PC, Lüders H, Dinner D, Wyllie E. Comparison of scalp electroencephalogram with subdural electrocorticogram recordings and functional mapping in frontal lobe epilepsy. *Arch Neurol*. 1993;50:294–9.

56. Elsharkawy AE, Alabbasi AH, Pannek H, Schulz R, Hoppe M, Pahs G, et al. Outcome of frontal lobe epilepsy surgery in adults. *Epilepsy Res.* 2008;81:97–106.
57. Bautista RE, Spencer DD, Spencer SS. EEG findings in frontal lobe epilepsies. *Neurology.* 1998;50:1765–71.
58. Ramantani G, Boor R, Paetau R, Ille N, Feneberg R, Rupp A, et al. MEG versus EEG: influence of background activity on interictal spike detection. *J Clin Neurophysiol Off Publ Am Electroencephalogr Soc.* 2006;23:498–508.
59. Kobayashi E, Bagshaw AP, Jansen A, Andermann F, Andermann E, Gotman J, et al. Intrinsic epileptogenicity in polymicrogyric cortex suggested by EEG-fMRI BOLD responses. *Neurology.* 2005;64:1263–6.
60. Yamazaki M, Tucker DM, Fujimoto A, Yamazoe T, Okanishi T, Yokota T, et al. Comparison of dense array EEG with simultaneous intracranial EEG for interictal spike detection and localization. *Epilepsy Res.* 2012;98:166–73.
61. Yamazaki M, Tucker DM, Terrill M, Fujimoto A, Yamamoto T. Dense array EEG source estimation in neocortical epilepsy. *Front Neurol.* 2013;4:42.
62. Feindel W, Penfield W, Jasper H. Localization of epileptic discharge in temporal lobe automatism. *Trans Am Neurol Assoc.* 1952;56:14–7.
63. Penfield W, Flanigin H. Surgical therapy of temporal lobe seizures. *AMA Arch Neurol Psychiatry.* 1950;64:491–500.
64. Bailey P, Gibbs FA. The surgical treatment of psychomotor epilepsy. *J Am Med Assoc.* 1951;145:365–70.
65. Siegel AM, Williamson PD. Parietal lobe epilepsy. *Adv Neurol.* 2000;84:189–99.
66. Foldvary N, Klem G, Hammel J, Bingaman W, Najm I, Lüders H. The localizing value of ictal EEG in focal epilepsy. *Neurology.* 2001;57:2022–8.
67. Ebersole JS. Noninvasive localization of epileptogenic foci by EEG source modeling. *Epilepsia.* 2000;41 Suppl 3:S24–33.

APPENDIX

*A REALISTIC MULTIMODAL MODELING APPROACH FOR THE EVALUATION OF
DISTRIBUTED SOURCE ANALYSIS: APPLICATION TO SLORETA*

A realistic multimodal modeling approach for the evaluation of distributed source analysis: application to sLORETA

D Cosandier-Rim  l  ¹, G Ramantani^{2,4} , J Zentner³, A Schulze-Bonhage² and M D  mpelmann²

¹ Bernstein Center, University of Freiburg, Hansastr. 9a, 79104 Freiburg, Germany

² Faculty of Medicine, Epilepsy Center, Medical Center—University of Freiburg, University of Freiburg, Breisacher Str. 64, 79106 Freiburg, Germany

³ Faculty of Medicine, Neurosurgery, Medical Center—University of Freiburg, University of Freiburg, Breisacher Str. 64, 79106 Freiburg, Germany

E-mail: matthias.duempelmann@uniklinik-freiburg.de

Received 26 July 2016, revised 2 July 2017

Accepted for publication 5 July 2017

Published 18 August 2017



CrossMark

Abstract

Objective. Electrical source localization (ESL) deriving from scalp EEG and, in recent years, from intracranial EEG (iEEG), is an established method in epilepsy surgery workup. We aimed to validate the distributed ESL derived from scalp EEG and iEEG, particularly regarding the spatial extent of the source, using a realistic epileptic spike activity simulator. *Approach.* ESL was applied to the averaged scalp EEG and iEEG spikes of two patients with drug-resistant structural epilepsy. The ESL results for both patients were used to outline the location and extent of epileptic cortical patches, which served as the basis for designing a spatiotemporal source model. EEG signals for both modalities were then generated for different anatomic locations and spatial extents. ESL was subsequently performed on simulated signals with sLORETA, a commonly used distributed algorithm. ESL accuracy was quantitatively assessed for iEEG and scalp EEG. *Main results.* The source volume was overestimated by sLORETA at both EEG scales, with the error increasing with source size, particularly for iEEG. For larger sources, ESL accuracy drastically decreased, and reconstruction volumes shifted to the center of the head for iEEG, while remaining stable for scalp EEG. Overall, the mislocalization of the reconstructed source was more pronounced for iEEG. *Significance.* We present a novel multiscale framework for the evaluation of distributed ESL, based on realistic multiscale EEG simulations. Our findings support that reconstruction results for scalp EEG are often more accurate than for iEEG, owing to the superior 3D coverage of the head. Particularly the iEEG-derived reconstruction results for larger, widespread generators should be treated with caution.

Keywords: computational modeling, source localization, EEG, intracranial, scalp

(Some figures may appear in colour only in the online journal)

1. Introduction

Electrical source localization (ESL) aims to localize the sources of electric currents within the brain that give rise to recordable potential fields [1]. ESL is increasingly used as an adjunctive method for surgical planning in patients with

drug-resistant focal epilepsy [2]. Several ESL methods have been proposed, based on either the focal dipolar or the distributed modeling approach. Distributed ESL methods, in contrast to their dipolar counterparts, may depict extended sources simultaneously, but are under-determined and require constraints to achieve a unique solution [1].

In the context of epilepsy surgery, both scalp EEG and invasive EEG may be applied to delineate the epileptogenic

⁴These authors contributed equally to this work.

zone [3]. Scalp EEG guides eligibility for further evaluation or even direct resection, but invasive EEG may still be required to further define the localization and extent of the epileptogenic zone [3]. ESL derived from scalp EEG has gradually gained its place in the presurgical evaluation of patients with focal epilepsy over the last 20 years. However, large parts of the brain, such as deep generators, are inaccessible to scalp electrodes and thus to scalp EEG-based ESL. Most importantly, the impact of volume conduction on the generation of scalp potentials—and thus on ESL accuracy—is not fully resolved and thus constitutes the topic of extensive research, particularly regarding the development of forward models [4]. ESL derived from intracranial EEG (iEEG) has been recently developed to further refine the epileptogenic zone delineation, particularly regarding deep sources. However, iEEG-based solutions are only reliable for adequately sampled brain regions. ESL based on scalp EEG or iEEG has been previously validated against the invasive delineation of the epileptogenic zone [1, 5, 6] and the postsurgical outcome [7–11]. However, none of these reference methods is a true gold standard. The invasive delineation of the epileptogenic zone may imply a sampling bias [10–13], and the surgical resection volume may exceed the volume of the epileptogenic zone. The comparison of ESL solutions based on different EEG scales and their reciprocal validation is clearly challenging.

Moreover, the matching of scalp EEG to iEEG signals and, eventually, to their cortical substrates, constitutes a fundamental issue in electrophysiology and has been previously addressed in patient as well as in simulation studies [14]. Additional to the denser sampling of cortical generators provided by subdural recordings compared to a 10–20 scalp EEG coverage, iEEG shows little field spread, whereas scalp EEG visibility depends on widespread synchronized activity [11, 15]. Multiscale EEG studies, deriving from both recordings and/or simulations, provide a unique opportunity to investigate the interrelations between cortical generators and their subdural and scalp correlates. In particular, realistic simulations of epileptic generators and resulting interictal EEG spikes offer an excellent opportunity to validate ESL in an entirely controlled environment as to the localization and extent of the generator. Thus, distributed ESL methods deriving from a parceled source space have been shown to accurately depict epileptic sources within a wide range of spatial extents ($10\text{mm}^2\text{--}40\text{cm}^2$), provided that their localization is restricted to the cortical surface [16]. Nevertheless, estimating the extent of reconstructed sources remains problematic, since the significance of different contributions of these sources for the generation of measured EEG components is yet unclear.

In this paper, we propose a multiscale evaluation environment [17] that relies on a real-data-based modeling framework for generating simultaneous iEEG and scalp EEG signals. We used our environment and numerical simulations to evaluate ESL, as implemented by the sLORETA (standardized low-resolution brain electromagnetic tomography) algorithm [18], a distributed ESL method with good performance regarding spike localization for both EEG scales [9, 19]. Our objective was to compare the accuracy of distributed ESL derived from scalp EEG and iEEG recordings.

2. Methods

2.1. Multiscale evaluation environment

2.1.1. Clinical data. The MRI and EEG data of two patients with drug-resistant focal epilepsy undergoing presurgical evaluation in our institution [13, 20–22] were used to design the modeling framework and provide an assessment environment comparable with the clinical setting. The study was granted approval by the institutional research ethics board, and patients gave their written informed consent.

2.1.1.1. Patients. These two patients underwent presurgical evaluation in the Epilepsy Center Freiburg in 2008 and 2010. They were selected according to the following criteria: (a) they underwent both scalp and subdural long-term video-EEG recordings (figure 1(A)); (b) they presented an *epileptogenic zone* localized in the lateral convexity, albeit in different lobar/sublobar localizations; (c) they had a full intracranial coverage of this *epileptogenic zone* with a grid electrode array; and (d) they subsequently underwent resective epilepsy surgery, with histopathology confirming focal cortical dysplasia (FCD).

2.1.1.2. MRI data. We used the 3D T1-weighted MRI performed before electrode implantation to provide realistically shaped volume conductor models for the numerical simulations (figure 1(C)). We considered three electrically homogeneous compartments: brain, skull, and scalp. The segmented brain surface boundary consisted of 3446 vertices and 6888 polygons, the skull boundary of 510 vertices and 1016 polygons, and the scalp boundary of 616 vertices and 1228 polygons. We set the conductivity at 0.33 S m^{-1} for the brain, 0.00825 S m^{-1} for the skull, and 0.33 S m^{-1} for the scalp [23]. We performed the segmentation, BEM mesh generation, and forward calculations with the ASA software package (ANT Neuro, Enschede, The Netherlands) using the isolated problem approach [24].

2.1.1.3. EEG data. Scalp EEG recordings were performed according to the international 10–20 system with 33 electrodes in patient #1 (Fp1, Fp2, F3, F4, C3, C4, P3, P4, O1, O2, F7, F8, T7, T8, P7, P8, Fz, Cz, Pz, FT10, FT9, TP10, TP9, T10, T9, FC2, FC1, FC6, FC5, CP2, CP1, CP6, CP5) and 29 electrodes in patient #2 (Fp1, Fp2, F3, F4, C3, C4, P3, P4, O1, O2, F7, F8, T3, T4, T5, T6, Fz, Cz, Pz, T1, T2, FC1, FC2, FC5, FC6, CP1, CP2, CP5, CP6). iEEG recordings were performed with an 8×8 subdural grid electrode array placed over the right temporo-parieto-occipital junction in patient #1 (figure 3(A)) and over the left fronto-central region in patient #2 (figure 5(A)). Subdural electrode positions were derived from electrode artifacts in the 3D T1-weighted MRI datasets performed 1–2 d after electrode implantation [25], as shown on the curvilinear reformatting of the cortical surface from the pre- and post-implant 3D T1-weighted MRI datasets (figures 3–6(A)). With an electrode diameter of 4 mm, the electrode artifact diameter was $<12\text{ mm}$. Electrode positions were identified using a simultaneous display of the curvilinear reconstruction of the brain surface and three orthogonal slices. The

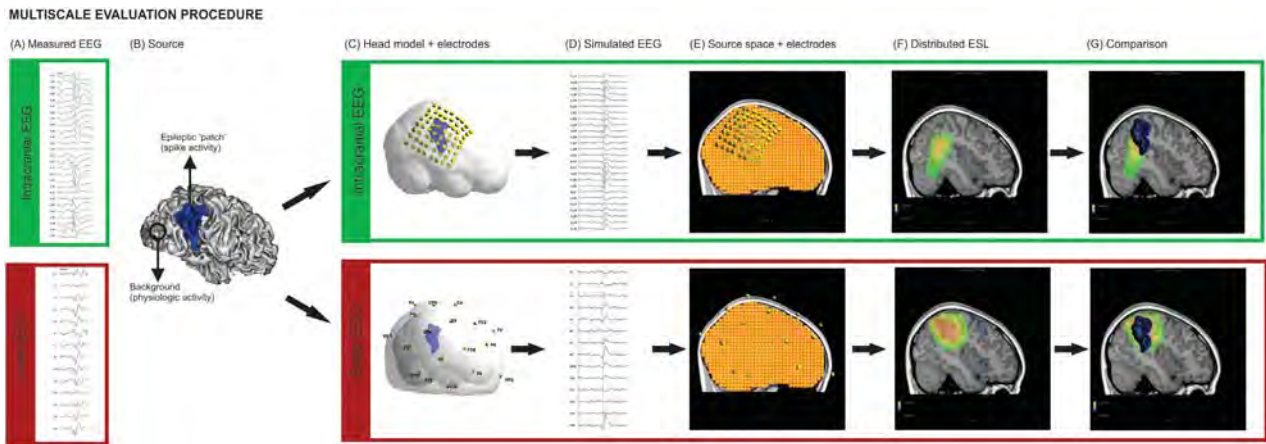


Figure 1. Multiscale evaluation procedure. Schematic overview of the multiscale evaluation environment. (A) Measured EEG on both scales, intracranial and scalp EEG. (B) Spatiotemporal source model. A widespread epileptic source is represented as a ‘patch’ on the neocortical surface, depicted in blue. Current dipoles inside the patch are assigned to epileptic activity (spikes), whereas current dipoles outside the patch are assigned to physiologic (background) activity. (C) Subdural grid and scalp electrodes with the respective realistic head models used for the EEG forward calculations. (D) Simulated EEG signals for each modality. (E) Source position and electrodes project on a MRI slice. (F) Source reconstruction results based on the intracranial EEG and scalp EEG recordings. (G) Comparison of source reconstruction accuracy for the two modalities.

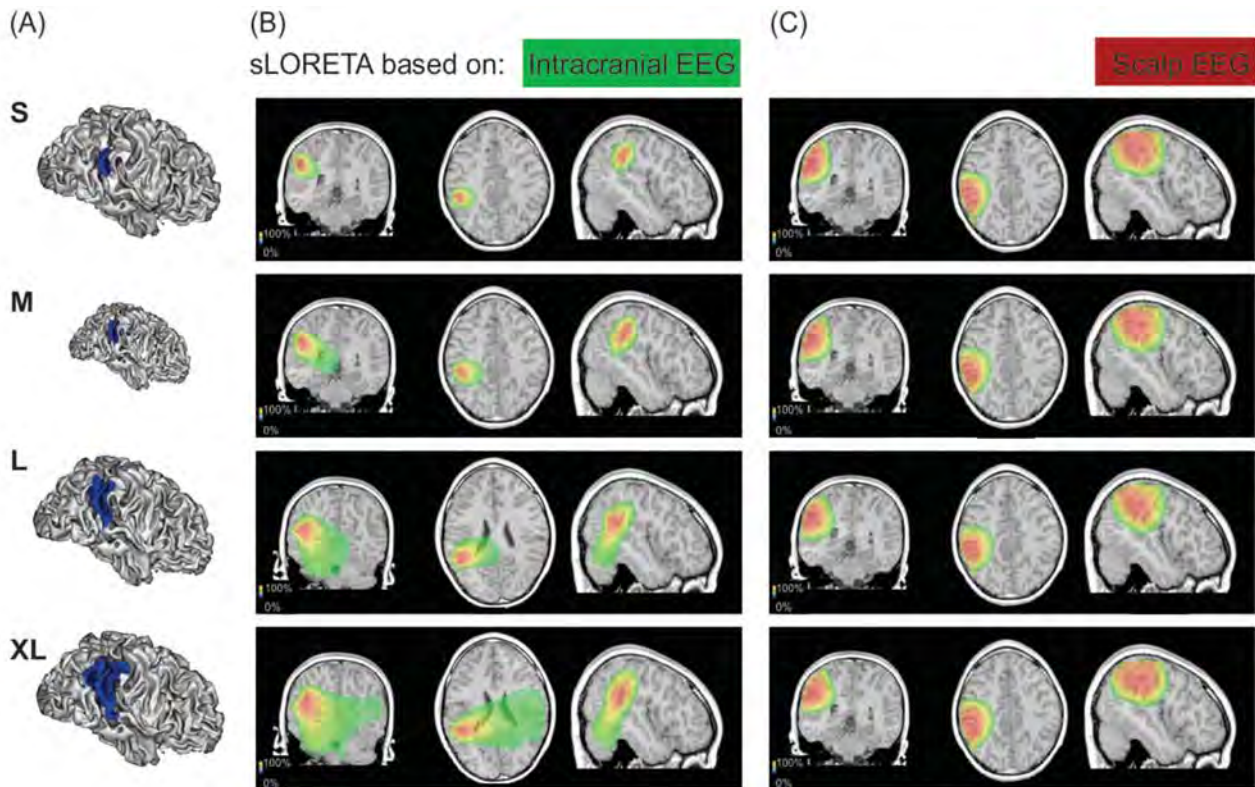


Figure 2. Impact of the epileptic source size on source localization accuracy. ESL performed with sLORETA based on intracranial EEG and scalp EEG recordings for different source sizes, exemplified in the configuration CFG1. (A) Epileptic source sizes considered in the study: small: S (5 cm²), medium: M (10 cm²), L: large (20 cm²), and extra large: XL (40 cm²). (B) Source reconstruction results derived from intracranial EEG recordings for all four source sizes. (C) Source reconstruction results derived from scalp EEG recordings for all four source sizes. For visualization purposes, sLORETA reconstructions were scaled to the respective maximum, and the result was set to transparency for points with sLORETA values below the identified ‘optimal’ threshold in both scales.

artifacts of the implanted electrodes in the curvilinear reformatting of the MRI after electrode implantation, the derived electrode positions on the same reformatting—overlying the curvilinear reformatting of the MRI before electrode implantation, as co-registered with the medium sized patch- and the

brain boundary are given in figures 3(A) and 5(A). For the two additional configurations, the electrode positions are shown with the curvilinear reformatting of the MRI before electrode implantation and the volume conductor model (figures 4(A) and 6(A)).

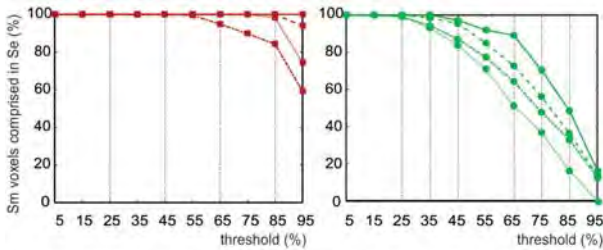
A. Electrodes on curvilinear reformatted MRI and mesh



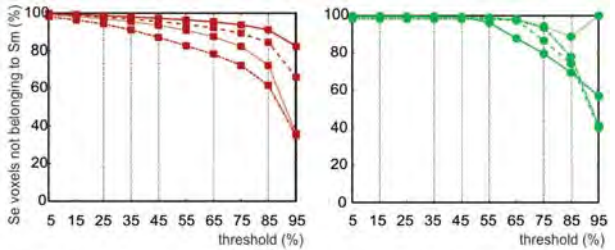
B. Patches on cortical layer in four different sizes



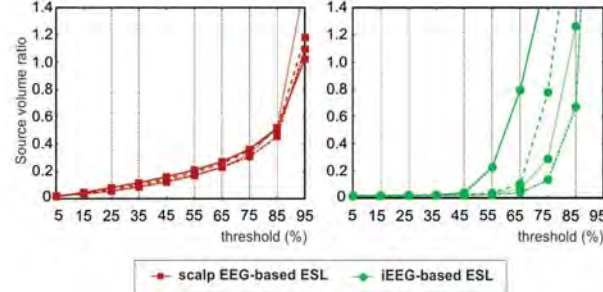
C. True Positive Rate



D. False Positive Rate



E. Source Volume Ratio



F. Source Barycenter Distance

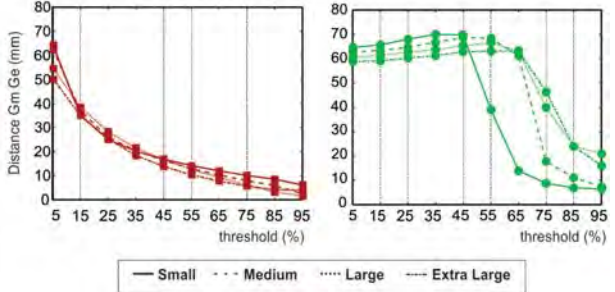


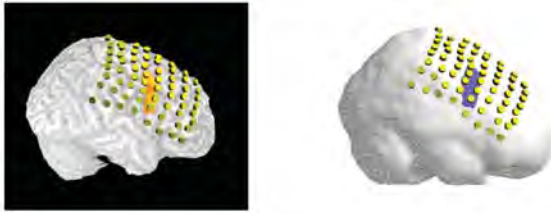
Figure 3. Anatomical configurations of electrodes and patches for CFG1 and accuracy measures. (A) From left to right: curvilinear reformatting of the MRI after electrode implantation with electrode contact and cable artifacts, curvilinear reformatting of the MRI after electrode implantation with overlaying derived electrode contacts, curvilinear reformatting of the MRI before implantation with a medium sized patch and electrode contacts, BEM surface with a medium sized patch and electrode contacts. (B) Curvilinear reformatting of the MRI before electrode implantation showing the location and extent of the four different patch sizes. Accuracy measures for varying thresholds: (C) true positive rate: TPR (optimum 100%), (D) false positive rate: FPR (optimum 0%), (E) source volume ratio: SVR (optimum 1.0) and (F) source barycenter distance: SBD, where S_m are cubes in the actual source volume compared to the cubes containing the reconstructed source volume S_e , G_m is the barycenter of the actual sources and G_e the barycenter of the estimated sources (optimum 0.0mm).

For the numerical simulations, subdural and scalp electrode positions were projected to the nearest vertex of the brain or to scalp compartment surfaces. The projection of the electrodes to the BEM surface nodes resulted in a distortion of the regular shape of the grid. The distance between each electrode location, as derived from the MRI after electrode implantation, and the corresponding projected position was <5.2 mm. This distance is in the accuracy range given by the difference between the artifact size compared to the actual electrode size. Furthermore, it should be noted that a CT- and MRI-study [26]

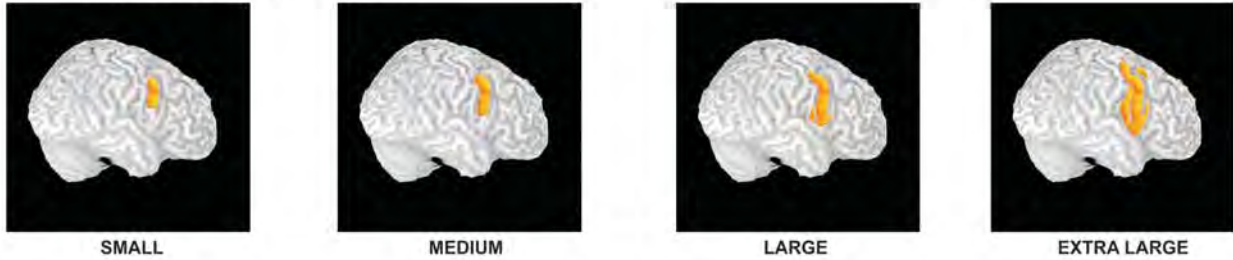
has previously reported 2.5–8.5mm errors for two patients, not considering possible shifts during iEEG recording. Thus, the electrode shift due to the contact projection to the nodes of the mesh in our study is in the range of errors inherent in image registration and processing.

2.1.2. EEG generation model. Simulations were performed using a previously developed computational model of EEG generation [27], which combines a spatiotemporal representation of EEG sources, i.e. the neuronal populations in the neocortex,

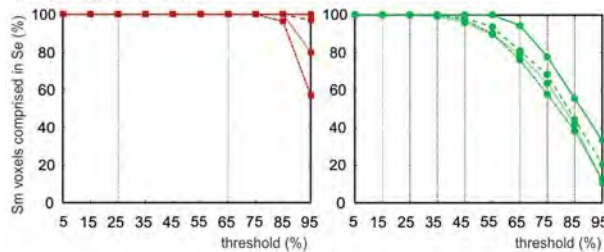
A. Electrodes on curvilinear reformatted MRI and mesh



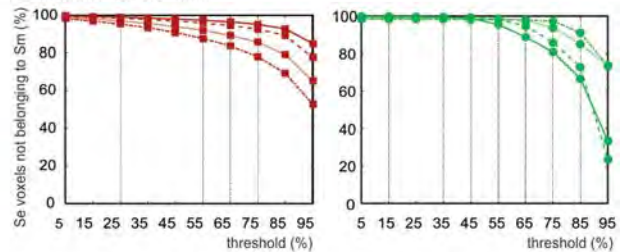
B. Patches on cortical layer in four different sizes



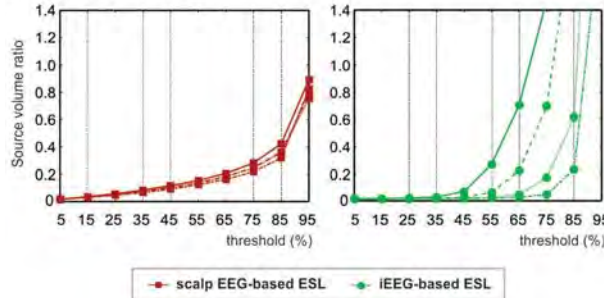
C. True Positive Rate



D. False Positive Rate



E. Source Volume Ratio



F. Source Barycenter Distance

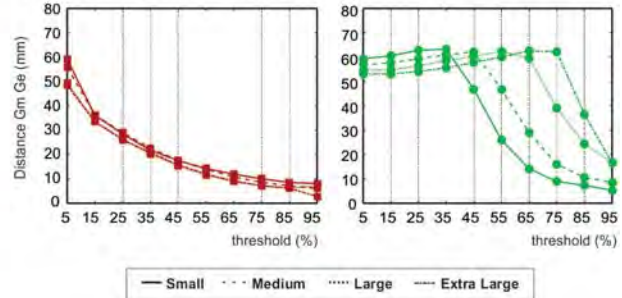


Figure 4. Anatomical configurations of electrodes and patches for CFG2 and accuracy measures: (A) from left to right: curvilinear reformatting of the MRI before electrode implantation with a medium sized patch and electrode contacts, BEM surface with a medium sized patch and electrode contacts. (B) Curvilinear reformatting of the MRI before electrode implantation showing the location and extent of the four different patch sizes. Accuracy measures for varying thresholds: (C) true positive rate: TPR (optimum 100%), (D) false positive rate: FPR (optimum 0%), (E) source volume ratio: SVR (optimum 1.0) and (F) source barycenter distance: SBD, where S_m are cubes in the actual source volume compared to the cubes containing the reconstructed source volume S_e , G_m is the barycenter of the actual sources and G_e the barycenter of the estimated sources (optimum 0.0 mm).

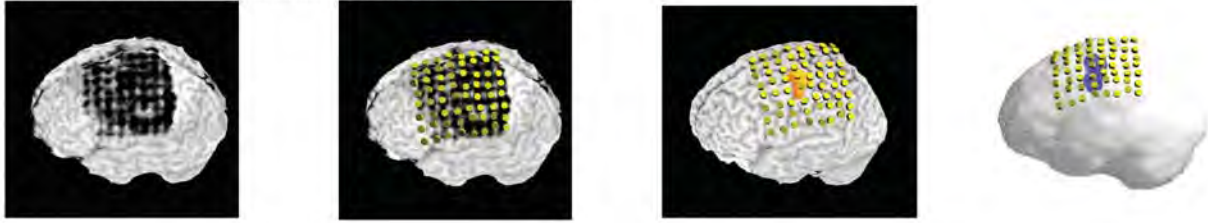
with a biophysically relevant account of the transmission of this neocortical activity to the recording electrodes. The main principles of our EEG generation model are summarized below.

2.1.2.1. Sources. The spatiotemporal EEG source model (figure 1(B)) relies on the combination of a distributed dipole source model that describes the spatial features of the sources, and a model of coupled neuronal populations that simulates the time-courses of these dipole sources).

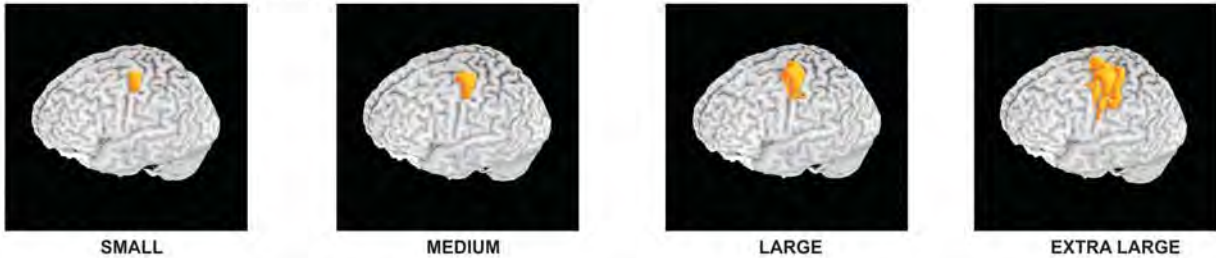
Assuming that the EEG sources are restricted to the pyramidal neurons of the neocortex, i.e. the subcortical structures

are not considered, they were represented as dipole layers distributed over the neocortical surface. The 3D geometry of these dipole layers is accounted for by a realistic mesh of the neocortical surface that allows for a detailed representation of neocortical convolutions. This mesh, used for defining dipole positions and orientations, was generated from the segmentation (gray matter/white matter interface) of the 3D MRI patient images using the BrainVisa software (www.brainvisa.info). This approach provides a high-resolution representation of the cortical surface. The average surface of each mesh triangle, presumably corresponding to a distinct population of neurons,

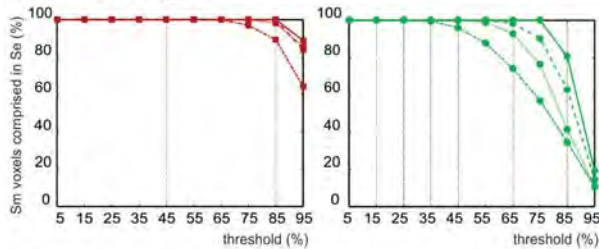
A. Electrodes on curvilinear reformatted MRI and mesh



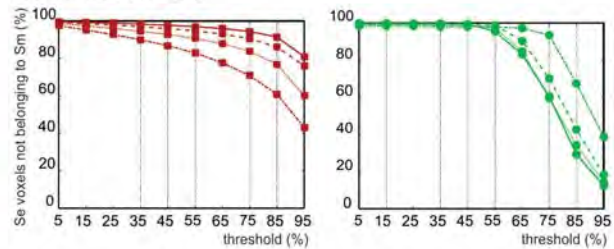
B. Patches on cortical layer in four different sizes



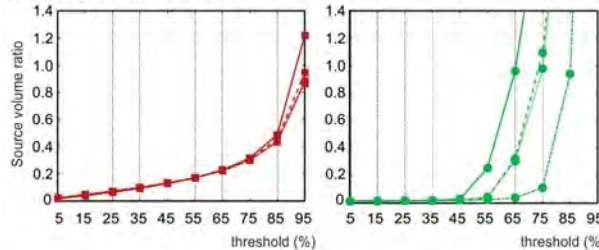
C. True Positive Rate



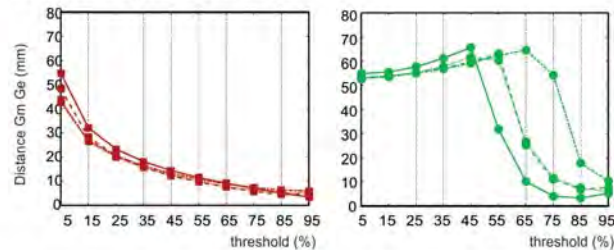
D. False Positive Rate



E. Source Volume Ratio



F. Source Barycenter Distance



—•— scalp EEG-based ESL —•— iEEG-based ESL — Small - - - Medium Large - . - . Extra Large

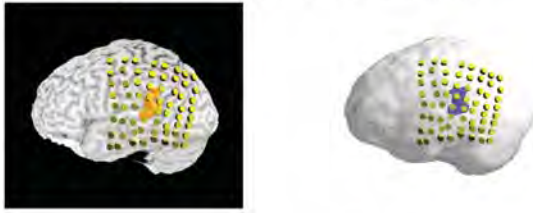
Figure 5. Anatomical configurations of electrodes and patches for CFG3 and accuracy measures: (A) from left to right: curvilinear reformatting of the MRI after electrode implantation with electrode contact and cable artifacts, curvilinear reformatting of the MRI after electrode implantation with overlaying derived electrode contacts, curvilinear reformatting of the MRI before implantation with a medium sized patch and electrode contacts, BEM surface with a medium sized patch and electrode contacts. (B) Curvilinear reformatting of the MRI before implantation showing the location and extent of the four different patch sizes. Accuracy measures for varying thresholds: (C) true positive rate: TPR (optimum 100%), (D) false positive rate: FPR (optimum 0%), (E) source volume ratio: SVR (optimum 1.0) and (F) source barycenter distance: SBD, where Sm are cubes in the actual source volume compared to the cubes containing the reconstructed source volume Se, Gm is the barycenter of the actual sources and Ge the barycenter of the estimated sources (optimum 0.0mm).

equaled 1 mm^2 . A single dipole was thus located at the barycenter of each triangle, and normally oriented to its surface (according to the columnar organization of the neocortex) [27].

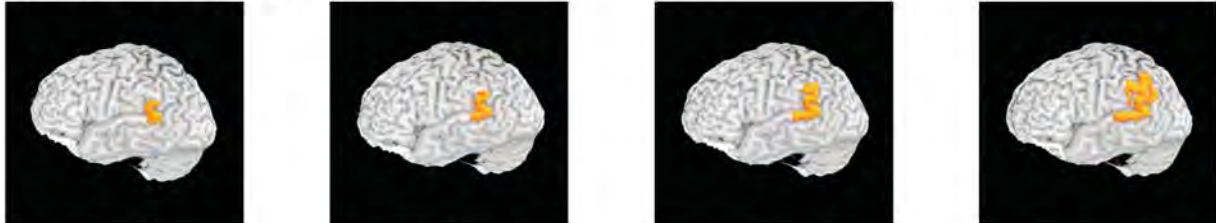
Assuming that the neocortex is organized as a network of neuronal populations, the time-courses of dipole intensities representing neuronal electrical activities were generated by a model of coupled neuronal populations [26]. In brief, each neuronal population contains two subsets of neurons, corresponding to the main pyramidal cells and local interneurons, which mutually interact through excitatory and inhibitory feedback. Neuronal populations

are also interrelated through excitatory connections, representing the average density of action potentials fired by the pyramidal cells. Interestingly, two conditions (physiologic and epileptic) can be obtained in the model from two different parameter settings (excitatory and inhibitory gains in feedback loops and degree and direction of coupling between interconnected populations) [26]. These settings thus served to simulate the time-courses of ‘epileptic sources’, i.e. dipoles associated to epileptic spike activity, and ‘physiologic sources’, i.e. dipoles associated to physiologic background activity.

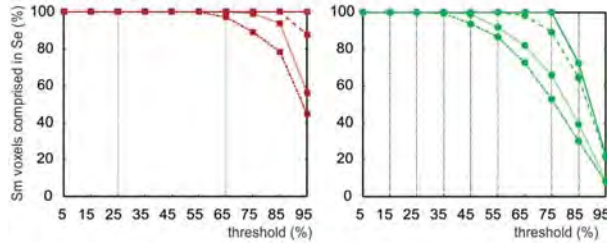
A. Electrodes on curvilinear reformatted MRI and mesh



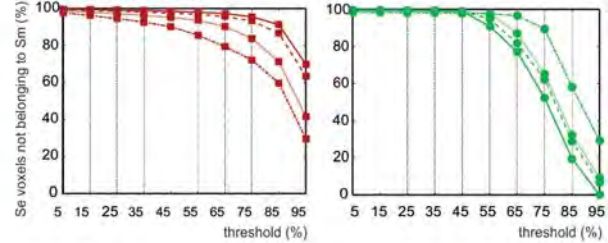
B. Patches on cortical layer in four different sizes



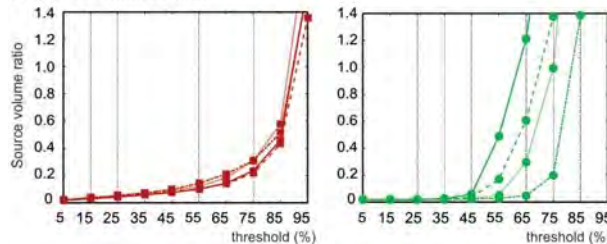
C. True Positive Rate



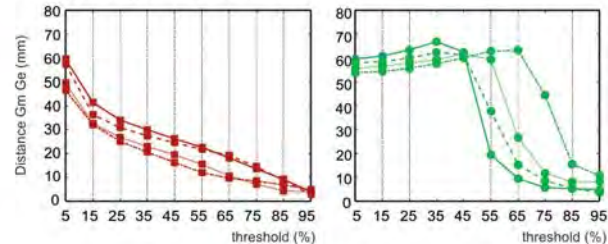
D. False Positive Rate



E. Source Volume Ratio



F. Source Barycenter Distance



Legend: ■ scalp EEG-based ESL ■ iEEG-based ESL
— Small - - - Medium ⋯ Large - · - · Extra Large

Figure 6. Anatomical configurations of electrodes and patches for CFG4 and accuracy measures: (A) from left to right: curvilinear reformatting of the MRI before electrode implantation with a medium sized patch and electrode contacts, BEM surface with a medium sized patch and electrode contacts. (B) Curvilinear reformatting of the MRI before implantation showing the location and extent of the four different patch sizes. Accuracy measures for varying thresholds: (C) true positive rate: TPR (optimum 100%), (D) false positive rate: FPR (optimum 0%), (E) source volume ratio: SVR (optimum 1.0) and (F) source barycenter distance: SBD, where Sm are cubes in the actual source volume compared to the cubes containing the reconstructed source volume Se, Gm is the barycenter of the actual sources and Ge the barycenter of the estimated sources (optimum 0.0mm).

2.1.2.2. EEG signals. The EEG signals were simulated by solving the ‘EEG forward problem’, i.e. by calculating the electric field potentials generated by the given sources in the head volume conductor. In this study, signals were computed both at scalp electrodes (scalp EEG) and at subdural grid electrodes (iEEG) (figure 1(D)), for a 100 s-duration. Forward calculations were performed in realistically shaped volume conductor models, using the isolated problem approach of the boundary element method. Scalp potentials were calculated in a three-compartment (brain, skull, and scalp) head model, and subdural potentials were calculated in a one-compartment (brain) head model. For the latter, it was assumed that currents

in the skull and outside the skull had no relevant contribution to potentials recorded at the brain surface. The minimum distance of a dipole to a subdural electrode was 4 mm. This is close to the threshold regarding numerical instabilities of the forward calculation. However, numerical instabilities in our study are unlikely, since the simulated signals showed no abrupt changes in their spatiotemporal properties, as verified by visual inspection.

2.1.3. Numerical simulations. In this study, a widespread epileptic source was considered and represented as a ‘patch’ with fixed size and location on the neocortical surface. Dipoles

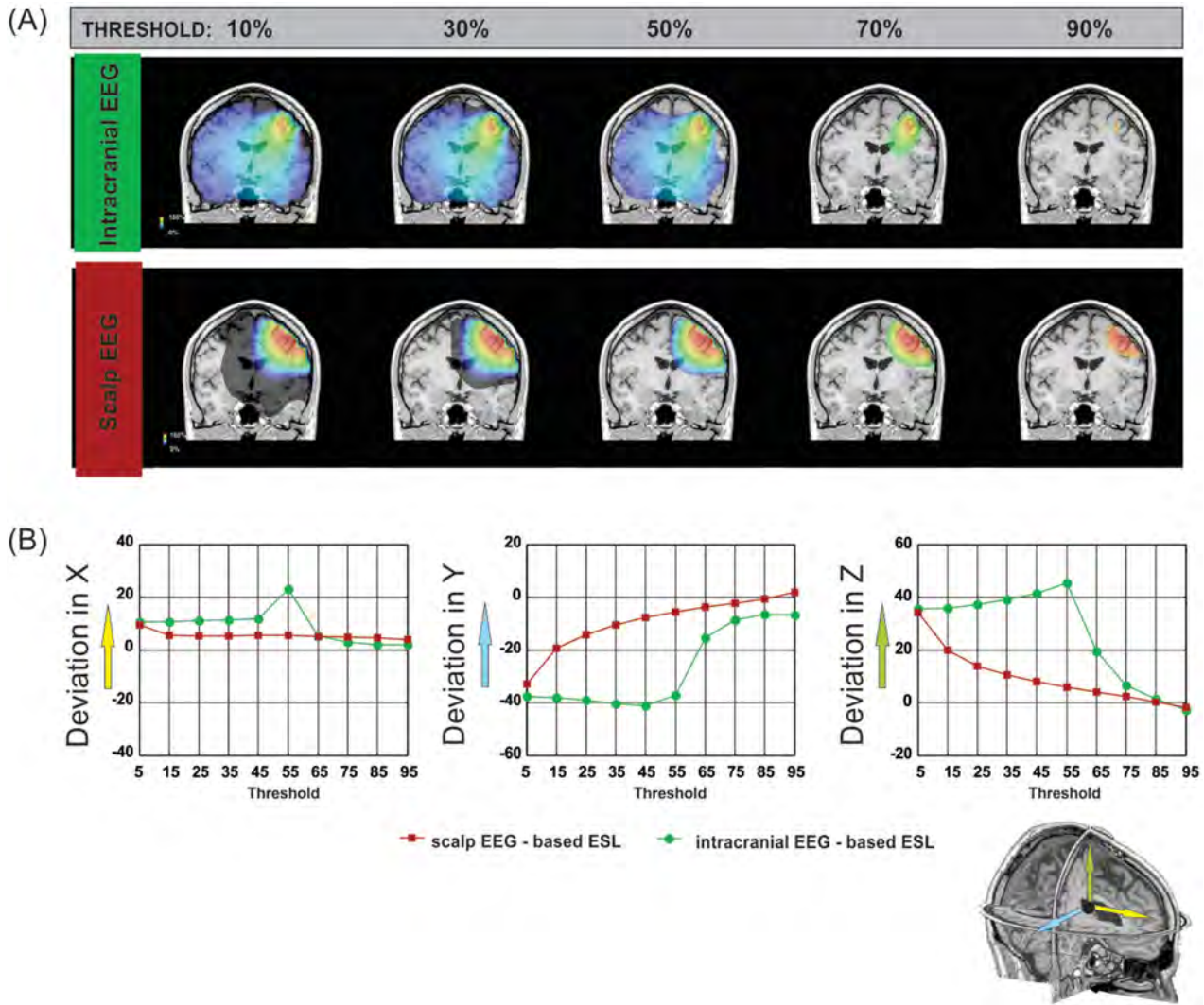


Figure 7. Impact of the threshold on source localization accuracy. The impact of the sLORETA threshold on ESL accuracy is illustrated for the medium-sized source in the configuration CFG3. (A) Examples of source reconstruction results for different threshold values and for both EEG modalities. (B) Variation of the Source Barycenter Distance: SBD deviation in the three directions (X, Y, Z), depending on the threshold.

located inside the patch were assigned epileptic spike activities, whereas dipoles outside the patch were assigned physiologic background activities (figure 1(B)). Physiologic activity was obtained for ‘standard’ parameter values, whereas epileptic activity (spikes) was obtained for model parameters adjusted according to hypotheses related to epileptogenesis (increase of excitation/inhibition ratio within neuronal populations and/or increase of inter-population coupling strength).

To account for the effects of neocortical surface and head geometry, simulations were performed for four different configurations (CFG1 to CFG4), deriving from patient data (CFG1 and CFG3), and including an arbitrarily chosen variation (CFG2 and FCG4) for each patient. CFG1 and CFG2 were epileptic patches located in the right parietal (figure 3(B)) and right frontal (figure 4(B)) regions in the head model of patient #1. CFG3 and CFG4 were epileptic patches located in the left frontal (figure 5(B)) and left parietal (figure 6(B)) regions in the head model of patient #2. For all four configurations, we assumed that the epileptic patch was located directly under the

center of the 8×8 grid electrode array, to ensure full iEEG coverage of the source (figures 3–6(A)).

Finally, for each configuration, we considered four different patch surface areas to illustrate a small (S, 5cm^2), medium (M, 10cm^2), large (L, 20cm^2) and extra large (XL, 40cm^2) epileptic source (figures 3–6(B)). Thus, we considered a total of 16 modeled neocortical epileptic patches.

2.2. Source reconstruction

In this study, ESL was performed by sLORETA (figure 1(F)), a commonly used distributed 3D inverse procedure, as implemented in the ASA software package (ANT Neuro, Enschede, The Netherlands). sLORETA is based on images of standardized current density, as derived from the current density estimate given by the minimum norm estimate and standardized by its variance, including both the actual source variance and the variation due to noise in the measurements [18]. The reconstruction points of sLORETA solutions were distributed

Table 1. RMBD values for all four configurations and four patch sizes, in the two EEG modalities.

Source configuration	Scalp EEG S (mm)	Scalp EEG M (mm)	Scalp EEG L (mm)	Scalp EEG XL (mm)	iEEG S (mm)	iEEG M (mm)	iEEG L (mm)	iEEG XL (mm)
CFG1	3.9	6.9	4.6	6.2	7.7	6.6	20.6	15.0
CFG2	9.6	8.2	6.6	2.0	5.6	10.0	17.4	12.4
CFG3	5.5	4.7	3.0	4.1	5.1	10.4	6.3	10.0
CFG4	4.6	6.2	7.7	6.7	2.8	4.6	7.7	12.3

on a regular cubic lattice of 5 mm edge length covering the brain volume, as given by the brain boundary of the volume conductor model. No further spatial restrictions of the source space were applied. This methodology allows for the reconstruction of 3D activity distributions, including deep sources, such as sulcal generators. sLORETA was computed for the interval 100ms before to 100ms after the peak of a spike average based on 20 simulated events. To guarantee stable results for the inverse procedure, we estimated the regularization parameter for the analysis interval by assessing the noise covariance, according to the general cross-validation method [28]. We thus calculated the regularization parameter from the signal of the full analysis interval and applied this value to all samples. The sLORETA algorithm computed results sample-wise. In our quantitative comparisons and their illustration (figures 2–7), we considered the mean value of the distribution over the analysis interval. For display purposes, we used a sensitivity threshold to separate source positions with relevant contributions to the average spike in figures of representative sLORETA reconstructions (figures 1(F), (G), 2 and 7(A)). We empirically selected a threshold for each source size and configuration to include most of the original patch extent, while avoiding an overestimation of the generating volume.

2.3. Quantification of the source reconstruction accuracy

The accuracy of iEEG and scalp EEG source reconstruction, as comparatively illustrated in figure 1(G), was quantitatively assessed using the following measures: true positive rate (TPR), false positive rate (FPR), source volume ratio (SVR), source barycenter distance (SBD), and reconstruction maximum to source barycenter distance (RMBD).

In our study, the point sets of the actual source (i.e. the neocortical epileptic patch in the model) and the reconstructed source (i.e. the result of the sLORETA algorithm) were generated independently and therefore presented different 3D positions. The point sets of the actual source derived from the cortical surface reconstruction of the patients' MRI, while the point sets of the reconstructed source were located on a regular 3D grid. This disparity precludes the use of well-established measures such as the sum of the squared differences between the actual and the reconstructed magnitudes or the correlation between the magnitudes of the two distributions [16]. To overcome this limitation, we divided the head volume into cubes of 5 mm edge length and assigned each cube to one of the following four states: (1) containing *neither* actual source points *nor* reconstructed source points, (2) containing *only* actual source points, (3) containing *only* reconstructed source points,

and (4) containing *both* actual and reconstructed source points. The TPR, FPR, and SVR measures rely on this methodology, whereas the SBD and RMBD measures rely directly on the 3D positions of point sets.

True positive rate—TPR, representing *sensitivity*, is the percentage of correctly estimated cubes in the reconstructed source volume, i.e. those containing both actual source points and reconstructed source points:

$$\text{TPR} = \frac{\text{No. of cubes containing both actual and reconstructed source points}}{\text{No. of cubes containing only actual source points}} \times 100.$$

Higher TPR values correspond to better source reconstruction results.

False positive rate—FPR is the percentage of incorrectly estimated cubes in the reconstructed source volume, i.e. those containing only reconstructed source points and no actual source points:

$$\text{FPR} = \frac{\text{No. of cubes containing only reconstructed and no actual source points}}{\text{No. of cubes containing reconstructed source points}} \times 100.$$

Lower FPR values correspond to better source reconstruction results. FPR provides a more intuitive measure than specificity, which represents the true negative rate.

Source volume ratio—SVR is the ratio of the number of cubes in the actual source volume to the number of cubes in the reconstructed source volume.

$$\text{SVR} = \frac{\text{No. of cubes in the actual source volume}}{\text{No. of cubes in the reconstructed source volume}}.$$

SVR values below 1 indicate an overestimation of the source volume, whereas values above 1 indicate an underestimation of the source volume.

Source barycenter distance—SBD is the Euclidean distance between the barycenter of the actual and the reconstructed source. The actual and reconstructed source barycenters were given by the mean values of the x , y , z coordinates of the dipoles contained within the neocortical epileptic patch and of the reconstructed sources. This measure describes the distance between the centers of mass of the two irregularly shaped volumes.

Reconstruction maximum to source barycenter distance—RMBD is the Euclidean distance between the barycenter of the actual source and the reconstruction point with the highest value of the sLORETA metric. This measure gives an estimate regarding the localization error of the ESL maximum and is independent from thresholding of the source reconstruction results.

3. Results

The simulated iEEG and scalp EEG data were used to generate a spike average for each configuration. Spikes generated by simulation showed a spatial extent and magnitude similar to the recorded spikes of the patients, but exhibited a comparably less sharp morphology and a longer duration (figures 1(A) and (D)). The signal-to-noise ratio (signal power divided by noise power, computed over all channels) of averaged spikes in an interval 100 ms before to 100 ms after the peak, compared to a 100 ms interval ending 400 ms before the spike peak, was 8.5–184.5 dB for simulated scalp data and 42.1–138.7 dB for simulated iEEG data. The maximum amplitudes of scalp EEG spike averages were in the range of 20–213 μV . The maximum amplitudes of iEEG spike averages were in the range of 330–1578 μV .

A first general observation is that the reconstruction accuracy was similar for the four source configurations (figures 3–6). As exemplified by the configuration CFG1 in figure 2, the sLORETA source reconstruction derived from iEEG and scalp EEG presented a maximum directly below the epileptic patch for all four configurations and epileptic source sizes. However, the extent of the reconstruction varied considerably between different source sizes and between the two EEG scales. For the two smaller patches, the activation volume of the scalp EEG-based reconstruction exceeded that of the iEEG-based reconstruction. For the two largest patches, the iEEG-based reconstruction was more extensive than the scalp EEG-based ESL, and considerably blurred, extending to the contralateral hemisphere. It should be noted that these results were obtained for empirically selected ‘optimal’ thresholds, as discussed in 2.2. Overall, ESL results differed between the two EEG scales as to the true positive and false positive rate, the source volume and location, as illustrated in the following paragraphs.

3.1. Sensitivity and false positive rate

In scalp EEG-based ESL, the *sensitivity* (TPR) approached 100% for the smallest patch in all configurations: the original patch was fully included in the reconstruction volume (figures 3–6(C)). For larger patches, the reconstruction volume covered $\geq 80\%$ of the original volume, when applying a sensitivity threshold $\geq 80\%$ of the maximum value. In iEEG-based ESL, similarly to scalp EEG-based ESL, most of the original patch was included in the reconstruction volume for the smallest patch size for low threshold values ($\leq 25\%$). The reconstruction volume covered $\geq 80\%$ of the original volume, when applying a sensitivity threshold $\geq 75\%$ of the maximum value. For the largest patch size, the original patch was included in the reconstruction volume at $< 45\%$ of the maximum value. Overall, for iEEG-based source reconstruction, lower sensitivity threshold values had to be applied to include 80% of the original patch. This limit decreased considerably for larger generators.

All reconstruction volumes showed a high false positive rate (FPR) for all configurations and patch sizes (figures 3–6(D)), indicating a systematic overestimation of the extent

of the actual source. Only increasing the threshold over 65% leads to a lower FPR. For both EEG modalities, the FPR remained similarly stable independent of source size up to roughly the same threshold. For higher threshold values, the FPR showed some spread depending on the modality, source size and configuration.

3.2. Source volume

For both EEG modalities, SVR values remained < 1 for all configurations and source sizes, indicating a systematic overestimation of the source volume (figures 3–6(E)). This was only reversed for scalp EEG-based ESL when suppressing reconstruction points with a metric $< 90\%$ of its maximum value and for iEEG-based ESL when suppressing reconstruction points with a metric $< 55\%$ of its maximum value. The observed very low SVR values suggest that reconstruction volumes exceeded by far the volume of the corresponding model. For both EEG modalities, SVR increased with source size. This highlights the increasing overestimation of source volume for larger epileptic sources. Overall, SVR values were higher for iEEG-based ESL than for scalp EEG-based ESL. An underestimation of the actual source size only occurred when applying a reconstruction metric $> 55\%$ of the reconstruction maximum for the smallest patch size and 75–85% of the reconstruction maximum for the largest patch size.

3.3. Source location

The impact of the actual source size on the accuracy of the reconstructed source location is presented in figures 3–6(F). The effect of the patch size on the source barycenter distance (SBD) varied to a great extent between the two EEG scales. The SBD values obtained from iEEG exceeded those obtained from scalp EEG for all source sizes and configurations independent of the threshold value. For scalp EEG, SBD values diminished continuously with increasing threshold values. For iEEG, SBD values remained constant for threshold values up to 35–45% to decrease rapidly after a deflection point at 45–75%. This deflection point appeared at higher thresholds for larger original patch sizes.

The distance between the reconstruction maximum and the source barycenter (RMBD) ranged between 2.0 mm and 20.6 mm for all configurations, patch sizes, and EEG scales (table 1). For scalp EEG-based ESL, the highest RMBD was only 9.6 mm, with the average RMBD remaining below 6.5 mm for all patch sizes. For iEEG-based ESL, the average RMBD was below 8.0 mm for the small and medium patch sizes, but exceeded 12.0 mm for the two largest patch sizes.

3.4. Impact of the threshold

The sensitivity threshold applied to sLORETA limits the ESL solution with the assumption that points below a certain percentage of the maximum reconstruction magnitude do not contribute substantially to the generator of the activity. The impact of the threshold on ESL accuracy is illustrated in figure 7. As shown in figure 7(A), a very low threshold

will result in the inclusion of too many brain regions in the reconstructed source, while a very high threshold will result in the exclusion of core elements of the source. Thus, the two extremes are 0% (the source is the whole brain) and 100% (the source narrows down to only one or only a few cubes). Especially for iEEG-based ESL, vast areas of the brain, including the contralateral hemisphere, lie above the threshold value for thresholds below 50% of the maximum activation. Only the thresholds of 70% and 90% show a focal activation. For scalp EEG-based ESL, activation volumes are considerably smaller at low thresholds compared to iEEG-based ESL, already appearing focal for a threshold value of 50%, but shrink less at high thresholds (>65%).

Taking a closer look at the main orientations of reconstructed source extension, leading to a potential blurring of ESL results, figure 7(B) illustrates the SBD as a function of the threshold along the following three axes: back-to-front (x -axis), left-to-right (y -axis), and bottom-to-top (z -axis). With the sole exception of the 55% threshold value for iEEG-based ESL, the deviation in the back-to-front direction was limited and was further decreased with increasing thresholds. For the left-to-right axis, the reconstructed barycenters appeared more mesial than their counterparts from the original patch at all thresholds for iEEG-based ESL and at a <85% threshold for scalp EEG-based ESL. The distance between the barycenters decreased monotonically for the scalp EEG-based ESL, but slightly increased for the iEEG-based ESL, before abruptly decreasing from a 60% threshold onwards. For the bottom-to-top axis, the distance between the barycenters decreased monotonically for scalp EEG-based ESL, but not for iEEG-based ESL. For the latter, only threshold values >55% were associated with decreasing distances between barycenters.

4. Discussion

In this simulation study, we comparatively evaluated the accuracy of distributed ESL as performed by the sLORETA algorithm from scalp EEG and iEEG recordings. We particularly investigated the effect of the spatial extent of a given source, as this is a crucial factor in the presurgical evaluation of drug-resistant epilepsy.

4.1. Methodological framework

The accuracy of focal source models for ESL has been the subject of thorough analysis in simulation studies, especially regarding dipolar sources [29, 30]. On the contrary, the accuracy of distributed source models for ESL has been the subject of only a few studies so far [8, 9, 16, 31], despite their wide application [19]. This may be attributed to the lack of a solid framework as well as of reliable quantitative measures for the evaluation of simulation results, other than the assessment of the distance between the maxima of spatial distributions.

To our knowledge, this is the first comprehensive simulation study to evaluate the detection accuracy of distributed ESL methods, as applied to multiscale EEG recordings from both scalp and subdural electrodes. The assessment was performed using a novel and comprehensive modeling framework that

is based on a realistic distributed model of EEG generation for different modalities (e.g. iEEG, scalp EEG), using individual realistic head models to reconstruct a spatially distinct epileptic source [17, 27, 32–34]. This spatiotemporal model has the potential to represent realistic physiologic background activity as well as epileptic spike time-courses and source configurations in various anatomical locations and spatial extents.

For iEEG data, we used the real subdural grid electrode positions deriving from patient data as well as a further arbitrarily chosen configuration for each patient, to cover a wider range of realistic scenarios of subdural EEG explorations. Our findings support that the reconstruction accuracy of the epileptic patch depends only to a small degree on the precise location of the subdural grid electrode on the lateral convexity. For scalp EEG, we used the scalp electrode setups deriving from the recordings of the two patients that were performed with extended 10–20 configurations. In our study, we chose to use electrode configurations aligned to the actual patient recordings. However, further simulation studies with setups for 64, 128 or more scalp electrodes should be encouraged, since high-density recordings have been recently shown to provide superior ESL results [7, 35]. The application of our novel multiscale framework to high-density electrode configurations may outperform the ESL results obtained in the present study.

We consistently applied a boundary element model (BEM) for the generation of EEG data as well as for the forward simulation step in the inverse procedure. This model provides a realistic volume conductor representation for the human head. Although BEM provides an acceptable compromise between computational effort and accuracy, finite element models (FEM) have the potential to diminish accuracy related errors in future studies [36]. To obtain potentials at the electrodes, the electrode positions were projected to the nearest node, thus resulting in a less regular geometrical distribution of the grid electrodes compared to the actual contact distribution or to their orthogonal projection onto the outermost surface [37]. Nevertheless, the influence of this less regular distribution on the reconstruction results can be assumed as minor, since the same electrode positions were used for the generation of simulated spikes and for source reconstruction, despite the less regular spatial sampling compared to an actual grid electrode.

Finally, in our study, the dipole positions for the EEG signal simulation differed from the source positions of the reconstruction space, in contrast to a recent study [16]. For this reason, we applied a set of five accuracy measures to evaluate the scalp EEG- and iEEG-based ESL. This approach has the benefit of avoiding the so-called ‘inverse crime’ that may result in overoptimistic accuracy estimates of the inverse procedure.

4.2. Overestimation of the source volume

The volume of the epileptic patch in our study was overestimated by sLORETA, in line with previous simulation studies [9, 31]. This finding corresponds to a well-described property of the sLORETA algorithm that trades localization accuracy for spatial blurring. This low-resolution property results in

reconstructed sources that underestimate the source volume. In our evaluation framework, the source volume was underestimated only for the highest threshold values, as reflected in the lower TPR. These observations are illustrated in our exemplary plots of sLORETA solutions (figures 2–7(A)) and confirmed by our quantitative measures for both scalp EEG- and iEEG-based ESL. Indeed, all four configurations and patch sizes, almost without exception, presented high FPR and $SVR < 1$.

For the scalp EEG-based ESL, the overestimation of the source volume in our study may be partly attributed to the low-density scalp electrode coverage used for the simulations, selected to match the actual recordings of the two patients. Indeed, the denser and thus less ‘patchy’ coverage of the head in a recent simulation study [35] was shown to considerably reduce not only the distance between simulated and reconstructed sources but also the spatial spread of the sLORETA solution.

For the iEEG-based ESL, the overestimation of the source volume in our study was accompanied by a significant dispersion towards deep structures, whereas the modeled epileptic patches depicted sources in the neocortical surface. Indeed, the barycenters of the iEEG-based sLORETA solutions shifted to the inside of the brain on the mesial-to-lateral axis. This dispersion may be partly attributed to the electrode positions that are distributed in a 2D plane roughly parallel to the lateral convexity, crossing the mesial-to-lateral axis only by a small extent. The position of the subdural electrode array thus emphasizes deep sources. Furthermore, to localize sources distant from the plane of the subdural grid, sLORETA amplifies their contribution by augmenting small signal components of these sources. This feature of sLORETA results in a considerable dispersion in the direction perpendicular to the grid plane. Additional strip electrodes may refine iEEG-based sLORETA reconstruction, but are not expected to solve the issue of source volume overestimation [35].

Finally, in our study, we assumed that the epileptic patch was located directly under the center of the subdural electrode array, to ensure full coverage of the source and thus optimal reconstruction. Indeed, for iEEG-based sLORETA, the estimated extent of focal sources has only proven valid for sources close to the electrode contacts, and the overestimation of the activation volume by sLORETA has been particularly pronounced for distant sources [9]. This property of the algorithm should be kept in mind when using sLORETA for source reconstruction. Obtaining blurred solutions for sources distant from the recording electrodes is the price to pay for the zero localization error regarding well-defined sources.

4.3. Inferiority of intracranial EEG-derived reconstruction for large sources

Distributed source models are devised to reconstruct widespread generators of cortical activity in a realistic manner. Our sLORETA study shows that the accuracy of the reconstruction depends on the size of the epileptic patch used for the simulation.

For iEEG-based sLORETA results, high TPRs and low FPRs were achieved only for the smallest patch size (5 cm^2),

to drop drastically for larger patch sizes. Moreover, the distance between the barycenters of the simulated epileptic patch and the reconstructed source was higher for larger patches. Furthermore, the distance between the reconstruction maximum and the barycenters of the original patches reached up to 20 mm for the two largest patches. These results prompt the conclusion that an iEEG-based sLORETA reconstruction can accurately represent only small sources.

For scalp EEG-based sLORETA results, in contrast, we found no clear correlation between the reconstruction accuracy and the size of the patch. Some configurations presented favorable trends in accuracy measures with larger patch sizes, while others showed a decreasing accuracy. The changes in accuracy measures were overall less pronounced for scalp EEG- than for iEEG-based source reconstruction.

4.4. Superiority of scalp EEG-derived source reconstruction

Overall, iEEG is expected to provide a superior quality signal compared to scalp EEG [38], as well as a superior spatial sampling in close proximity to the generators of epileptic activity. At first glance it seems surprising that, in our study, the accuracy of source reconstruction is higher for scalp EEG than for iEEG. Indeed, scalp EEG-based reconstructions showed a higher sensitivity, a similar or even lower FPR, a lower SVR, SBD, and RMBD, for all configurations. For the larger patches, the disparity in accuracy measures between the two modalities augmented, with scalp EEG-derived ESL proving to be more stable and independent of the spatial extent of the source. Furthermore, the dispersion of the sLORETA solution towards deep structures was established only for the iEEG-based ESL.

The latter finding gives a valuable hint regarding the reasons of scalp EEG-based reconstruction superiority. As already discussed above, the iEEG electrodes are distributed practically in only two dimensions over the neocortical surface, thus overemphasizing potential sources in deep brain regions. The use of additional electrodes covering the contralateral hemisphere in a recent study [8] failed to substantially improve the iEEG-based ESL performed by the standard minimum norm or MUSIC approach. The use of contralateral electrodes marginally improved iEEG-based reconstruction performed by the sLORETA approach, with the resulting volume still remaining blurred [9]. Considering this property of sLORETA, the complete 3D coverage by scalp electrodes provides a coherent explanation for the superior results of scalp EEG-derived ESL. The favorable effect of 3D coverage by additional iEEG electrodes on sLORETA performance may lead to improved results in individual patients, in case additional electrode placement is required for clinical purposes.

In this study, we used numerical simulations to illustrate the synchronous propagation patterns of epileptic activity in circumscribed areas of the brain. However, spikes often show local, non-synchronous propagation patterns, with a more pronounced representation in iEEG compared to the simultaneous scalp EEG [14]. Hence, reconstruction based on iEEG may illustrate these propagation patterns better than scalp EEG. Further studies on numerical simulations including

spike propagation between different brain regions may add substantial information on this topic.

4.5. Impact of the threshold

To date, no established rules are available as to the optimal threshold values for distributed inverse solutions that ensure an accurate definition of the spatial extent of a given generator. Our findings show that sLORETA results clearly overestimate the source extent for thresholds <55%. All five quality measures exhibit a deflection point at a threshold close to this value. In particular, considering the differences in the barycenters of actual and reconstructed sources, it is evident that besides a continuous approximation of these points for scalp EEG-based source reconstruction, a rapid approximation between these points presents over a 55% threshold for iEEG-based source reconstruction. In contrast, threshold values $\geq 85\%$ may lead to solutions corresponding to only part of the generator. This latter scenario may have a higher impact than a solution including the distributed source but overestimating its extent, since it would mislead towards a partial view of the generator, with grave consequences in a clinical context. All exemplary figures present on a qualitative level, at least for the smaller patches and for a threshold selected as described above, a circumscribed activation delineating the volume of the actual patches.

The accurate delineation of the spatial extent for a reconstructed source poses a largely unsolved problem in the distributed algorithm approach. Our novel multiscale framework utilized in this study for the evaluation of sLORETA may also be suitable for investigating the relation between method related constraints and the volume of the reconstructed source in other distributed source models, e.g. minimum norm estimate, weighted minimum norm estimate or LORETA. This modeling approach has the potential to complement and enhance concepts introducing statistical tests [39] or parceling strategies [16], by diminishing subjectiveness in the determination of the generator extent in an inverse solution. In particular, an extended concept of parceling the source space from the cortical surface to 3D would be an interesting approach to be evaluated by the proposed framework.

5. Conclusion

In this study, we present a novel multiscale framework for the evaluation of distributed source models. This framework is based on realistic multiscale EEG (iEEG, scalp EEG) simulations and allows for a thorough investigation of the properties of distributed inverse models. The application of the framework to the widely used sLORETA method provides novel and valuable insights into method-related issues, especially regarding the spatial extent of reconstructed sources. Scalp EEG-based reconstruction results are often more accurate than iEEG-based results. In particular, iEEG reconstruction results for larger, widespread generators should be treated with caution.

ORCID iDs

G Ramantani  <https://orcid.org/0000-0002-7931-2327>

References

- [1] Plummer C, Harvey A S and Cook M 2008 EEG source localization in focal epilepsy: where are we now? *Epilepsia* **49** 201–18
- [2] Kaiboriboon K, L uders H O, Hamaneh M, Turnbull J and Lhatoo S D 2012 EEG source imaging in epilepsy—practicalities and pitfalls *Nat. Rev. Neurol.* **8** 498–507
- [3] Rosenow F and L uders H 2001 Presurgical evaluation of epilepsy *Brain* **124** 1683–700
- [4] Kybic J, Clerc M, Abboud T, Faugeras O, Keriven R and Papadopoulos T 2005 A common formalism for the integral formulations of the forward EEG problem *IEEE Trans. Med. Imaging* **24** 12–28
- [5] Michel C M, Murray M M, Lantz G, Gonzalez S, Spinelli L and de Peralta R G 2004 EEG source imaging *Clin. Neurophysiol.* **115** 2195–222
- [6] Rikir E, Koessler L, Gavaret M, Bartolomei F, Colnat-Coulbois S, Vignal J-P, Vespignani H, Ramantani G and Maillard L G 2014 Electrical source imaging in cortical malformation-related epilepsy: a prospective EEG-SEEG concordance study *Epilepsia* **55** 918–32
- [7] Brodbeck V, Spinelli L, Lascano A M, Wissmeier M, Vargas M-I, Vulliemoz S, Pollo C, Schaller K, Michel C M and Seeck M 2011 Electroencephalographic source imaging: a prospective study of 152 operated epileptic patients *Brain* **134** 2887–97
- [8] D umpelmann M, Fell J, Wellmer J, Urbach H and Elger C E 2009 3D source localization derived from subdural strip and grid electrodes: a simulation study *Clin. Neurophysiol.* **120** 1061–9
- [9] D umpelmann M, Ball T and Schulze-Bonhage A 2012 sLORETA allows reliable distributed source reconstruction based on subdural strip and grid recordings *Hum. Brain Mapp.* **33** 1172–88
- [10] Ramantani G, Cosandier-Rim el e D, Schulze-Bonhage A, Maillard L, Zentner J and D umpelmann M 2013 Source reconstruction based on subdural EEG recordings adds to the presurgical evaluation in refractory frontal lobe epilepsy *Clin. Neurophysiol.* **124** 481–91
- [11] Ramantani G, D umpelmann M, Koessler L, Brandt A, Cosandier-Rim el e D, Zentner J, Schulze-Bonhage A and Maillard L G 2014 Simultaneous subdural and scalp EEG correlates of frontal lobe epileptic sources *Epilepsia* **55** 278–88
- [12] Koessler L, Cecchin T, Colnat-Coulbois S, Vignal J-P, Jonas J, Vespignani H, Ramantani G and Maillard L G 2015 Catching the invisible: mesial temporal source contribution to simultaneous EEG and SEEG recordings *Brain Topogr.* **28** 5–20
- [13] Ramantani G, Koessler L, Colnat-Coulbois S, Vignal J-P, Isnard J, Catenoix H, Jonas J, Zentner J, Schulze-Bonhage A and Maillard L G 2013 Intracranial evaluation of the epileptogenic zone in regional infrasyllvian polymicrogyria *Epilepsia* **54** 296–304
- [14] Ramantani G, Maillard L and Koessler L 2016 Correlation of invasive EEG and scalp EEG *Seizure* **41** 196–200
- [15] Tao J X, Ray A, Hawes-Ebersole S and Ebersole J S 2005 Intracranial EEG substrates of scalp EEG interictal spikes *Epilepsia* **46** 669–76
- [16] Grova C, Daunizeau J, Lina J-M, B enar C G, Benali H and Gotman J 2006 Evaluation of EEG localization methods

- using realistic simulations of interictal spikes *NeuroImage* **29** 734–53
- [17] D mpelmann M, Cosandier-Rim el e D, Ramantani G and Schulze-Bonhage A 2015 A novel approach for multiscale source analysis and modeling of epileptic spikes *37th Annual Int. Conf. of the IEEE Engineering in Medicine and Biology Society* vol 2015 pp 6634–7
- [18] Pascual-Marqui R D 2002 Standardized low-resolution brain electromagnetic tomography (sLORETA): technical details *Methods Find. Exp. Clin. Pharmacol.* **24** 5–12
- [19] Plummer C, Wagner M, Fuchs M, Vogrin S, Litewka L, Farish S, Bailey C, Harvey A S and Cook M J 2010 Clinical utility of distributed source modelling of interictal scalp EEG in focal epilepsy *Clin. Neurophysiol.* **121** 1726–39
- [20] Ramantani G et al 2017 Posterior cortex epilepsy surgery in childhood and adolescence: predictors of long-term seizure outcome *Epilepsia.* **58** 412–9
- [21] Ramantani G et al 2014 Epilepsy surgery for glioneuronal tumors in childhood: avoid loss of time *Neurosurgery* **74** 648–57; discussion 657
- [22] Ramantani G et al 2017 Frontal lobe epilepsy surgery in childhood and adolescence: predictors of long-term seizure freedom, overall cognitive and adaptive functioning *Neurosurgery* *nyx340*
- [23] Gonalves S I, de Munck J C, Verbunt J P A, Bijma F, Heethaar R M and Lopes da Silva F 2003 *In vivo* measurement of the brain and skull resistivities using an EIT-based method and realistic models for the head *IEEE Trans. Biomed. Eng.* **50** 754–67
- [24] Zanow F and Peters M J 1995 Individually shaped volume conductor models of the head in EEG source localisation *Med. Biol. Eng. Comput.* **33** 582–8
- [25] Kovalev D, Spreer J, Honegger J, Zentner J, Schulze-Bonhage A and Huppertz H-J 2005 Rapid and fully automated visualization of subdural electrodes in the presurgical evaluation of epilepsy patients *AJNR Am. J. Neuroradiol.* **26** 1078–83
- [26] Dykstra A R, Chan A M, Quinn B T, Zepeda R, Keller C J, Cormier J, Madsen J R, Eskandar E N and Cash S S 2012 Individualized localization and cortical surface-based registration of intracranial electrodes *NeuroImage* **59** 3563–70
- [27] Cosandier-Rim el e D, Merlet I, Badier J M, Chauvel P and Wendling F 2008 The neuronal sources of EEG: modeling of simultaneous scalp and intracerebral recordings in epilepsy *NeuroImage* **42** 135–46
- [28] Grech R, Cassar T, Muscat J, Camilleri K P, Fabri S G, Zervakis M, Xanthopoulos P, Sakkalis V and Vanrumste B 2008 Review on solving the inverse problem in EEG source analysis *J. Neuroeng. Rehabil.* **5** 25
- [29] Kobayashi K, Yoshinaga H, Oka M, Ohtsuka Y and Gotman J 2003 A simulation study of the error in dipole source localization for EEG spikes with a realistic head model *Clin. Neurophysiol.* **114** 1069–78
- [30] Merlet I and Gotman J 1999 Reliability of dipole models of epileptic spikes *Clin. Neurophysiol.* **110** 1013–28
- [31] Hauk O, Wakeman D G and Henson R 2011 Comparison of noise-normalized minimum norm estimates for MEG analysis using multiple resolution metrics *NeuroImage* **54** 1966–74
- [32] Cosandier-Rim el e D, Bartolomei F, Merlet I, Chauvel P and Wendling F 2012 Recording of fast activity at the onset of partial seizures: depth EEG versus scalp EEG *NeuroImage* **59** 3474–87
- [33] Cosandier-Rim el e D, Merlet I, Bartolomei F, Badier J-M and Wendling F 2010 Computational modeling of epileptic activity: from cortical sources to EEG signals *J. Clin. Neurophysiol.* **27** 465–70
- [34] Cosandier-Rim el e D, Badier J-M, Chauvel P and Wendling F 2007 A physiologically plausible spatio-temporal model for EEG signals recorded with intracerebral electrodes in human partial epilepsy *IEEE Trans. Biomed. Eng.* **54** 380–8
- [35] Song J, Davey C, Poulsen C, Luu P, Turovets S, Anderson E, Li K and Tucker D 2015 EEG source localization: sensor density and head surface coverage *J. Neurosci. Methods* **256** 9–21
- [36] Rullmann M, Anwander A, Dannhauer M, Warfield S K, Duffy F H and Wolters C H 2009 EEG source analysis of epileptiform activity using a 1 mm anisotropic hexahedra finite element head model *NeuroImage* **44** 399–410
- [37] Gramfort A, Papadopoulos T, Olivi E and Clerc M 2011 Forward field computation with OpenMEEG *Comput. Intell. Neurosci.* **2011** 923703
- [38] Ball T, Kern M, Mutschler I, Aertsen A and Schulze-Bonhage A 2009 Signal quality of simultaneously recorded invasive and non-invasive EEG *NeuroImage* **46** 708–16
- [39] Sperli F, Spinelli L, Seeck M, Kurian M, Michel C M and Lantz G 2006 EEG source imaging in pediatric epilepsy surgery: a new perspective in presurgical workup *Epilepsia* **47** 981–90

ABSTRACT/RESUME

CONTRIBUTION OF INTERICTAL AND ICTAL EPILEPTIC SOURCES TO SCALP EEG

Several in vitro, in vivo, and simulation studies have been performed in the past decades aiming to clarify the interrelations of cortical sources with their scalp and invasive EEG correlates. The amplitude ratio of cortical potentials to their scalp EEG correlates, the extent of the cortical area involved in the discharge, as well as the localization of the cortical source and its geometry, have been each independently linked to the recording of the cortical discharge with scalp electrodes. Simultaneous multiscale EEG recordings with scalp, subdural and depth electrodes, applied in presurgical epilepsy workup, offer an excellent opportunity to address this fundamental issue. Whereas past studies have considered predominantly neocortical sources in the context of temporal lobe epilepsy, the present work addresses deep sources, in mesial temporal and extra-temporal epilepsies. We showed that deep sources, such as those in mesial temporal or fronto-basal regions, are not visible, but are detectable in scalp EEG. Scalp EEG spikes correlate with extensive activation of the cortical convexity and high spike-to-background amplitude ratios.

Keywords: interictal spikes, source localization, intracranial recordings, refractory epilepsy, epilepsy surgery, electroencephalography

CONTRIBUTION DES SOURCES INTERICTALES ET ICTALES A L'EEG DE SCALP

Plusieurs études de simulation in vitro et in vivo ont été réalisées au cours des dernières décennies afin de clarifier les interrelations des sources corticales avec leurs corrélats électrophysiologiques enregistrés sur l'EEG invasif et l'EEG de scalp. L'amplitude des potentiels corticaux, l'étendue de l'aire corticale impliquée par la décharge, de même que la localisation et la géométrie de la source corticale sont des facteurs indépendants qui modulent l'observabilité et la contribution de ces sources sur l'EEG de surface. L'enregistrement simultané et multi-échelle de l'EEG de scalp et intra-crânien (avec des électrodes sous-durales ou profondes) durant l'exploration pré-chirurgicale des patients épileptiques offre une opportunité unique d'explorer cette question fondamentale. Alors que les études précédentes ont considéré essentiellement des sources néocorticales dans le contexte de l'épilepsie du lobe temporal, notre travail s'est intéressé à l'observabilité et la contribution de sources profondes temporales et frontales. Nous avons pu montrer : (1) que les sources épileptiques profondes enregistrées dans les régions temporales médianes et fronto-basales ne sont pas visibles par l'analyse visuelle de routine mais sont détectables après élimination du bruit de fond physiologique généré par les sources corticales de surface sus-jacentes ; (3) que l'amplitude des pointes enregistrées en surface est corrélée avec la surface d'activation corticale de la convexité et avec des ratios élevés d'amplitude pointes/activité de fond.

Mots clefs: pointes intercritiques, localisation de source, enregistrements intra-crâniens, EEG, SEEG, épilepsie réfractaire, chirurgie de l'épilepsie